A

Thesis

On

HYDRODYNAMIC STUDIES OF THREE-PHASE FLUIDIZED BED BY EXPERIMENT AND CFD ANALYSIS

Submitted By

Sambhurisha Mishra

(610CH304)

Under the Supervision of

Dr. Hara Mohan Jena

In partial fulfillment for the award of the Degree of

Master of Technology (Research)
In
Chemical Engineering

Department Of Chemical Engineering

National Institute Of Technology

Rourkela, Odisha, India

January 2013

Dedicated

To

My Parents

Manoj Kumar Mishra

&

Meena Kumari Satapathy

National Institute Of Technology Rourkela
Department Of Chemical Engineering

Certificate

*Certified that this Project thesis entitled "**Hydrodynamic Studies of Three-Phase Fluidized Bed by Experiment and CFD Analysis**" by*

Sambhurisha Mishra

(610 CH 304)

during the year 2010 - 2012 in partial fulfillment of the requirements for the award of the Degree of Master of Technology (Research) in Chemical Engineering at National Institute of Technology, Rourkela has been carried out under my supervision and this work has not been submitted elsewhere for a degree.

Date: 30.01.2013

Supervisor:

Dr. Hara Mohan Jena
Assistant Professor
Department of Chemical Engineering
National Institute of Technology
Rourkela.

Acknowledgement

I take this opportunity to express my profound gratitude and deep regards to my guide Dr. Hara Mohan Jena for his exemplary guidance, monitoring and constant encouragement throughout the course of this thesis. The blessing, help and guidance given by him time to time shall carry me a long way in the journey of life on which I am about to embark.

I take this opportunity to express my deep sense of gratitude to the members of my Master Scrutiny Committee Prof. Raghubansha Kumar Singh (HOD), Prof. (Mrs.) Abanti Sahoo of Chemical Engineering Department and Prof. Rupam Dinda of Chemistry Department for thoughtful advice during discussion sessions. I am also thankful to my teachers Dr. Pradip Chowdhury, Dr. Basudeb Munshi, Dr. Santanu Paria, Dr. Arvind Kumar, and Dr. Sujit Sen for constant encouragement and good wishes throughout the current work.

I am very mush thankful to my senior Akhilesh Pravakaran Khapre, Gaurav Kumar, Rajib Ghosh Chaudhuri, Sachin Mathur, Arvind Kumar, Bodhisattwa Chakraborty, Dhananjay Kumar, Pranati Sahoo, Divya Raja Vathsavai, Suman Choudhury, and Kailash Krishna Prasad; to my batch mates V. Balaji Patro, Tanmaya Lima, Sankaranarayanan Hariharan, Rajesh Tripathy, Anis Bakhsh, Prince George, Shivani Sharma, Sanjukta Bhoi, Lipika Kalo, Tapash Ranjan, Saswat Kumar, Tusar Ranjan Swain, Kalyan Hati and Stutee Bhoi; to my junior Chinmayee Patra, Aakanksha Pare, Sangram Patil and Sidharth Sankar Parhi for their cordial support, valuable information and guidance, which helped me in completing this task through various stages.

Last but not the least, thank to my lovable parents, sister, brother in law, and niece for incredible love and support and for the believing me unconditionally.

I am really grateful to almighty for those joyful moments I enjoyed and painful instances which made me tough and strong to face situations in life to come and for the exceptional journey and memories at National Institute of Technology Rourkela.

(Sambhurisha Mishra)

Table of Contents

List of Tables

List of Figures

Nomenclature

β:	Particulate loading, -
$\alpha_{d:}$	Volume fraction of discrete phase, -
α_c:	Volume fraction carrier phase, -
ρ_d:	Density of the dispersed phase (*d),* Kg m^{-3}
ρ_c:	Density of the carrier phase (*c*), kg m^{-3}
St:	Stoke number, -
τ_d:	Particle response time, s
t_s:	System response time, s
d_d:	Diameter of dispersed phase, m
μ_c:	Viscosity of carrier phase, Pa s
$L_{s:}$	Characteristics length, m
$V_{s.}$:	Characteristic velocity, m s^{-1}
V_q:	Volume of phase q. -
α_q:	Volume fraction of phase q, -
$\vec{\rho}_q$:	Effective density of phase q, Kg m^{-3}
ρ_q:	Physical density of the phase q, Kg m^{-3}
$\vec{v}_q$:	Velocity of phase *q*, m s^{-1}
$\dot{m}_{pq}$:	Mass transfer from phase *q* to phase *p*,
$\dot{m}_{qp}$:	Mass transfer from phase *p* to phase *q*
S_q:	Source term,-

$\bar{\bar{\tau}}_q$: q^{th} phase stress-strain tensor, Pa

μ_q: Shear viscosity of the phase q, m s^{-1}.

λ_q: Bulk viscosity of phase q, m s^{-1}.

$\vec{F}_q$: External body force, N

$\vec{F}_{lift,q}$: Lift force, N

$\vec{F}_{vm,q}$: Virtual mass force, N

$\vec{R}_{pq}$: Interaction between phases, -

p : Pressure, Pa

$\vec{g}$: Acceleration due to gravity, m s^{-2}

ρ_{rq}: Phase reference density of q^{th} phase, K m^{-3}

K_{pq}: Interphase momentum co-efficient, Kg s^{-1}

p_s: Solid pressure, Pa

α_s: Volume fraction of phase, -

ρ_s: Density of phase s, Kg m^{-3}

$\overrightarrow{v_s}$: Velocity of phase, s

$\bar{\bar{\tau}}_s$: s^{th} phase stress-strain tensor, Pa

K_{ls}: Fluid-solid exchange co-efficient, Kg s^{-1}

N: Total number of phases, -

K_{pq} : Fluid-fluid exchange co-efficient, Kg s^{-1}

K_{ls}: Fluid-solid and solid-solid exchange coefficient, Kg s^{-1}

f: Drag function, -

τ_p: Particulate relaxation time, s

d_p: Diameter of the bubbles of phase p, m

C_D : Drag co-efficient, -

Re : Reynolds number, -

ρ_{rp}: Mixture density of phase *p* and *r*, kg m^{-3}

μ_{rp}: Mixture viscosity of phase *p* and *r*, m s^{-1}.

α_p: Volume fraction of phase *p*, m s^{-1}.

μ_p: Viscosity of phase *p*, m s^{-1}.

α_r: Volume fraction of phase *r*, -

μ_r: Viscosity of phase *r*, m s^{-1}.

μ_l: Viscosity of liquid phase, m s^{-1}.

τ_s: Particulate relaxation time, s

d_s : Diameter of the particles of phase *s*, m

α_l: Volume fraction of liquid phase, -

ρ_l: Density of liquid phase, kg m^{-3}

$\vec{v}_l$: Velocity of liquid phase, m s^{-1}

e_{ls}: Coefficient of restitution,-

$C_{fr,ls}$: Coefficient of friction between the l^{th} and s^{th} solid phase particles,-

d_l: Diameter of particle of solid *l*, m

$g_{0,ls}$: Radial distribution coefficient, -.

Θ_s : Granular temperature, K

e_{ss}: Co-efficient of restitution for particle collisions, -

$g_{0,ss}$: Radial distribution function, -

S: Distance between grains, m

μ_s: Solid shear viscosity, m s^{-1}

$\mu_{s,col}$: Collision viscosity, m s^{-1}

$\mu_{s,kin}$: Kinetic viscosity, m s^{-1}

$\mu_{s,fr}$: Frictional viscosity, m s^{-1}

λ_s: Bulk viscosity, m s^{-1}

ϕ: Angle of internal friction, -

K_{Θ_s}: Diffusion co-efficient

Υ_{Θ_s}: Collisional dissipation of energy

Φ_{ls}: Energy exchange between l^{th} solid phase and s^{th}solid phase

$\vec{U}_{s,||}$: Particle slip velocity parallel to the wall, m s^{-1}

ϕ: Specularity co-efficient between particle and wall, -

$\alpha_{s,max}$ Volume fraction for particle at maximum packing, -

$\bar{\bar{\tau}}_q^{"}$: Reynolds stress tensors for continuous phase q, Pa

$\vec{U}_q$: Phase-weighted velocity, m s^{-1}

$\mu_{t,q}$: Turbulent viscosity, Pa s

ε_q: Dissipation rate, m^2 s^{-3}

C_μ: Constant, -

$L_{t,q}$: Length of turbulent eddies, m

Π_{k_q}=Π_{ε_q} : Influence of dispersed phase on continuous phase q

$G_{k,q}$: Turbulence kinetic energy, J m^{-2}

$\tau_{F,pq}$: Characteristic relaxation time, s

Γ_ϕ: Diffusion co-efficient for ϕ, -

$\nabla\phi$: Gradient of ϕ, -

S_ϕ: Source of ϕ per unit volume, -

N_{face}: Number of face enclosing cell, -

ϕ_f: Value of ϕ convected through face *f*, -

ρ_f: Density of ϕ convected through face *f*, kg m^{-3}

$\vec{v}_f$: Velocity of ϕ at face *f*, m s^{-1}

$\vec{A}_f$: Area of face *f*, m^2.

$\nabla.\phi_f$: Gradient of ϕ at face *f*,-

V: Cell volume, m^3

nb: Neighbour cell, -

a_p: Linearized co-efficient for ϕ, -

a_{nb}: Linearized co-efficient for ϕ_{nb}, -

I: Identity matrix, -

$\vec{F}$: Force vector, N

J_f : Mass flux through face f, kg m^{-2}

J_f^*: Face flux, N m^{-2}

$J_f^{'}$: Correction factor, -

d_f: Diameter of face, m

$p_{C_0}^{'}$: Cell pressure correction, Pa

$p^{'}$: Pressure correction, Pa

b : Source term, -

α : Under-relaxation factor, -

α_p: Under relaxation factor for pressure, -

U_{Lmf}: Minimum liquid fluidization velocity, m s^{-1}

Abstract

The complex hydrodynamics of three-phase (gas-liquid-solid) fluidized beds are not well understood due to complicated phenomena such as particle-particle, liquid-particle and particle-bubble interactions. In the present work both experimental and computational studies have been carried out on two and three dimensional fluidized beds to characterize there hydrodynamic behavior. Air, water and low density solid particles have been used as the gas, liquid and solid phase to analyze the system behaviors. Eulerian multi-phase model has been used to simulate the system by using the commercial CFD code ANSYS Fluent 13.0. Gidaspow and Schiller-Neumann drag models have been used to calculate inter-phase drag force. Two-equation standard *k*-ε model has been used to describe the turbulent quantities. CFD simulation of three-phase fluidized bed systems with a distributor plate is not seen in literature. In the present work fluidized bed with distributor having orifice diameter 0.002 m has been studied. Result obtained from the simulation shows that fluidized bed with distributor has higher values of bed expansion and gas holdup compared to that of fluidized bed without distributor plate. It is also observed that in the bed having distributor the velocity magnitudes of solid particles, the liquid and gas phases are high and more fluctuating than in the bed without distributor. Simulation result obtained from CFD simulation with low density solid material is found agree with the experimental finding.

CHAPTER-1

INTRODUCTION AND LITERATURE REVIEW

Fluidization is an operation by which fine solids are transformed into a fluid-like state through contact with gas or liquid or by both gas and liquid. Gas-liquid-solid fluidization is defined as an operation in which a bed of solid particles is suspended in gas and liquid media due to net drag force of the gas and/or liquid flowing opposite to the net gravitational force (or buoyancy force) on the particles. Such an operation generates considerable, intimate contact among the gas, liquid and the solid in the system and provides substantial advantages for application in physical, chemical or biochemical processing involving gas, liquid and solid phases. Fluidization is broadly of two types, viz. aggregative or bubbling and. The gas-liquid-solid fluidization with liquid as continuous phase is of particulate fluidization type, while aggregative fluidization is a characteristic of gas-liquid-solid system with gas as the continuous phase.

1.1. Advantages and disadvantages of three-phase fluidized bed:

There are several advantages of fluidized beds such as; ability to maintain a uniform temperature, significantly lower pressure drops which reduce pumping costs, catalyst may be withdrawn, reactivated, and added to fluidized beds continuously without affecting the hydrodynamics performance of the reactor, bed plugging and channeling are minimized due to the movement of solids, lower investments for the same feed and product specifications, new improved catalyst can replace older catalysts with minimal effort, high reactant conversion for reaction kinetics favoring completely mixed flow patterns, low intra particle diffusion resistance, gas-liquid and liquid-slid mass transfer resistance(shah, 1979; Beaton et al., 1986; Fan, 1989; Le Page et al., 1992; Jena, 2010). There are, however, also some disadvantages to fluidized beds such as; catalyst attrition due to particle motion, entrainment and carryover of particles, relatively larger reactor size compared to bed expansion, not suitable for reaction kinetics favoring plug flow pattern, low controllability over product selectivity for complex reaction and loss of driving force due to back mixing of particles in case transfer operations (Jena, 2010).

1.2. Modes of operation and flow regimes in three-phase fluidized bed:

Depending on the flow directions of the fluid phases, fluidized beds are classified as: co-current up-flow, co-current down-flow, counter-current, liquid batch with gas up-flow (Jena, 2010). Along with flow directions and the fluid phase which is continuous, the gas-liquid-solid fluidization is categorized mainly into four mode of operation. These mode are co-current three-phase fluidization with liquid as continuous phase, co-current three-phase fluidization with the gas as the continuous phase, inverse three-phase fluidization and fluidization represented by a turbulent contact absorber (TCA) (Jena et al.,2008).

Flow regime has a great role in three-phase fluidized bed and is important for its stable operation in a particular set of operating variables Fan (1989). Three-phase fluidized beds can operate: bubbling, slugging and transport regime. Within the bubbling regimes, there are two sub-categories: the dispersed bubbles and the coalesced bubble regimes. The separation between regimes is often qualitative and not well defined. Zhang (1996) and Zhang et al. (1997) identified seven distinct flow regimes for gas-liquid-solid co-current fluidized bed and identified a number of quantitative methods for determining the transitions as under:

- Dispersed bubble flow: Usually corresponds to high liquid velocities and low liquid velocities. Results in small bubbles of relatively uniform size. Little bubble coalescence despite high bubble frequency.
- Discrete bubble flow: Usually occurs at low liquid and gas velocities. It is similar to the previous regime with respect to small bubble size and uniform size. However, the bubble frequency is lower.
- Coalesced bubble flow: Usually found at low liquid velocities and intermediate gas velocities. The bubbles are larger and show a much wider size distribution due to increased bubble coalescence.
- Slug flow: This regime is characterized by large bullet shaped bubble with a diameter approaching that of the column and length that exceed the column diameter.
- Churn flow: Churn flow similar to the previous regimes, but much more chaotic and frothy.

- Bridging flow: A transitional regime between the churn flow and the annular flow where liquid and solid effectively form “bridges” across the reactor which is continuously broken and reformed.
- Annular flow: At extremely high gas velocities, a continuous gas phase appears in the core of the column.

Dispersed flow, discrete flow and coalesced flow are grouped under the heading “bubbling regimes”, while churn flow, bridging low and annular flow all be classified as belonging to the transport regime. (Jena, 2010)

1.3. Application of three-phase fluidized bed:

Among all the types of three-phase fluidized beds, three-phase concurrent gas-liquid-solid fluidized beds are used in a wide range of applications including hydro-treating and conversation of heavy petroleum and synthetic crude, coal liquefaction, methanol production, sand filter cleaning, electrolytic timing, conversion of glucose to ethanol, aerobic waste water treatment, and various other hydrogenation and oxidation reactions (Fan, 1989; Wild and Poncin, 1996; Jena, 2010).

In the waste water treatment various types of bioreactors are in use. The recent fluidized bed bioreactors are superior in performance due to immobilization of cells on solid particles reducing the time of treatment, volume of reactor is extremely small, lack of clogging of bio-mass and removal of pollutant like phenol even at lower concentrations (Jena et al., 2005). Numerous researches on various types of waste water treatment using gas-liquid-solid fluidized bed bioreactor have been reported in literature. In the fluidized bed system used in waste water treatment, low density solid matrix is used to immobilize the microbes as the system operates at low water and air velocities to avoid transportation of the particles from the bed.

1.4. Design aspects of three-phase fluidized bed:

Considerable progress has been made with respect to understanding of the phenomenon of gas-liquid-solid fluidization. The successful design and operation of a gas-liquid-solid fluidized bed system depends on the ability to accurately predict the fundamental properties of the system. To design a three-phase fluidized bed chemical reactor different aspects must be

predicted and quantified. Most often, to achieve desired reactor goals, fundamental knowledge like the effect of various operating parameters on the hydrodynamics may be required. For the given fluid and solid properties, the operating gas and liquid superficial velocity must then be set and the reactor size determined based upon the expected bed expansion and hold-ups.

Some of the common parameters used to describe the fluidization phenomena are:

- *Bed Pressure drop*: Measures the drag in combination with the buoyancy and phase holdups
- *Minimum fluidization velocity*: The minimum superficial velocity at which the bed becomes fluidized.
- *Gas holdup*: Measure the fractional volume occupied by the gas.
- *Liquid holdup*: Represents the fraction of the bed occupied by the liquid phase.
- *Solid holdup*: Measure the fractional volume occupied by solids.
- *Bed expansion ratio*: Measure the extent of fluidization of the bed.
- *Porosity*: Measures the volume occupied by both the liquid and the gas.
- *Phase velocity*: the velocity of individual phases in the fluidized bed.

1.5. Hydrodynamic studies of three-phase fluidized beds with low density particles:

Low density solid particles found huge application in bio reactor for aerobic waste water treatment. Hydrodynamics study of three-phase fluidized bed with low density particles are rarely seen in literature although a tremendous work is seen for moderate or high density solid particles. Nore, et al. (1992) have studied hydrodynamics, gas-liquid mass transfer and particle-liquid heat and mass transfer in three-phase fluidized bed of light particles under condition typical of biochemical application. They have used polypropylene beads with inclusion of mica and achieved a density ranging from 1130 to 1700 kg/m^3 as the solid phase. They have studied the effect of liquid and gas velocities on bed porosity and liquid holdup. Thy have reported increase in bed porosity for both increase in the gas velocity and the liquid velocity. Hydrodynamics of a gas-liquid-solid fluidized bed with low density solid [Kaldnes Miljotechnologies AS (KMS)] support was investigated by Sokół and Halfani (1999), they have found that value of minimum fluidization air velocity depend on the ratio of bed to

reactor volume and mass of cell growth on the particles. Thy have also established that the air hold depends on air velocity, ratio of bed to reactor volume and mass of biomass laden particles. The effect of operational parameters on biodegradation of organics in fluidized bed bioreactor with low density solid particles have been studied by Sokół (2001) and Sokół and Korpal (2004). Briens and Ellis (2005) have characterized the hydrodynamics of three-phase fluidized bed systems by statistical, fractal, chaos and wavelet analysis. The have determined the optimum fluid velocity and ratio of volume of bed to volume of reactor for largest degradation of phenol. The solid particles covered with a biofilm are fluidized by air and contaminated water by Allia et al. (2006) to confirm the operating stability, to identify the nature of mode flow and to determine some hydrodynamic parameters such as the minimum fluidization velocity, the pressure drop, the expansion, the bed porosity, the gas retention and the stirring velocity. Rajasimman and Karthikeyan (2006) have determined the optimum air holdup and expanded bed height for maximum aerobic digestion of starch wastewater in fluidized bed bioreactor with low density particles. .

Even though a large number of experimental studies are directed towards the quantification of flow structure and flow regimes identification for different process parameters and physical properties, the complex hydrodynamics of these reactor are not well understood due to complicated phenomena such as particle-particle, liquid-particle, and particle-particle interactions (Jena, 2010). As regard to mathematical modeling, computational fluid dynamics (CFD) simulation give detailed information about the local values of pressure, component of mean velocity, viscous and turbulent stresses, turbulent kinetics energy and turbulent energy dissipation rate, etc. Such information can useful in the understanding of the transport phenomena in the complex geometry like fixed beds.

1.6. Computational fluid dynamics:

CFD is a powerful tool for the prediction of the fluid dynamics in various type of system, thus, enabling a proper design of such systems. It is a sophisticated way to analyze not only for fluid flow behavior but also the processes of heat and mass transfer. The availability of high performance computing hardware and the introduction of user-friendly interfaces have led to the development of CFD packages available both for commercial and research

purposes. The various general purposes CFD packages in use are PHONICS, CFX, FLUENT, FLOW3D, and STAR-CD etc. Most of these packages are based on the finite volume method and are used to solve fluid flow and heat and mass transfer problems.

Basically two approaches are used namely, the Euler-Euler formulation based on the interpenetrating multi-fluid model, and the Euler-Lagrangian approach based on solving the Newton's equation of motion for the dispersed phase. The finite volume method (FVM) is one of the most versatile discrimination technique used for solving the governing equation for fluid flow and heat and mass transfer problems. The most compelling features of the FVM are that the resulting solution satisfied the conservation of quantities such as mass, momentum, energy and species. In the FVM, the solution domain is subdivided into continuous cells or control volume where the variable of interest is located at the centroid of the control volume forming a grid. The next step is to integrate the differential form of the governing equations over each control volume. Interpolation profiles are then assumed in order to describe the variation of the concerned variables between cell centroids. There are several schemes that can be used for discretization of governing equations e.g. central differencing, upwind differencing, power law differencing and quadratic upwind differencing schemes. The resulting equations are called discretized equation. In this manner the discretized equation expresses the conservation principle for the variable inside the control volume. These variable forms a set of algebraic equations which are solved simultaneously using special algorithm.

1.7. ANSYS FLUENT Software:

FLUENT is one of the widely used CFD package. ANSYS FLUENT software contain wide range of physical modeling capabilities which are used to model flow, turbulence, reaction and heat transfer for industrial application. Features of ANSYS FLUENT software:

- MESH FLEXIBILITY: ANSYS FLUENT software provide mesh flexibility. It has ability to solve flow problem using unstructured mesh. Mesh type which support in FLUENT include quadrilateral, triangular, hexahedral, tetrahedral, polyhedral, pyramid and prism. Due to automatic nature of creating mesh save time.
- MULTIPHASE FLOW: it is possible to model different fluid in a single domain in FLUENT.

- REACTION FLOW: modeling of surface chemistry, combustion as well as finite rate chemistry can be done in FLUENT.
- TURBULENCE: It offer a number of turbulence models to study the effect of turbulence in a wide range of flow regimes.
- DYNAMICS AND MOVING MESH: The user setup the initial mesh and instructs the motion, while FLUENT software automatically changes the mesh to follow the motion instructed.
- POST-PROCESSING AND DATA EXPORT: Users can post process their data in FLUENT software, creating among other things contour, path lines and vectors to display the data.

1.8. Computational fluid dynamic studies on three-phase fluidized beds:

Recently, several CFD models based on Eulerian multi-fluid approach have been developed for gas–liquid-solid flows (Matonis et al., 2002; Feng et al., 2005; Schallenberg et al., 2005). Comprehensive list of literature on modeling of three-phase fluidized beds are presented below.

Grevskott et al. (1996) have carried out computational fluid dynamic simulation of three phase slurry reactor by two fluid models, with the two phases treated in an Eulerian frame of reference. They have assumed equal pressure for both fluid phase, no mass transfer between the two-phase and a spatial averaging larger than the scale of the dispersed phase. The inter-phase momentum exchange terms modeled between the fluid phases were steady interfacial drag, added mass force and lift force. They have considered lift force only in the radial direction, since the drag force is dominating in the axial direction. They have also tested a new model for bubble size distribution and solid pressure. Their new bubble size model is found to improve the size distribution prediction compared to prior model. They have quantified the axial mean velocity and turbulent kinetic energy as function of radial position.

Mitra-Majumdar et al. (1997) have used computational fluid dynamics model to examine the structure of three-phase (air-water-glass beads) flow through a vertical column. In their study they proposed new co-relation to modify the drag between the liquid and the gas phase to account for the effect of solid particles on bubble motion. They also attempt to proposed

new co-relation for drag between the solid particles and the liquid phase to incorporate the effect of bubbles. They have used K- ϵ model for simulating the effect of turbulence on the flow field. They have characterized the variation of solid volume fraction axially and determined the radial velocity profile.

Jianping and Shonglin (1998) have used a two dimensional pseudo-two phase fluid dynamics model with turbulence calculate local values of axial liquid velocity and gas holdup in a concurrent gas-liquid-solid three-phase bubble column reactor. They have examined the effect of solid loading, superficial liquid velocity and superficial gas velocity on the local axial liquid velocity and local gas holdup. They have concluded that local axial liquid velocity and local gas holdup value are strongly influenced by solid loading and operating condition, local gas holdup and axial liquid velocity increased as the solid loading declined and under certain circumstance, the increased in superficial liquid velocity was seen to increase the local axial liquid velocity and decreased the local gas holdup.

Li et al. (1999) have carried out CFD simulation of gas bubbles rising in water in a small two dimensional bed glass beads. Solid flow in a fluidized bed is simulated by a combine method CFD with discrete particle method. They have applied a bubble induced force model, continuum surface force model and Newton third law respectively for the couplings of particle-bubbles, gas-liquid and particle liquid interactions. They have also included a close distance interaction model in particle-particle collision model, which consider liquid interstitial effect among particles. It is shown that their model can capture the bubble wake behavior such as wake structure and the shedding frequency. Their simulation results were in good agreement with experimental finding.

Zhang et al. (2000a) have conducted a discrete phase simulation to study the bubble and particle dynamics in a three phase fluidized bed at high pressure. They have employed the Eulerian volume-averaged method, the Lagrangian dispersed particle method, and the volume of fluid (VOF) method to describe the motion of liquid, solid particles, and gas bubbles. To describe the coupling effect of particle-bubble, gas-liquid, and particle-liquid interactions they have applied a bubble-induced force model, a continuum surface force (CSF) model, and Newton's third law. They have conducted simulations of the bubble rise velocity at various

solids holdups and pressures along with the maximum stable bubble size and the particle–bubble interactions. They have examined effects of the pressure and solids holdup on the bubble rise characteristics such as the bubble rise velocity, bubble shape and trajectory.

Zhang et al. (2000b) have developed a computational scheme for discrete-phase simulation of a gas-liquid-solid fluidization system and a two-dimensional code based on it. The volume-averaged method, the dispersed particle method, and the volume-of-fluid (VOF) method have been used to account for the flow of liquid, solid particles, and gas bubbles respectively. The gas-liquid interfacial mass, momentum and energy transfer have been described by a continuum surface force (CSF) model. They have introduced a close-distance interaction (CDI) model which illustrates the motion of the particle prior to its collision; upon collision, the hard sphere model have been employed. The particle-bubble interactions have been formulated by incorporating the surface tension force in the equation of motion of particles. The particle-liquid interaction have been brought into the liquid phase Navier-Stokes (N-S) equations through the use of Newton's third law of motion. The volume-averaged liquid phase N-S equations have been solved using the time-split two-step projection method. The simulation results using this scheme have been verified for bed expansion and pressure drop in liquid-solid fluidized beds. The simulations of a single bubble rising in a liquid-solid suspension and the particle entrainment by a bubble on the surface of the bed have been conducted and the results are in agreement with the experimental findings.

Padial et al. (2000) have used finite-volume flow simulation technique to study the three dimensional simulation of three phase flow in a conical-bottom draft-tube bubble column. They have employed an unstructured grid method along with a multifield description of the multiphase flow dynamics. They have observed the same loss of column circulation as experimental when the column is operated with the draft tube in its highest position.

Li et al. (2001) have conducted a discrete phase simulation (DPS) to investigate multi-bubble formation dynamics in gas-liquid-solid fluidization systems. They have developed and employed a numerical technique based on computational fluid dynamics (CFD) with the discrete particle method (DPM) and volume tracking represented by the volume-of-fluid (VOF) method for simulation. They have applied a bubble-induced force (BIF) model, a

continuum surface force (CSF) model, and Newton's third law to account for the couplings of particle-bubble, bubble-liquid and particle-liquid interactions, respectively. In the formulation of particle-particle collision model they have consider a close interactive effect between colliding particles. They have conducted two-dimensional simulations of behavior of bubble formation from multi-orifices in liquids and liquid-solid suspensions at high pressures up to 19.4 MPa under constant gas flow conditions. They have indicated that the liquid flow dynamics induced by adjacent bubbles and bubble wake significantly affects the multi-bubble formation process.

Matonis et al. (2002) have developed experimentally verified computational fluid dynamic model for gas-liquid-solid flow. A three-dimensional transient computational code for the coupled Navier-Strokes equations for each phase has been used. Their simulation shows a down flow of particles in the center of the column, and an up flow near the wall, and a nearly uniform particle concentration. They have characterized the local solid velocity.

Chen and Fan (2004) have developed two dimensional Eulerian–Lagrangian model for three-phase Fluidization and used Level-set method for interface tracking and Sub-Grid Scale (SGS) stress model for bubble-induced turbulence to characterize the bubble rise velocity, bubble shapes and their fluctuations, and bubble formation. They have discussed the effect of particle concentration on these phenomena.

Glover and Generalis (2004) have presented an alternate approach to the modeling of solid-liquid and gas-liquid-solid flow for a 5:1 height to width ratio bubble column. They have developed a modified transport equation for the volume fraction of a dispersed phase for the investigation of turbulent buoyancy driven flows.

Feng et al. (2005) have developed a 3-dimensional computational fluid dynamics (CFD) model to simulate the structure of gas-liquid-TiO2 nanoparticles three-phase flow in a bubble column. The have been compared with experimental data for model validation. Their time-averaged and time-dependent predictions are successful on instantaneous local gas holdup, gas velocity, and liquid velocity.

Wiemann and Mewes (2005) have presented a numerical method for the calculation of the three- dimensional flow fields in bubble columns based on a multi fluid model. The mean

bubble volume has been obtained from population balance equation. For calculation of three phase gas-liquid-solid flow, solid phase have been considered numerically by an additional Eulerian phase. They have obtained the local and the integrated volume fraction of gas in the bed from CFD simulation.

Zhang and Ahmadi (2005) have used an Eulerian-Lagrangian computational model for simulation of gas-liquid-solids flows in three phase slurry reactors. They have used a volume-averaged system of governing equations for liquid flow model whereas motion of bubbles and particles are evaluated by the Lagrangian trajectory analysis procedure. They have assumed that the bubbles remain spherical and their shape variations have been neglected. They have included two-way interactions between bubble-liquid and particle-liquid in the analysis. The discrete- phase equation include drag, lift, buoyancy, and virtual mass forces. They have accounted for particle-particle interaction and bubble-bubble interaction by the hard sphere model approach. They have included bubble coalescence in the model. They have studied the transient flow characteristics of three phase flow and the effect of bubble size on variation of flow characteristics. The simulation result shows dominance of time-dependent staggered vortices on the transient characteristics. The bubble size significantly affects the characteristics of three-phase flows and flows with larger bubbles appear to evolve faster.

Annaland et al. (2005) has presented a hybrid model for the numerical simulation of gas-liquid-solid flow using a combine front tracking (FT) for dispersed gas bubbles and solid particle present in the continuous liquid phase. They have presented the physical foundation of the combined FT-DP model with illustrative computational results highlighting capabilities of this hybrid model. They have studied effect of bubble-induced particle mixing focusing on the effect of the volumetric particle concentration. In addition they have quantified the retarding effect on bubble rising velocity due to presence of suspended solid particles.

Schallenberg et al. (2005) have used a computational fluid dynamic model to calculate a three-phase (air-water-solid particles) flow in a bubble column. They have used the K-ε turbulence model extended with term accounting for the bubble-induced turbulence to calculate the eddy viscosity of the liquid phase. Bubble-bubble and particle-particle interaction have been considered as well as a direct momentum transfer between the two

dispersed phases bubbles and solid particles. The local volume fractions of the dispersed phase have been considered of the calculation of the drag coefficient between the dispersed phases and the continuous phases. They have compared the measured local gas and solid holdup as well as measured liquid velocity with the corresponding calculated result. They have observed good agreement between the measured and the calculated results.

Cao et al. (2009) have modeled gas-liquid-solid circulating fluidized bed by two dimensional, Eulerian–Eulerian–Lagrangian (E/E/L) approaches. E/E/L model combined with Two Fluid Model (TFM) and Distinct Element Method (DEM). Based on generalized gas–liquid two fluids *k*-*ε* model, the modified gas–liquid TFM is established. They have studied the local liquid velocity and radial distribution of local phase hold-ups

Muthiah et al. (2009) have carried out computational fluid dynamics to characterize the dynamics of three-phase flow in cylindrical fluidized bed, run under homogeneous bubble flow and heterogeneous flow condition. They performed simulation for air-water-glass beads in a fluidized bed of height of 0.6 m and diameter of 0.1 m and diameter of solid of 0.05 m to study the flow pattern. They have used Eulerian-Eulerian multiphase model with K-ϵ turbulence for liquid phase. They observed from their simulation result that an appropriate mesh and a robust numerical solver are crucial for getting accurate solution. They have also observed that higher gas velocity, higher value of solid loading and lower particles diameter make the system diameter faster.

O'Rourke et al. (2009) have developed 3D model and used Eulerian finite difference approach to simulate gas-liquid-solid fluidized bed. The mathematical model using multiphase particle-in-cell (MP-PIC) method is used for calculating particle dynamics (collisional exchange) in the computational-particle fluid dynamics (CPFD). Mass averaged velocity of solid and liquid and particle velocity fluctuation, collision time, liquid droplet distribution has been characterized by them.

Paneerselvam et al. (2009) have developed a three dimensional transient model to simulate the local hydrodynamics of a gas-liquid-solid three phase fluidized bed reactor using the CFD method. The flow field predicted by CFD simulation shows a good agreement with the experimental data of literature. From the validated CFD model, they carried out the

computation of the solid mass balance and various energy flows in fluidized bed reactors. They also studied the influence of different inter-phase drags models for gas-liquid interaction on gas holdup in their work.

Sivaguru et al. (2009) have carried out the CFD analysis of three-phase fluidized bed to predict the hydrodynamics. They have taken liquid phase as water that continuously flow, whereas the gas phase is air which flow discretely throughout the bed. Ceramic particle of 1 mm diameter, density of 2650 kg/m^3 have been used as solid phase. The solid and liquid phases have been represented by the mixture model. The air has been injected from the bottom of the fluidized bed by mean of discrete phase method (DPM). They have obtained the simulation result using porous jump and porous zone model to represent the distributor. They have found that porous zone model is best applicable in Industries, since stability of operating condition is achieved even with non-uniform air, water flow rate and with different bed height. The work shows a good agreement of simulated pressure drop value of the fluidized bed with the experimental finding.

Nguyen et al. (2011) have carried out CFD simulation using commercial CFD package FLUENT 6.2 to understand the hydrodynamics of three phase fluidized bed. They have investigated the complex hydrodynamics of three phase fluidized bed such as bed expansion, holdup for two phases, bed pressure drop, and fluidized bed voidage and velocity profile. They have used Euler-Euler multiphase approach for predicting the overall performance of gas –liquid-solid fluidized bed and Gidaspow model is used as drag model for simulation. Result obtained by them shows that the liquid holdup increased with the inlet liquid velocity and gas holdup increases with flow rate of gas and decreased with increased in liquid flow rate.

Hamidpour et al (2012) have performed CFD simulations of gas-liquid-solid fluidized beds in a full three dimensional, unsteady multiple-Euler frame work by mean of the commercial software FLUENT. They have investigated the significance of implementing accurate numerical schemes as well as the choice of available K-ε turbulence models (standard, RNG, realizable), solid wall boundary condition and granular temperature model. The result indicated that in order to minimize numerical diffusion artifacts and to enable valid

discussions on the choice of physical models, third order numerical schemes need to be implemented. They have observed that the realizable turbulence formulation was unable to produce the expected solid gulf-stream pattern (i.e. rising solid particles in the core and descending solid particles near the wall) in the three phase fluidized bed whereas the RNG and K-ε models were able to better capture depiction of flow patterns. They have obtained the best prediction of flow characteristics with a laminar model formulation accounting for the solid phase viscosity and the molecular viscosities of the two fluids.

The report on the computational models for the hydrodynamics characteristics of three-phase fluidized bed is limited. Most of these CFD studies are based on steady state, 2D axisymmetric, Eulerian multi-fluid approach. But in general, three phase flows in fluidized bed reactors are intrinsically unsteady and are composed of several flow processes occurring at different time and length scales. The unsteady fluid dynamics often govern the mixing and transport processes and is inter-related in a complex way with the design and the operating parameters like reactor and sparger configuration, gas flow rate and solid loading. Hardly there is any literature which focused on the effect various variables on the liquid minimum fluidization velocity, the bed expansion and phase holdup behaviour. Computational Model with a distributor plate at the bottom of the three-phase fluidized bed is not seen in literature although it is actually present in a physical fluidized bed. The presence of distributor is likely to affect the flow behaviour of phases in the bed and so also the other hydrodynamic characteristics. The experimental hydrodynamic study of three-phase fluidized bed is meager and no literature describes the hydrodynamic study of low density particles in a three phase fluidized bed by CFD simulation and experiment together. Thus the present work has been carried out with the following main objectives.

1.9. Research objectives:

The main objectives of the present research work are summarized below:

- Hydrodynamic study on three-phase fluidized bed with low density particles (Plastic beads) using water and air as liquid and gas phase.
- To compare the hydrodynamic properties obtained from experiment with those obtained from CFD simulation.

- To study the CFD simulation of hydrodynamic behaviors of three dimensional (3D) fluidized bed and compare with the results of 2D model.
- To study the effect of the presence of distributor plate on the bed dynamics by CFD simulation and compare the results with those obtained from the simulation of bed without distributor.

1.10. Thesis summary:

This thesis comprises of five chapters v.i.z. Introduction and Literature Survey, Experimental setup and technique, Computational Flow Model and Numerical Methodology, Result and Discussion and Conclusion and Future scope of the work.

- *Chapter 1,* the background information, literature review and objective of the present work is discussed.
- *Chapter 2* deals with the experimental set up and detail of the system under experimental investigation. It also includes experimental procedure.
- *Chapter 3* deals with the computational models, the numerical methods, mesh quality, boundary condition, material description etc. used in the CFD simulation.
- *Chapter 4* the results of various hydrodynamics properties obtained from experiment and the simulation have represented graphically and discussed.
- *Chapter 5* deals with overall conclusion. Future recommendations based on the research outcome are suggested. The major findings of the work are also summarized.

CHAPTER – 2

EXPERIMENTAL SET-UP AND TECHNIQUES

A three-phase (gas-liquid-solid) fluidized bed is designed and fabricated to study the hydrodynamic characteristics (like: pressure drop, minimum fluidization velocity, bed expansion and phase holdup) of low density particle (plastic beads) using water as liquid phase and air as the gas phase.

2.1. Experimental setup:

The fluidized bed assembly consists of three sections, viz., the test section, the gas-liquid distributor section, and the gas-liquid disengagement section. Fig. 2.1 shows the schematic representation of the experimental setup used in the three-phase fluidization study. Fig. 2.2 gives the photographic representation of the experimental setup. The test section is the main component of the fluidized bed where fluidization takes place. It is a vertical cylindrical Plexiglas column of 0.1 m internal diameter and 1.88 m height consisting three pieces of persepex columns assembled by flange and nut bolt arrangement with rubber gasket in-between.

To prevent particle entrainment a 16-mesh screen has been attached to the top of the column for the fluidization study. The gas-liquid distributor is located at the bottom of the test section and is designed in such a manner that uniformly distributed liquid and gas mixture enters the test section. The distributor section made of Perspex is fructo-conical of 0.31 m in height, and has a divergence angle of 4.5^0. The liquid inlet of 0.0254 m in internal diameter is located centrally at the lower cross-sectional end. The higher cross-sectional end is fitted to the test section, with a perforated distributor plate made of G.I. sheet of 0.001 m thick, 0.12 m diameter having open area equal to 20 % of the column cross-sectional area with either a 16 mesh (BSS) stainless steel screen in between.

The distributor plate has 288 openings of 0.002 m, 0.0025 m and 0.003 m in triangular pitch arranged in 10 concentric circles of about 0.005 m radial gap. The size of the holes has been increased from the inner to the outer circle. This has been done with a view to have less pressure drop at the distributor plate and a uniform flow of the liquid into the test section. Figs.

2.3(a) and 2.3(b) represent the photographic view of the gas-liquid distributor section and the distributor plate. An antenna-type air sparger (Fig. 2.3(c)) of 0.09 m diameter with 50 number of 0.001 m holes has been fixed below the distributor plate for the generation of uniform bubbles to flow along the column cross-section of the fluidizer. In the gas-liquid distributor section, the gas and the liquid streams are merged and passed through the perforated grid. The mixing section and the grid ensured that the gas and the liquid are well mixed and evenly distributed into the bed.

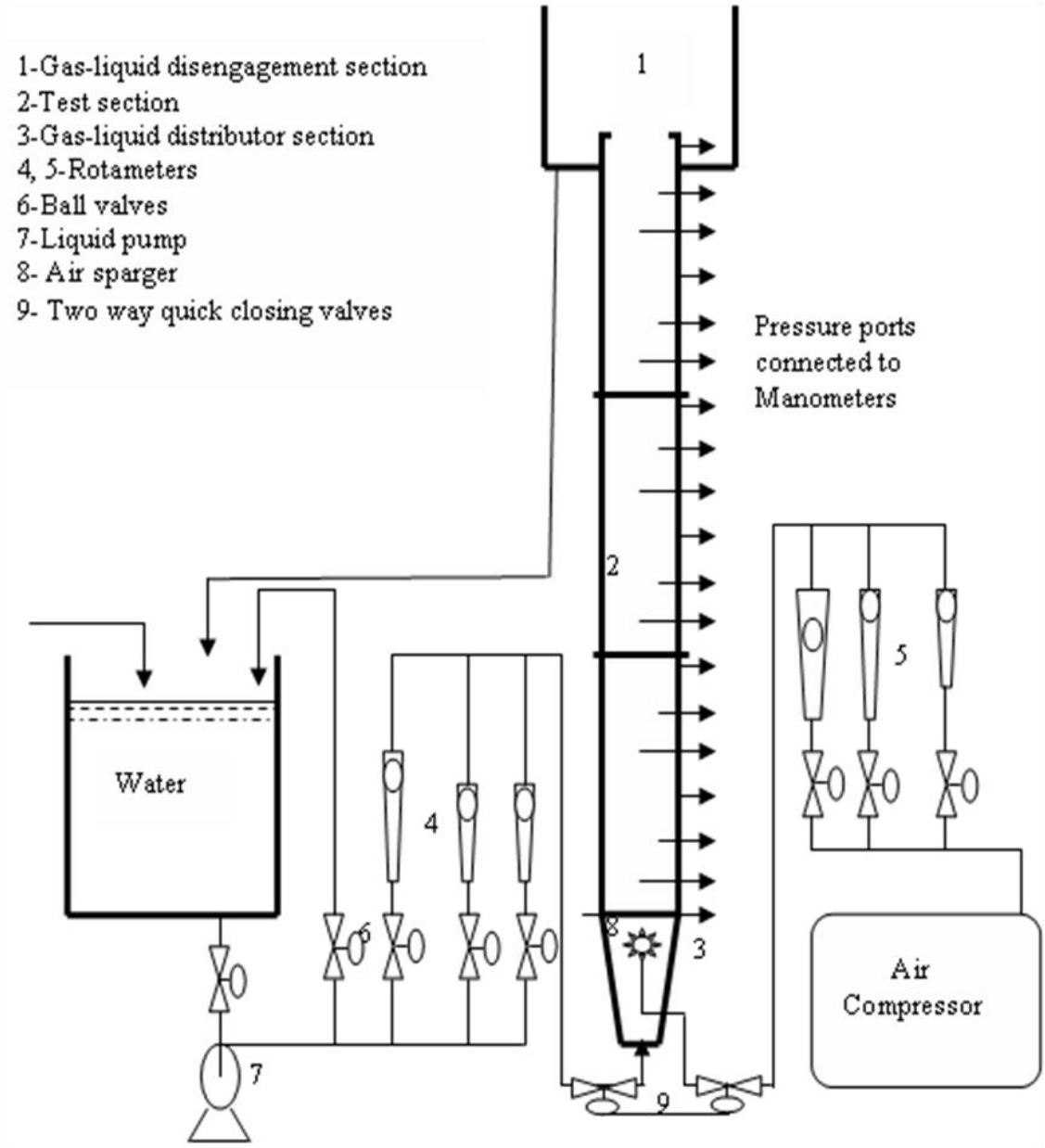

Fig. 2.1. Schematic representation of the experimental setup.

Fig. 2.2. Photographic view of the experimental set-up.

(a) **(b)** **(c)**

Fig. 2.3. Photographic view of: (a) the gas-liquid distributor, (b) distributor plate, (c) air sparger.

The gas-liquid disengagement section at the top of the fluidizer is a cylindrical section of 0.26 m internal diameter and 0.34 m height, assembled to the test section with 0.08 m of the test section inside it, which allows gas to escape and liquid to be circulated through the outlet of 0.0254 m internal diameter at the bottom of this section.

Table 2.1. Equipment characteristics and operating conditions

SET-UP	
Test section (Cylindrical Plexiglas column)	
Diameter, m	0.1
Height, m	1.88
Gas-liquid distributor section (fructo-conical)	
Height, m	0.31
Diameter of the ends, m	0.0508, 0.1
Tapered angle	4.5^0
Gas-liquid disengagement section (Cylindrical)	
Diameter, m	0.26
Height, m	0.34
Air sparger (antenna type)	
Orifice size, m	0.001 (50 nos.)
Distributor plate (GI)	
Diameter, m; thickness, m	0.12; 0.001
(holes in 10 concentric circles extend to 0.001m from centre)	0.005
Gap between circumference of holes, m	centre:1, circle-1 (c-1): 6, c-2: 12, c-3: 21
0.002 m holes (40 nos)	c-4: 22, c-5: 28, c-6: 34, c-7: 39, c-8: 19
	c-8: 19, c-9: 40, c-10: 47
0.0025 m holes (142 nos)	
0.003 m holes (106 nos)	
Liquid reservoirs	
Dimension, m; capacity, lit.	0.42 x 0.32 x 0.70; 94

For the measurement of pressure drop in the bed, the pressure ports have been provided and fitted to the manometer filled with carbon tetrachloride as the manometric fluid. The inner end of the pressure ports have been covered by means of 16 wire mesh SS sieve to prevent solids entering into the pressure tubing connected to the manometer.

In actual practice, oil free compressed air from a centrifugal compressor (3 phase, 1 Hp, 1440 rpm) used to supply the air at nearly constant pressure as fluidizing gas. This was done by continuously monitoring the pressure in the compressor air tank and adjustment of the bypass

line. The air was injected into the column through the air sparger at a desired flow rate using calibrated rotameter. Water was pumped to the fluidizer at a desired flow rate using water rotameter. Centrifugal pumps of different capacity (CRI, single phase, 0.5 HP, 2880 rpm, discharge capacity of 120 lpm) was used to deliver water to the fluidizer along with a bypass line. Two calibrated rotameters with different ranges each for water as well as for air were used for the accurate record of the flow rates. Water rotameters used were of the range 0 to 20 lpm and 5 to 100 lpm. Air rotameters were of the range 0 to 10 lpm and 5 to 50 lpm.

2.2. Measurement of properties of the solids and the fluids:

2.2.1. Particle size

The diameter of spherical plastic beads has been determined by slide callipers. The average diameter of 10 individual particles randomly selected has been used as the particle size.

2.2.2. Particle density

The density of the plastic beads has been measured using the water displacement method in which the packing voidage was obtained by displaced water volume when the particles were placed into a graduated cylinder filled with water. The plastic beads used are taken from the market having through hole at the centre. The hole has been filled by mechanical seal to increase the density more than that of water.

2.3. Experimental procedure:

The three-phase solid, liquid and gas are glass beads, tap water and oil free compressed air, respectively. The scope of the experiment is presented in Table 2.2. The air-water flow was co-current and upwards. Accurately weighed amount of material was fed into the column and adjusted for a specified initial static bed height. Water was pumped to the fluidizer at a desired flow rate using water rotameter. The air was then introduced into the column through the air sparger at a desired flow rate using air rotameter. Two calibrated rotameters with different ranges each for water as well as for air have been used for the accurately record of the flow rates. All experiments have been started with the column completely filled with water and glass beads and the initial level of manometer adjusted to have zero level. For liquid-solid experiment the liquid flow rate was gradually increased. Approximately five minutes were allowed to make sure that the steady state was reached. Then the readings of the

manometers and the expanded heights of the bed were noted. For gas-liquid-solid experiment, with a little flow of liquid close to zero, the air was slowly introduced and gradually increased to the desired flow rate after which the liquid flow rate was increased and the readings were noted down, as mentioned above. The procedure was repeated for different values of initial static bed height, particle size and gas velocity. In some experiment the liquid velocity is kept constant at experimental minimum fluidization velocity or at some fraction or multiple of minimum fluidization velocity, and then the gas velocity is varied to see the movement of the particles in the bed.

Table 2.2. Scope of the present investigation

A. Properties of gas, liquid and solid phase			
Gas phase	**Density (kg/m^3)**	**Viscosity (Pa.s)**	**Surface tension (kg/m^2)**
Air at 30^0C	1.166	$1.794x10^{-5}$	-
Liquid phase at 30^0C			
Water	995.7	0.000798	0.0712
Solid phase	**Particle Size (d_p), cm**	**Particle density (ρ_p), kg/m^3**	
Plastic beads	0.8	1172	
	1.16	1164	
	1.54	1155	
B. Experimental conditions			
Operating variables		**Range**	
Superficial gas velocity:		$0< U_g < 0.0382$ m/s	
Superficial liquid velocity (for fluidization study):		$0.004246 < U_L < 0.1062$ m/s	
Bed Parameters			
Initial static bed height in cm:	12.2, 24.7, 35.2, 41		

CHAPTER - 3

COMPUTATIONAL FLOW MODEL AND NUMERICAL METHODOLOGY

CFD is a powerful tool for the prediction of the fluid dynamics in various types of systems, thus, enabling a proper design of such systems. The availability of affordable high performance computing hardware and the introduction of user-friendly interfaces have led to the development of several CFD packages available both for commercial and research purposes. Most of the packages are based on the finite volume method. The Finite Volume Method (FVM) is one of the most versatile discrimination techniques used for solving the governing equations for fluid flow. The most compelling features of the FVM are that the resulting solution satisfies the conservation of quantities such as mass and momentum. This is exactly satisfied for any control volume as well as for the whole computation domain. Even a coarse grid solution exhibits exact integral balances. Apart from this, it can be applied to any type of grids (structured or unstructured, Cartesian or body fitted), and especially to complex geometries. In the finite volume method, the solution domain is subdivided into continuous cells or control volumes where the variable of interest is located at the centroid of the control volume forming a grid. The next step is to integrate the differential form of the governing equations over each control volume. Interpolation profiles are then assumed in order to describe the variation of the concerned variables between cell centroids. There are several schemes that can be used for discretization of governing equations e.g. central differencing, upwind differencing, power-law differencing and quadratic upwind differencing schemes. The resulting equation is called the discretized equation. In this manner the discretization equation expresses the conservation principle for the variable inside the control volume. These variables form a set of algebraic equations which are solved simultaneously using special algorithm.

Advances in physical models, numerical analysis and computational power enable simulation of the multi-phase flow characteristics in two and three dimensional circumstances. Today,

computational fluid dynamics CFD has emerged as a new paradigm for modeling multiphase flow and fluidization, as seen from the literature review for three-phase reactors. As described in the objective, the purpose of this study is to investigate numerically the hydrodynamic behaviour of a three-phase gas-liquid-solid fluidized bed. The hydrodynamic behaviour studied numerically is the bed pressure drop, minimum fluidization velocity, bed expansion and phase hold-ups.

In the present work three geometries of a physical unit has been considered. First a two dimensional (2D) geometry without distributor is simulated with CFD tools to check the present findings with previous ones available which are mostly based on two 2D models. Then a three dimensional geometry without distributor is considered to see the variations in the hydrodynamic parameters by the addition of one more dimension making the geometry more likely the physical unit. Finally a 2D geometry with a distributor plate is being simulated to see the effect of distributor on the hydrodynamic behavior. A distributor is actually present in a physical unit. 3D geometry with distributor has not taken up simulation as it requires more computational power which is limited by the m/c. Commercial CFD package ANSYS FLUENT has been used in modeling and simulation of various geometries considered.

Three-phase fluidization involve gas, liquid and solid phases, hence for computational study choosing of appropriate multiphase model play an important role in the simulation result. There are different multiphase models available in commercial software ANSYS FLUENT. In the present work a series of computational models available in FLUENT have been used. The details of various models and numerical schemes used in the present work are discussed in this chapter.

3.1. Computational model for multiphase flow:

Advance in computational fluid mechanics have provided the basis for further insight into the dynamics of multiphase flow. Currently there are two approaches for the numerical calculation of multiphase flow: The Eulerian-Lagrangian approach and the Euler-Euler approach. In the Euler-Euler approach, the different phases are treated mathematically as

interpenetrating continua. Since the volume of a phase cannot be occupied by the other phase the concept of phasic volume fraction is introduced. These volume fractions are assumed to be continuous function of space and time and their sum is equal to one. Conservation equations for each phase are derived to obtain a set of equations which have similar structure for all phase. The equations are closed by providing constitutive relations that are obtained from empirical information or in the case of granular flow by application of kinetic theory. For volume averaged information on any hydrodynamic property the Euler-Euler approach is suitable for its simplicity.

3.1.1. Choosing an appropriate Eulerian model:

There are three different Euler-Euler multiphase models are available. *The volume of fluid (VOF) model:* The VOF model is a surface-tracking technique applied to a fixed Eulerian mesh. It is designed for two or more immiscible fluids are of interest. In the VOF model, a single set of momentum equation is shared by the fluids, and the volume fraction of each of the fluids in each computational cell is tracked throughout the domain. *The mixture model:* The mixture model is designed for two or more phases (fluid or particulate). As in the Eulerian model, the phases are treated as interpenetrating continua. The mixture model solves for the mixture momentum equations as prescribes relatives velocity to describe the dispersed phases. *The Eulerian model:* The Eulerian model is the most complex of the multiphase model. It solves a set of *n* momentum and continuity equations for each phase. Through the pressure and interphase exchange coefficients coupling are achieved. The manner in which this coupling is handled depends upon the type of phases involved; granular (fluid solid) flows are handled differently than non-regular (fluid-fluid) flows. For granular flows, the properties are obtained from the application of kinetic theory. Momentum exchange between the phases is also depends upon the type of mixture being modeled.

An appropriate multiphase model for the multiphase system can be determined from the flow regime. For slug, and stratified/free surface flows VOF model are used. For slurry flow, hydro transport, bubbly, droplet, and particle-laden flows in which the phase mix and/or dispersed phase volume fractions exceed 10% either mixture model or Eulerian model are used. For

general, complex multiphase flows that involve multiple flow regimes, select the aspect of flow that is of most interest and choosing of model that is of most appropriate. There are some parameters that help to identify the appropriate multiphase model: the particulate loading, β, and Stoke number, *St*.

Particulate loading effect:

It is defined as the mass density ratio of the dispersed phase (d) to that of carrier phase (c).

$$\beta = \frac{\alpha_d \rho_d}{\alpha_c \rho_c} \tag{3.1}$$

It has a major impact on phase interactions. Depending on the particulate loading, the degree of interaction of phases can be divided into the following three categories. *For very low loading,* the coupling between the phase is one-way (i.e. the fluid carrier influence the particle via drag and turbulence, but particles have no influence on the fluid carrier). The discrete phase, mixture and Eulerian models can handle this type of problem correctly. F*or intermediate loading,* the coupling is two way (i.e. the fluid carrier influences the particulate phase via drag and turbulence, but the particles in turn influence the carrier fluid via reduction in mean momentum and turbulence). All three models are applicable in this case, but some other factors are needed to take into account to decide which model is more appropriate. *For high loading,* there is two-way coupling plus particle pressure and viscous stresses due to the particles (four-way coupling). Only the Eulerian model will handle this type of problem correctly.

Significance of Strokes number:

The Stokes number can be defined as the relation between the particle response times the system response time. For the system with intermediate particulate loading, the value of Strokes number can help to select the appropriate model.

$$St = \frac{\tau_d}{t_s} \tag{3.2}$$

where $\tau_d = \frac{\rho_d d_d^2}{18\,\mu_c}$ and t_s is the based on the characteristics (L_s) and characteristic velocity (V_s) of the system under investigation*:* $t_s = L_s / V_s$. *For St << 1.0 or = 1.0,* the particle will follow

closely and any of the three model is applicable. *For St > 1.0,* the particle will move independently of the flow, either the discrete phase or Eulerian model is applicable.

In the present work, an Eulerian granular multiphase model is adopted where gas, liquid, and solid phase are all treated as continua, interpenetrating and interacting with each other everywhere in the computational domain. With the Eulerian multiphase model, the number of secondary phase is limited only by memory requirement and convergence behavior. Any number of secondary phases can be modeled provided that sufficient memory is available. Eulerian multiphase model does not distinguish between fluid-fluid and fluid-solid (granular) multiphase flows. A granular phase is simple one that involves at least one phase that has been designated as a granular phase. The pressure field is assumed to be shared by all the three phases, in proportion to their volume fraction. Solid-phase shear and bulk viscosities are obtained by applying kinetic theory of granular flows.

Limitation of the Eulerian multiphase model: The Reynolds Stress turbulence model is not available on a per phase basis, inviscid flow is not allowed, melting and solidification are not allowed, and Particle tracking (using the Lagrangian dispersed phase model) interacts only with the primary phase. Streamwise periodic flow with specified mass flow rate cannot be modeled when the Eulerian model is used, and when tracking particles in parallel, the DPM model cannot be used with the Eulerian multiphase model if the shared memory option is enabled.

3.2. Conservation equations:

The motion of each phase is governed by respective mass and momentum conservation equations.

Conservation of mass: $$\frac{\partial}{\partial t}\left(\alpha_q \rho_q\right) + \nabla.\left(\alpha_q \rho_q \vec{v}_q\right) = 0 \qquad (3.3)$$

where ρ_q is the density of the phase, $\alpha_q$is the volume fraction and $\vec{v}_q$is the volume fraction of the phase $q = L, g, s$. The volume fraction of the three phases satisfies the flowing condition:

$$\alpha_L + \alpha_g + \alpha_s = 1 \qquad (3.4)$$

Conservation of momentum: The conservation of momentum equation for the fluid phase is

$$\frac{\partial}{\partial t}\left(\alpha_q \rho_q \vec{v}_q\right) + \nabla.\left(\alpha_q \rho_q \vec{v}_q \vec{v}_q\right) = -\alpha_q \nabla p + \nabla.\bar{\bar{\tau}}_q + \alpha_q \rho_q \vec{g} + \vec{F}_{i,q} \quad (3.5)$$

where q is for liquid and gas phases, $\bar{\bar{\tau}}_q$ is the stress-strains tensor of liquid and gas phase and $\vec{g}$ is the acceleration due to gravity.

The conservation of momentum for the solid phase is

$$\frac{\partial}{\partial t}(\alpha_s \rho_s \vec{v}_s) + \nabla.(\alpha_s \rho_s \vec{v}_s \vec{v}_s) = -\alpha_s \nabla p - \nabla.p_s + \nabla.\bar{\bar{\tau}}_s + \alpha_s \rho_s \vec{g} + \vec{F}_{i,s} \quad (3.6)$$

where p_s is the s^{th} solid pressure, and $\bar{\bar{\tau}}_s$is the stress-strains tensor of solid phase .

$$\bar{\bar{\tau}}_q = \alpha_q \mu_q\left(\nabla.\vec{v}_q + \nabla.\vec{v}_q^T\right) + \alpha_q\left(\lambda_q - \frac{2}{3}\mu_q\right)\nabla.\vec{v}_q\bar{\bar{I}} \quad (3.7)$$

$$\bar{\bar{\tau}}_s = \alpha_s \mu_s(\nabla.\vec{v}_s + \nabla.\vec{v}_s^T) + \alpha_s\left(\lambda_s - \frac{2}{3}\mu_s\right)\nabla.\vec{v}_s\bar{\bar{I}} \quad (3.8)$$

3.2.1. Interphase Exchange Co-efficient:

The inter phase momentum exchange terms F_i are composed of a linear combination of different interaction forces between different phases such as the drag force, the lift force and the added mass force, etc., and is generally represented as

$$F_i = F_D + F_L + F_M \quad (3.9)$$

In a recent review, the effect of various interfacial forces has been discussed by Rafique et al. (2004). They reported that the effect of added mass can be seen only when high frequency fluctuations of the slip velocity occur and they also observed that the added mass force are much smaller than the drag force in bubbly flow. By default, Fluent does not include the added or virtual mass force. In the previous studies, lift force has been applied to a few 2D simulations of gas–liquid flows. But, it has been often omitted in 3D simulation of bubble flows. The main reason for this is the lack of understanding about the complex mechanism of lift forces in gas–liquid flows (Bunner and Tryggvason, 1999). Also depending on the bubble size, a negative or positive lift coefficient is used in the literature in order to obtain good agreement between simulation and experiment. Recently Sokolichin et al. (2004) suggested that the lift force should be omitted as long as no clear experimental evidence of their direction and magnitude is available and neglecting the lift force can still lead to good

comparison with experimental data as reported by Pan et al. (1999, 2000). The lift force is insignificant compared to the drag force. Hence, only the drag force is included for inter-phase momentum exchange in the present CFD simulation. The inter-phase force depends on the friction, pressure, cohesion and other effects and is subject to the conditions that $F_{D,jk} = -F_{D,kj}$ and $F_{D,jj} = 0$, where, subscripts j and k represent various phases. The inter-phase force term is defined as:

$$F_{D,jk} = K_{jk}(u_j - u_k) \tag{3.10}$$

where $K_{jk}(= K_{kj})$ is the inter-phase momentum exchange coefficient.

In the present work, the liquid phase is considered as a continuous phase and both the gas and the solid phases are treated as dispersed phases. The inter phase drag force between the phases is discussed below.

Fluid-fluid exchange co-efficient: For fluid-fluid flow, each secondary phase is assumed to form droplets or bubbles. This exchange co-efficient can be written in the following general form

$$K_{pq} = \frac{\alpha_q \alpha_p \rho_p f}{\tau_p} \tag{3.11}$$

where f is the drag function, is defined differently for the different exchange co-efficient models and τ_p, the "particulate relaxation time", is defined as

$$\tau_p = \frac{\rho_p d_p^2}{18\,\mu_q} \tag{3.12}$$

where d_p is the diameter of the bubbles or droplets of phase p**.** Nearly all definition of f include a drag co-efficient *(* C_D) that is based on the relative Reynolds number (*Re*). It is the drag function that differs among the exchange co-efficient models. For all these situations, K_{pq} should trend to zero. Whenever the primary phase is not present with in the domain, to enforce this f is always multiplied by the volume fraction of the primary phase q as shown in equation (3.13).

In the present model we have used Schiller and Naumann model to define the drag function *f.*

$$f = \frac{C_D Re}{24} \tag{3.13}$$

Where $C_D = 24\,(1 + 0.15\,Re^{0.687})/\,Re \qquad Re \leq 1000$

$C_D = 0.44 \qquad Re \geq 1000$

and *Re* is the relative Reynolds number. The relative Reynolds number for the primary phase *q* and secondary phase is obtained from

$$Re = \frac{\rho_{rp}|\vec{v}_r - \vec{v}_p|d_{rp}}{\mu_{rp}} \tag{3.14}$$

where $\mu_{rp} = \alpha_p\mu_p + \alpha_r\mu_r$ is the mixture viscosity of the phase *p* and *r*.

Fluid-solid Exchange Co-efficient: The fluid-solid exchange co-efficient K_{sl} can be written in the following general form.

$$K_{sl} = \frac{\alpha_s\rho_s f}{\tau_s} \tag{3.15}$$

where f is defined differently for the different exchange co-efficient model and τ_s**,** the particulate relaxation time.

$$\tau_s = \frac{\rho_s d_s^2}{18\,\mu_l} \tag{3.16}$$

where d_s is the diameter of the particles of phase *s*. All definition of *f* includes a drag function (C_D) that is based on the relative Reynolds number (Re_s). It is this drag function that differs among the exchange co-efficient models.

In our present study, we have taken Gidaspow model, combination of Wen and Yu model and the Ergun equation.

When $\alpha_l > 0.8$**,** the fluid solid exchange coefficient K_{sl} is of the following form:

$$K_{sl} = \frac{3}{4}C_D\frac{\alpha_s\alpha_l\rho_l|\vec{v}_s - \vec{v}_l|}{d_s}\alpha_l^{-2.65} \tag{3.17}$$

where $C_D = \frac{24}{\alpha_l Re_s}[\,1 + 0.15(\alpha_l Re_s)^{0.687}]$ (3.18)

where Re_s is defined as,

$$Re_s = \frac{\rho_l d_s |\vec{v}_s - \vec{v}_l|}{\mu_l} \tag{3.19}$$

l is the l^{th} fluid phase, s is for the s^{th} solid phase particles and d_s is the diameter of the s^{th} solid phase particles

when $\alpha_l \leq 0.8$,

$$K_{ls} = \frac{3(1 + e_{ls})\left(\frac{\pi}{2} + C_{fr,ls}\frac{\pi^2}{8}\right).\alpha_s\rho_s\alpha_l\rho_l(d_l + d_s)^2 g_{0,ls}|\vec{v}_l - \vec{v}_s|}{2\pi(\rho_l d_l^3 + \rho_s d_s^3)} \tag{3.20}$$

where e_{ls}= the coefficient of restitution

$C_{fr,ls}$= the coefficient of friction between the l^{th} and s^{th} solid phase particles.

d_l = diameter of the particle of solid l

$g_{0,ls}$ = the radial distribution coefficient.

3.3. Closure law for solid pressure:

For granular flow in the compressible regime (i.e. where the solid volume fraction is less than its maximum allow value), a solid pressure is calculated independently and used for the pressure gradient term,$\nabla . p_s$, in the granular-phase momentum equation. Because a Maxwellian velocity distribution used for the particles, a granular temperature is introduced into the model, and appears in the expression for the solid pressure and viscosities. The solid pressure is composed of a kinetic term and a secondary term due to particle collisions.

$$p_s = \alpha_s\rho_s\Theta_s + 2\rho_s(1 + e_{ss})\alpha_s^2 g_{0,ss}\Theta_s \tag{3.21}$$

Where e_{ss} is the co-efficient of restitution for particle collisions, $g_{0,ss}$ is the radial distribution function, and Θ_s is the granular temperature. The granular temperature Θ_s is proportional to the kinetic energy of the fluctuating particle motion. In ANSYS FLUENT a default value of 0.9 for Θ_s is use and can be adjusted to suit the particle type. The function $g_{0,ss}$ is a distribution function that governs the transition from the "compressible" condition with

$\alpha_s < \alpha_{s,max}$, where the spacing between the solid particles can continue to decrease, to incompressible condition with $\alpha = \alpha_{s,max}$, where no further decrease in space can occurs. The value of 0.63 is the default for $\alpha_{s,max}$.

3.3.1. Radial distribution function:

The radial distribution function, $g_o$is a correction factor that modifies the probability of collision between grains when the solid granular phase became dense. This function may also be interpreted as the non-dimensional distance between spheres:

$$g_o = \frac{s + d_p}{s} \tag{3.22}$$

where *s* is the distance between grains. From equation (3.22) it can be observed that for a dilute solid phase $s \to \infty$, and therefore $g_o \to 1$. In the limit when solid phase contact, $s \to 0$ and $g_o \to \infty$. For a one solid phase,

$$g_o = [1 - (\frac{\alpha_s}{\alpha_{s,max}})^{1/3}]^{-1} \tag{3.23}$$

3.3.2. Solid shear stresses:

The solid shear stresses contains shear and bulk viscosities arising from particle momentum exchange due to translation and collision. A frictional component of viscosity can also be included to account for the viscous-plastic transition that occurs when particle of solid phase reach the maximum solid volume fraction. The collision and kinetics parts and the optional frictional part are added to give the solid shear viscosity.

$$\mu_s = \mu_{s,col} + \mu_{s,kin} + \mu_{s,fr} \tag{3.24}$$

Collision viscosity: The collision part of the shear viscosity is modeled as

$$\mu_{s,col} = \frac{4}{5}\alpha_s \rho_s d_s g_{o,ss}(1 + e_{ss})(\frac{\Theta_s}{\pi})^{1/2}\alpha_s \tag{3.25}$$

Kinetic viscosity:

$$\mu_{s,kin} = \frac{\alpha_s d_s \rho_s \sqrt{\Theta_s \pi}}{6(3 - e_{ss})}\left[1 + \frac{2}{5}(1 + e_{ss})(3e_{ss} - 1)\alpha_s g_{o,ss}\right] \tag{3.26}$$

Bulk viscosity: The bulk viscosity account for the resistance of the granular particle to compression and expansion.

$$\lambda_s = \frac{4}{3}\alpha_s \rho_s d_s g_{o,ss}(1+e_{ss})({}^{\Theta_s}/_{\pi})^{\frac{1}{2}} \tag{3.27}$$

Frictional viscosity: In dense flow at low shear, where the secondary volume fraction for a solid phase nears the packing limit, the generation of stress is mainly due to friction between particles.

In the present, we have taken Schaeffer's expression

$$\mu_{s.fr} = \frac{p_s \sin\phi}{2\sqrt{I_{2D}}} \tag{3.28}$$

where p_s is the solids pressure,ϕ is the angle of internal friction, and I_{2D} is the second invariant of the deviatoric stress tensor.

3.4. Granular temperature:

The granular temperature for the s^{th} solids phase is proportional to the kinetic energy of random motion of particles. The transport equation derived from kinetic theory take the form

$$\frac{3}{2}\left[\frac{\partial}{\partial t}(\rho_s \alpha_s \Theta_s) + \nabla.(\rho_s \alpha_s \vec{v}_s \Theta_s)\right] = \left(-p_s\bar{\bar{I}} + \bar{\bar{\tau}}_s\right):\nabla.\vec{v}_s + \nabla.\left(K_{\Theta_s}\nabla.\Theta_s\right) - \Upsilon_{\Theta_s} + \Phi_{ls} \tag{3.29}$$

where

$\left(-p_s\bar{\bar{I}} + \bar{\bar{\tau}}_s\right):\nabla.\vec{v}_s$ = the generation of energy by solid stress tensor

$K_{\Theta_s}\nabla.\Theta_s$ = the diffusion of energy ($K_{\Theta_s}$is the diffusion co-efficient)

Υ_{Θ_s} = the collisional dissipation of energy

Φ_{ls} = the energy exchange between the l^{th} phase or solid phase and the s^{th} solid phase.

$K_{\Theta_s}.\nabla.\Theta_s$describe the diffusive flux of granular energy. The diffusion co-efficient for granular energy, $K_{\Theta_s}$is given by

$$K_{\Theta_s} = \frac{15\, d_s \rho_s \alpha_s \sqrt{\Theta_s \pi}}{4(41-33\eta)}\left[1+\frac{12}{5}\eta^2(4\eta-3)\alpha_s g_{0,ss}+\frac{16}{15\pi}(41-33\eta)\eta\alpha_s g_{0,ss}\right] \quad (3.30)$$

where

$$\eta = \tfrac{1}{2}(1+e_{ss})$$

The collisional dissipation of energy, Υ_{Θ_s}, represents the rate of energy dissipation within the s^{th} solid phase due to collision between particles. This term is represented by the expression derived by

$$\Upsilon_{\Theta_m} = \frac{12(1-e_{ss}^2)g_{0,ss}}{d_s\sqrt{\pi}}.\rho_s\alpha_s^2\Theta_s^{3/2} \quad (3.31)$$

The transfer of the kinetic energy of random fluctuations in particle velocity from the s^{th} solid phase to the l^{th} fluid or solid phase is represented by ϕ_{ls}

$$\phi_{ls} = -3K_{ls}\Theta_s \quad (3.32)$$

For a granular phase s, we may write the shear force at the wall in the following form:

$$\vec{\tau}_s = -\frac{\pi}{6}\sqrt{3\phi}\frac{\alpha_s}{\alpha_{s,max}}\rho_s g_0\sqrt{\Theta_s\vec{U}_{s,||}} \quad (3.33)$$

here $\vec{U}_{s,||}$ is the particle slip velocity parallel to the wall, ϕ is the specularity co-efficient between the particle and the wall, $\alpha_{s,max}$ is the volume fraction for the particle at maximum packing, and g_0 is the radial distribution function that is the model dependent. The general boundary conditions for granular temperature at the wall take the form

$$q_s = \frac{\pi}{6}\sqrt{3\phi}\frac{\alpha_s}{\alpha_{s,max}}\rho_s g_0\sqrt{\Theta_s}\,\vec{U}_{s,||} - \frac{\pi}{4}\sqrt{3}\frac{\alpha_s}{\alpha_{s,max}}(1-e_{sw}^2)\rho_s g_0\Theta_{sw}^2 \quad (3.34)$$

3.5. Closure law for turbulence:

To describe the effect of turbulent fluctuation of velocities in a multiphase flow, the number of terms to be modeled in the momentum equations is large, and this make the modeling of turbulence in multiphase simulations extremely complex. There are three methods for modeling turbulence in multiphase flow mixture turbulence model, dispersed turbulence

model and turbulence model for each phase. In the present work dispersed turbulence model is applied.

$K-\varepsilon$ Dispersed model: This model is applicable only when there is clearly one primary continuous phase and rest are dispersed dilute secondary phases. In this case, interparticle collision collisions are negligible and the dominant process in the random motion of the secondary phase is the influence of the primary phase turbulence. Fluctuating quantities of the secondary phases can therefore be given in term of the mean characteristics of the primary phase and the ratio of the mean particle relaxation time and eddy-particle relaxation time.

Turbulence in the continuous phase: The eddy viscosity model is used to calculate average fluctuation quantities. The Reynolds stress tensors for continuous phase q take the following form

$$\bar{\bar{\tau}}_q^{"} = -\frac{2}{3}\left(\rho_p k_q + \rho_q v_{t,q}.\nabla.\vec{U}_q\right)\bar{\bar{I}} + \rho_q v_{t,q}\left(\nabla.\bar{\bar{U}}_q + \nabla.\vec{U}_q^T\right) \tag{3.35}$$

where $\vec{U}_q$ is the phase-weighted velocity.

The turbulent viscosity $\mu_{t,q}$ is written in the term of the turbulent kinetic energy of phase *q.*

$$\mu_{t,q} = \rho_q C_\mu \frac{k_q^2}{\varepsilon_q} \tag{3.36}$$

and a characteristic time of the energetic turbulence eddies is defined as

$$\tau_{t,p} = \frac{3}{2} C_\mu \frac{k_q}{\varepsilon_q} \tag{3.37}$$

where $\varepsilon_q$is the dissipation rate and C_μ = 0.9

The length scale of the turbulent eddies is

$$L_{t,q} = \sqrt{\frac{3}{2}}\, C_\mu \frac{k_q^{3/2}}{\varepsilon_q} \tag{3.38}$$

Turbulent prediction are obtained from the modified K − ε model

$$\frac{\partial}{\partial t}\left(\alpha_q \rho_q k_q\right) + \nabla.\left(\alpha_q \rho_q \vec{U}_q k_q\right) = \nabla.\left(\alpha_q \frac{\mu_{t,q}}{\sigma_k} \nabla k_q\right) + \alpha_q \rho_q \varepsilon_q + \alpha_q \rho_q \Pi_{k_q} \quad (3.39)$$

and

$$\frac{\partial}{\partial t}\left(\alpha_q \rho_q \varepsilon_q\right) + \nabla.\left(\alpha_q \rho_q \vec{U}_q k_q\right) = \nabla.\left(\alpha_q \frac{\mu_{t,q}}{\sigma_\varepsilon} \nabla \varepsilon_q\right) + \alpha_q \frac{\varepsilon_q}{k_q}\left(C_{1\varepsilon} G_{k,q} - C_{2\varepsilon} \rho_q \varepsilon_q\right) + \alpha_q \rho_q \Pi_{\varepsilon_q} \quad (3.40)$$

here $\Pi_{k_q}$and Π_{ε_q}represent the influence the dispersed phase on the continuous phase *q*, and $G_{k,q}$ is production of turbulence kinetic energy.

The term $\Pi_{k_q}$is derived from the instantaneous equation of the continuous phase and takes the following form, where *M* represent the number of secondary phases.

$$\Pi_{kq} = \sum_{p=1}^{M} \frac{k_{pq}}{\alpha_q \rho_q}\left(k_{pq} - 2k_q + \vec{v}_{pq}.\vec{v}_{dr}\right) \quad (3.41)$$

Turbulence in dispersed phase: Time and length scale which characterize the motion are used to evaluate dispersion co-efficient correlation functions, and the turbulent kinetic energy of each dispersed phase.

The characteristic relaxation time connected with inertial effects acting on a dispersed phase p is defined as

$$\tau_{F,pq} = \alpha_p \rho_q K_{pq}^{-1}\left(\frac{\rho_p}{\rho_q} + C_v\right) \quad (3.42)$$

The Lagrangian integral time scale calculated along the particle trajectories, mainly affected by the crossing trajectories, mainly effect, is defined as

$$\tau_{t,pq} = \frac{\tau_{t.q}}{\sqrt{(1 + C_\beta \xi^2}} \quad (3.43)$$

where

$$\xi = \frac{\left|\vec{v}_{pq}\right| \tau_{t,q}}{L_{t,q}} \quad (3.44)$$

and

$$C_\beta = 1.8 - 1.35(cos\,\theta)^2 \tag{3.45}$$

where θ is the angle between the mean particle velocity and the mean relative velocity.

The ratio between these characteristic time is written as,

$$\eta_{pq} = \frac{\tau_{t,pq}}{\tau_{F,pq}} \tag{3.46}$$

turbulence quantities for dispersed phase p as

$$k_p = k_q \left(\frac{b^2+\eta_{pq}}{1+\eta_{pq}}\right) \tag{3.47}$$

$$k_{pq} = 2k_q \left(\frac{b+\eta_{pq}}{1+\eta_{pq}}\right) \tag{3.48}$$

$$D_{t,pq} = \frac{1}{3} k_{pq} \tau_{t,pq} \tag{3.49}$$

$$D_p = D_{t,pq} + \left(\frac{2}{3}k_p - b\frac{1}{3}k_{pq}\right)\tau_{F,pq} \tag{3.50}$$

$$b = (1 + C_v)\left(\frac{\rho_p}{\rho_q} + C_v\right) \tag{3.51}$$

and C_v = 0.5 is the added mass coefficient.

3.6. Numerical Methodology:

In ANSYS FLUENT control-volume based technique is used to convert a general scalar transport equation to an algebraic equation that is solved numerically. This control volume technique consists of integrating the transport equation about each control volume, resulting in a discrete equation that expresses the conservation law on a control-volume basis. Considering the unsteady conservation equation of a scalar quantity ϕ in equation (3.52) discretization of this equation can be written in equation (3.53).

$$\int \frac{\partial \rho\phi}{\partial t}.dV + \oint \rho\phi\vec{v}dA = \oint \Gamma_\phi.\nabla\phi.d\vec{A} + \int_V S_\phi dV \tag{3.52}$$

where ρ = density

$\vec{v}$ = velocity vector

Γ_{ϕ} = diffusion co-efficient for ϕ

$\nabla\phi$ = gradient of ϕ

S_{ϕ} = source of ϕ per unit volume.

equation (3.52) is applied to each cell in the computational domain.

$$\frac{\partial \rho\phi}{\partial t}V + \sum_{f}^{N_{face}} \rho_f \vec{v}_f \phi_f \vec{A}_f = \sum_{f}^{N_{face}} \Gamma_{\phi} . \nabla . \phi_f + S_{\phi} \quad (3.53)$$

where N_{face} = number of face enclosing cell.

ϕ_f = value of ϕ convected through face f

$\rho_f \vec{v}_f \phi_f \vec{A}_f$ = mass flux through face.

$\vec{A}_f$ = area of face f

$\nabla . \phi_f$ = gradient of ϕ at face f

V = cell volume.

The discretized scalar transport equation contain unknown scalar contain unknown scalar variable ϕ at a cell center as well as the unknown value in the surrounding neighbor cells. The equation, in general, be non-linear with respect to these variable. A linearized form of equation (3.53) can be written as

$$a_p\phi = \sum_{nb} a_{nb}\phi_{nb} + b \quad (3.54)$$

nb is the neighbor cell, and $a_p$and a_{nb} are the linearized co-efficient for ϕ and ϕ_{nb} .

The number of neighbor for each cell depends on a mesh topology, but typically equals the number of faces enclosing the cell. This results in a set of algebraic equation with sparse co-efficient matrix. These linear systems of equation are solved using a point implicit (Gauss-Seidel) linear equation solver in conjunction with an algebraic multigrid (AMG) method.

Algebraic Multigrid (AMG): In this algorithm, the coarse level equation are generate without the use of any geometry or re-discretization on the coarse level. The advantage being that no

coarse meshes have to be constructed or stored, and no fluxes or source term need to be evaluated on the coarse level. The scalar AMG solver is used for the solution of linear systems obtained from the discretization of the individual transport equation

$$a_{ij}x_{ij} = b_{ij} \tag{3.55}$$

Gauss-Seidel Method: This method is a technique for solving a linear system of equation one at a time and in sequence. It uses the previously computed results as soon as they became available. It performs two sweeps on the unknown in forward and backward direction.

The Gauss-Seidel procedure can be illustrated using the scalar system equation (3.55).

The forward sweep can be written as

$$x_i^{k+\frac{1}{2}} = (b_i - \sum_{j<1} a_{ij} x_j^{k+\frac{1}{2}} - \sum_{j>1} a_{ij} x_j^k)/a_{ii} \tag{3.56}$$

$$(i = 1, \dots\dots\dots\dots\dots, N)$$

where *N* is the number of unknowns.

The forward sweep is followed by backward sweep which can be written as:

$$x_i^{k+1} = (\, b_i - \sum_{j<1} a_{ij} x_j^{k+\frac{1}{2}} - \sum_{j>1} a_{ij} x_j^{k+1})/a_{ii} \tag{3.57}$$

3.6.1. Spatial Discretization:

The discrete values of the scalar ϕ at the cell center (C_0 and C_1 in figure 3.1*)* are stored default in ANSYS FLUENT. However, face values ϕ_f are required for the convection term in equation (3.53) and must be interpolated from the cell center value. This is accomplished using an upwind scheme. Upwinding means that the face value ϕ_f is derived from quantities in the cell upstream or "upwind", relative to the direction of the normal velocity v_n. The diffusion terms in equation (3.53) are central difference and always second order accurate.

First-Order Upwind Scheme: When first order accuracy is desired, quantities at cell faces are determined by assuming that the cell-center values of any field variable represent a cell-average value and hold throughout the entire cell; the face quantities are identical to the cell

quantities. Thus when first order upwind is selected the face value ϕ_f is set equal to the cell-center value of ϕ in the upstream cell.

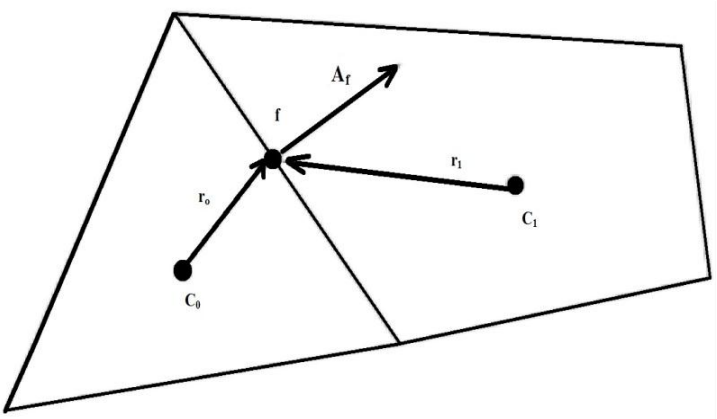

Fig. 3.1. Control volume used to illustrate discretization of a scalar transport equation.

Second-Order Upwind Scheme: When second-order accuracy is desired, quantities at cell faces are computed using multi-dimensional linear reconstruction approach. In this approach, higher order accuracy is achieved at cell faces through a Taylor series expansion of the cell centered solution about the cell centroid. Thus when second order upwind is selected, the face value ϕ_f is computed using the following expression.

$$\phi_{f,sou} = \phi + \nabla.\phi\vec{r} \tag{3.58}$$

where ϕ and $\nabla.\phi$ are the cell-centered value and it's gradient in the upstream cell centroid to the face centroid. This formulation required the determination of gradient $\nabla.\phi$ in each cell. Finally the gradient is the limited so that no new maxima or minima are introduced.

3.6.2 Evaluation of gradient and derivative:

Gradient are needed not only for constructing values of a scalar at the cell faces, but also computing secondary diffusion terms and velocity derivatives. The gradient $\nabla.\phi$ of a given variable ϕ is used to discretize the convection and diffusion term in the flow conservation equation. The gradients are computed according to the following methods, Green-Gauss cell-based, Green-Gauss node-based and Least squares cell-based. In present work, least square cell-based method is used.

Least-Square Cell-Based: In this method the solution is assumed to vary linearly in figure 3.2.the change in cell value in between C_0 and Ci along the vector δr_i from centroid of the cell $C_0$to cell C_i can be expressed as

$$(\nabla\phi)_{C_0}.\Delta r_i = \left(\phi_{C_i} - \phi_{C_0}\right) \tag{3.59}$$

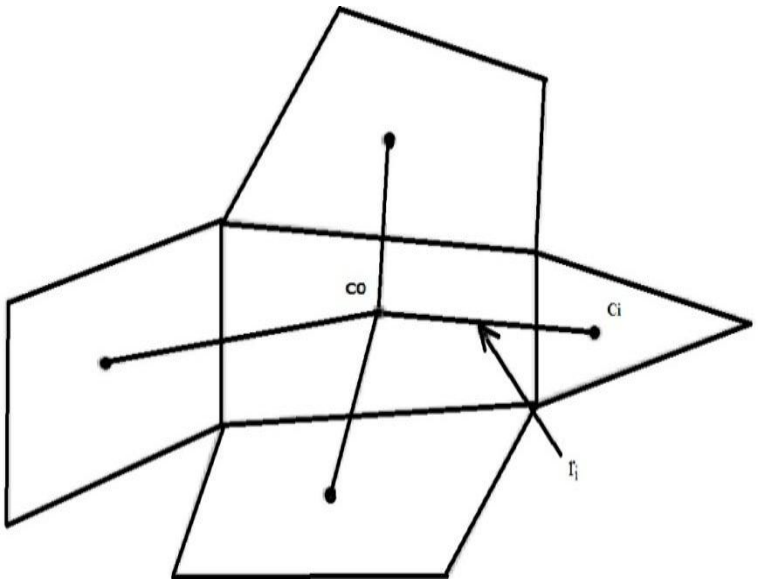

Fig. 3.2. Cell centroid evaluation.

If we write similar equation for each cell surrounding the cell C_0, following form obtained which can be written in compact form.

$$[\,J\,]\,(\nabla.\phi)_{C_0} = \Delta\phi \tag{3.60}$$

where $[\,J\,]$ is the co-efficient matrix which is purely a function of geometry.

The above linear system of equation is over-determined and can be solved by decomposing the co-efficient matrix, resulted a matrix of weight of each cell. The gradient at the cell center can then be computed by multiplying the weight factor by the difference vector $\nabla\phi = \left(\phi_{C_1} - \phi_{C_0}\right)$.

$$(\phi_x)_{C_0} = \sum_{i=1}^{n} W_{i0}^{x}\left(\phi_{C_i} - \phi_{C_0}\right) \tag{3.61}$$

$$(\phi_y)_{C_0} = \sum_{i=1}^{n} W_{i0}^{y}\left(\phi_{C_i} - \phi_{C_0}\right) \tag{3.62}$$

$$(\phi_z)_{C_0} = \sum_{i=1}^{n} W_{i0}^{z}\left(\phi_{C_i} - \phi_{C_0}\right) \tag{3.63}$$

3.6.3. Pressure-Velocity Coupling:

Considering the steady-state continuity and momentum equation in integral form

$$\oint \rho \, \vec{v}. d\vec{A} = 0 \tag{3.64}$$

$$\oint \rho \vec{v} \vec{v} d\vec{A} = -\oint pI. d\vec{A} + \oint \bar{\bar{\tau}} d\vec{A} + \int_V \vec{F} dV \tag{3.65}$$

where I is the identity matrix, $\bar{\bar{\tau}}$ is the stress tensor and $\vec{F}$ is the force vector.

The discretized momentum equation can be obtained by setting $\phi = u$ (i.e. x-momentum equation).

$$a_p u = \sum_{nb} a_{nb} U_{nb} + \sum p_f A \, \vec{\imath} + S \tag{3.66}$$

If the pressure field and face mass fluxes are known equation (3.66) can be solved and a velocity field obtained. However the pressure field and face mass fluxes are not known a prior and must be obtained as a part of solution.

ANSYS FLUENT uses a co-located scheme, where pressure and velocity are stored at cell centers. The value of the pressure variation between cell C_0 and $C_1$is required solving the equation. An interpolation scheme is required to compute the face value of pressure from the cell values.

$$P_f = \frac{\frac{P_{C_0}}{a_{p,C_0}} + \frac{P_{C_1}}{a_{p,C_1}}}{\frac{1}{a_{p,C_0}} + \frac{1}{a_{p,C_1}}} \tag{3.67}$$

This procedure works well as long as the pressure variation between cell centers is smooth. When there are jumps or large gradient in momentum source term between control volumes, the pressure profile has a high gradient at the cell face, and cannot be interpolate using this scheme. In such case it is necessary to pack the mesh in the region of high gradient to resolve the pressure variation adequately. Several alternate schemes such as linear scheme, second-order scheme, PRESTRO and body-force- weighted scheme are available for cases in which the standard pressure interpolation scheme is not valid.

The continuity equations have the following discrete equation

$$\sum_{f}^{N_{face}} J_f A_f = 0 \tag{3.68}$$

where J_f is the mass flux through face $f, \rho v_n$.

To further proceed, it is necessary to relate the face value of velocity, $\vec{v}_n$ to the stored value of velocity at the cell centered linear interpolation of cell-centered velocities to the face result in unphysical checker boarding of pressure. The face value of velocity is not averaged linearly; instead, momentum weighted averaging, using weighting factors based on the a_p coefficient from equation (3.68) is performed. Using this procedure, the face value, J_f, may be written as

$$\begin{aligned} J_f &= \rho_f \frac{a_{p,C_0} v_{n,C_0} + a_{p,C_1} v_{n,C_1}}{a_{p,C_0} + a_{p,C_1}} + d_f((p_{C_0} + (\nabla p)_{C_0} \vec{r}_0) - \left(p_{C_1} + (\nabla p)_{C_1} \vec{r}_1\right)\Big) \\ &= \vec{J}_f + d_f\left(p_{C_0} - p_{C_1}\right) \end{aligned} \tag{3.69}$$

where p_{C_0}, p_{C_1} and v_{n,C_0}, v_{n,C_1} are pressure and normal velocity, respectively, with in the two cells on either side the face, and $\vec{J}_f$ contain the influence of velocities in these cell. The term d_f is a function a_p, the average of the momentum equation a_p coefficient for the cells on either side of the face f.

Semi-Implicit Method for Pressure Linked Equations (SIMPLE): SIMPLE algorithm is a widely used numerical procedure to solve the Navier-Stokes equations. It uses a relation between velocity and pressure corrections to enforce mass-conservation and to obtain pressure field. If the momentum equation are solved using a guessed pressure field p^*, the resulting face flux, J_f^* from equation(3.70).

$$J_f^* = \vec{J}_f^* + d_f\left(p_{C_0} - p_{C_1}^*\right) \tag{3.70}$$

doesn't satisfy the continuity equation. Consequently, a correction J_f' is added to the face flux J_f^* so that the corrected face flux, J_f

$$J_f = J_f^* + J_f' \tag{3.71}$$

satisfying the continuity. The SIMPLE algorithm postulate that J_f' can be written as

$$J_f' = d_f\left(p'_{C_0} - p'_{C_1}\right) \tag{3.72}$$

where p'_{C_0} is the cell pressure correction.

The SIMPLE algorithm substitutes the flux correction equation into a discrete continuity equation to obtain a discrete equation for the pressure correction p' in the cell.

$$a_p p' = \sum_{nb} a_{nb} p'_{nb} + b \tag{3.73}$$

where the source term b is the net flow rate into the cell.

$$b = \sum_{f}^{N_{face}} J_f^* A_f \tag{3.74}$$

The pressure-correction equation may be solved using the AMG method. Once the solution is obtained, the cell pressure and the face flux are corrected using

$$p = p^* + \alpha_p p' \tag{3.75}$$

$$J_f = J_f^* + d_f\left(p'_{C_0} - p'_{C_1}\right) \tag{3.76}$$

where α_p is the under relaxation factor for pressure. The corrected face flux, J_f satisfy the discrete continuity equation (3.76) identically during each iteration.

3.6.4. Under-relaxation of Variable:

The under-relaxation of variables is used in all cases for some material properties in the non-iterative time advancement solver (NITA) for solution variables and in pressure based coupled algorithm where this explicit under-relaxation is used for momentum and pressure. Because of non-linearity of the equation set, it is necessary to control the change of ϕ. This is typically achieved by under-relaxation of variable, which reduces the changes of ϕ produced during each iteration. In a simple form, the new value of the variable ϕ within a cell depend upon the old value, ϕ_{old} , the computed change in ϕ, $\Delta\phi$, and the under-relaxation factor α, as follow

$$\phi = \phi_{old} + \alpha\Delta\phi \tag{3.77}$$

In ANSYS FLUENT, the default under-relaxation parameters for all variables are set to value that are near optimal for the largest number of possible cases. It is good practice to begin a calculation using the default under-relaxation factors. If the residual continue to increase after the first 4 or 5 iteration, reduce the under-relaxation factor.

3.7. Geometry and Mesh:

Two numbers of two dimensional computational geometries, one without distributor and the other with distributor and a three dimensional computational geometry without distributor of the fluidization column have been generated by using DESIGN MODELLER available in ANSYS software. Fig.3.3. shows the line diagram of the fluidized beds used in simulation. After the creation of geometry of the fluidized bed meshing has been done for each of the geometry. The meshes of various geometries are shown in Fig. 3.4. Detail of the type, size and number of elements with different computational meshes are listed in the Table 3.1.

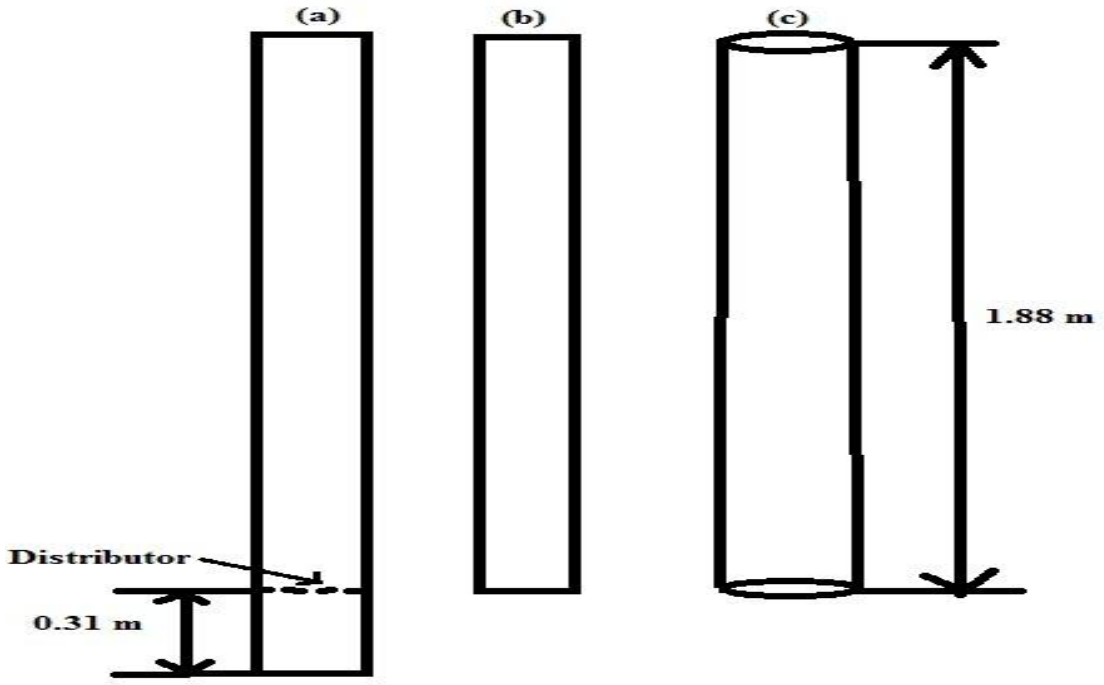

Fig. 3.3. Line diagram of computational geometry fluidized bed: (a) 2D fluidized bed with distributor, (b) 2D fluidized bed without distributor (c) 3D fluidized bed without distributor.

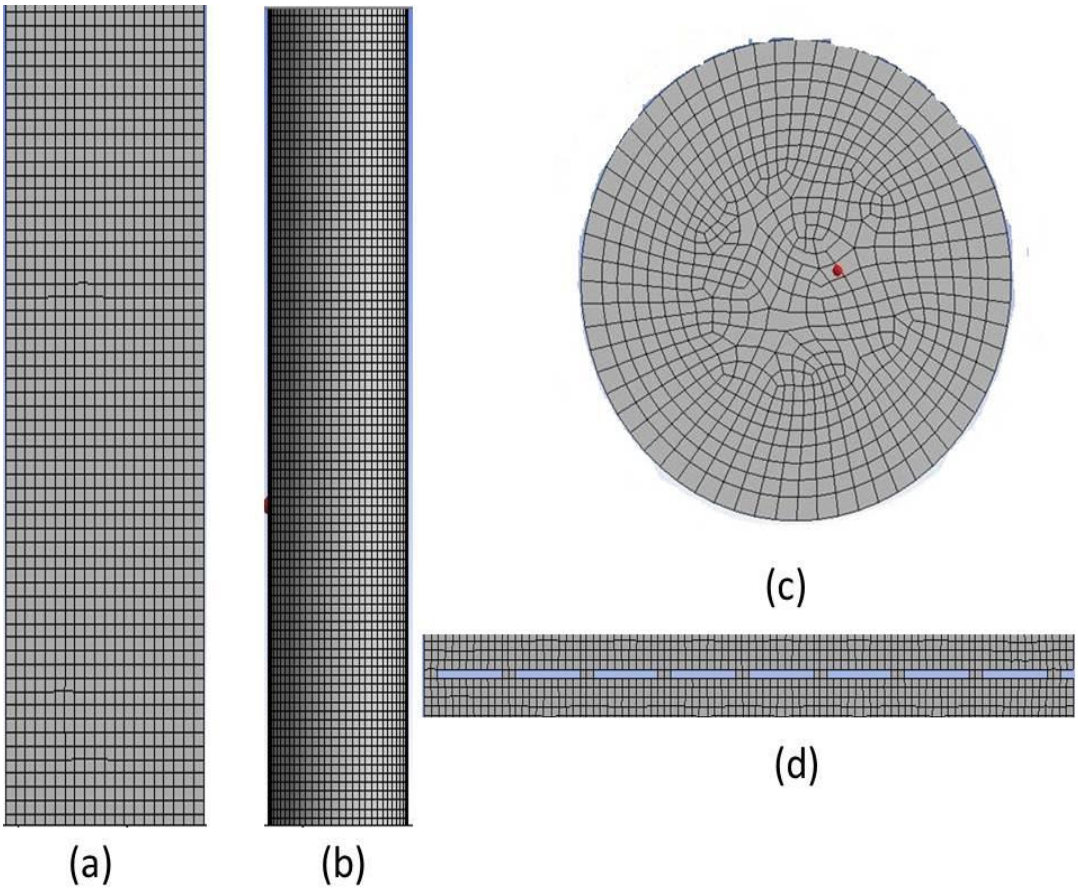

Fig. 3.4. (a) 2D mesh without distributor; (b) 3D mesh; (c) cross-sectional view of 3D mesh; (d) Mesh around the distributor plate in case of 2D mesh with distributor.

Table 3.1. Meshing configuration used in the computations of fluidized bed

2D fluidized bed (without distributor):	
Mesh type	Quadrilateral mesh
Element size	0.005 m
Number of Node	15834
Number of Element	7520
2D fluidized bed (with distributor):	
Mesh type	Quadrilateral mesh
Element size	0.001 m
Number of Node	443436
Number of Element	219330
3D fluidized bed (without distributor) :	
Mesh type	Hexahedral mesh
Element size	0.005 m
Number of node	253172
Number of element	240030

3.8. Boundary and initial conditions:

In order to obtain a well-posed system of equations, reasonable boundary conditions for the computational domain have to be implemented. Inlet boundary condition is a uniform liquid and gas velocity at the inlet, and outlet boundary condition is the pressure boundary condition, which is set as 1.013×105 Pa. Wall boundary conditions are no-slip boundary conditions for the liquid phase and free slip boundary conditions for the solid phase and the gas phase. The higher viscous effect and higher velocity gradient near the wall have been dealt with the standard wall function method. At initial condition the solid volume fraction of 0.59 for glass beads and 0.56 for plastic beads of the static bed height of column has been used and the volume fraction of the gas at the inlet and in the free board region is based on the inventory. Table 3.2 represents the detail description of the boundary and initial conditions used in simulation.

Table 3.2. Description of systems used in simulation

Diameter of column:	0.1 m	
Height of column:	1.88 m	
Solid phase	Glass beads	plastics beads
Particle size, mm:	2.18	8, 11.6, 15.4
Particle density, Kg/m^3:	2470	1155
Initial static bed height, m:	0.171, 0.213	0.122
Bed inventory, kg:	1.965, 2.450	0.59
Superficial liquid velocity:	0.004246 to 0.138 m/s	
Static bed voidage:	0.41	
Superficial gas velocity:	0 to 0.1019 m/s	
Liquid phase (water), 300˚C		
Viscosity, Pas:	$7.98x10^{-4}$	
Density, Kg/m^3:	995.7	
Gas phase (air), 300C		
Viscosity, Pas:	$1.794x10^{-5}$	
Density, Kg/m^3:	1.166	

CHAPTER-4

RESULTS AND DISCUSSIONS

Hydrodynamic behaviour of a fluidized bed is to be precisely known for better design and operation of a fluidized bed. Thus in the present work an attempt has been made to characterize the three-phase fluidized bed by experiment with low density particles having application as bioreactor and by numerical simulation using CFD tool. Results obtained from experiment and simulations are analyzed and discussed. Simulations are also carried out using glass beads as the solid phase in the fluidized bed with distributor and without distributor to study the variation in hydrodynamic behaviour due to the effect of distributor. Hydrodynamic properties studied by the experiment are validated with the simulation results.

4.1. Experimental Results:

Experiments have been carried out for plastic beads as reported in chapter-2 by varying the gas and the liquid velocities and the results are represented graphically.

4.1.1. Bed pressure drop and minimum fluidization velocity:

In the present study, pressure drop in the fluidized bed has been measured by using manometers filled with carbon tetrachloride as manometric fluid connected to pressure tapping in the column as described in chapter-2. All experiments have been started with the column completely filled with water and plastic beads up to a desired height with the initial level of manometer adjusted to have zero. For liquid-solid experiment the liquid flow rate was gradually increased. For gas-liquid-solid experiment with different liquid and gas flow rate has been carried out in two different manners: one with little flow of liquid close to zero, the air was slowly introduced and gradually increased to the desired flow rate after which the liquid flow rate was increased and the readings were noted down and the other is keeping the liquid flow rate constant at some value may be minimum liquid fluidization velocity or some fraction or multiple of that and gas flow rate was gradually varied.

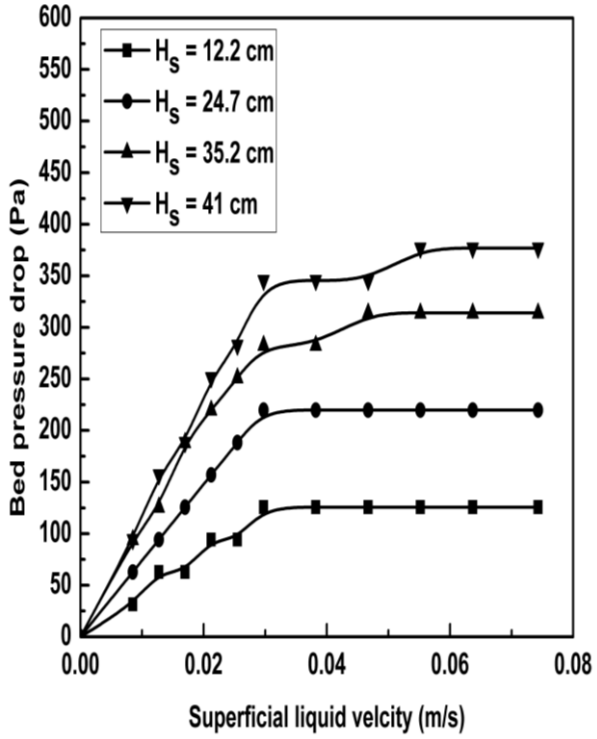

Fig. 4.1. Variation of bed pressure drop with liquid velocity at different static bed heights of 0.0154 m plastic beads.

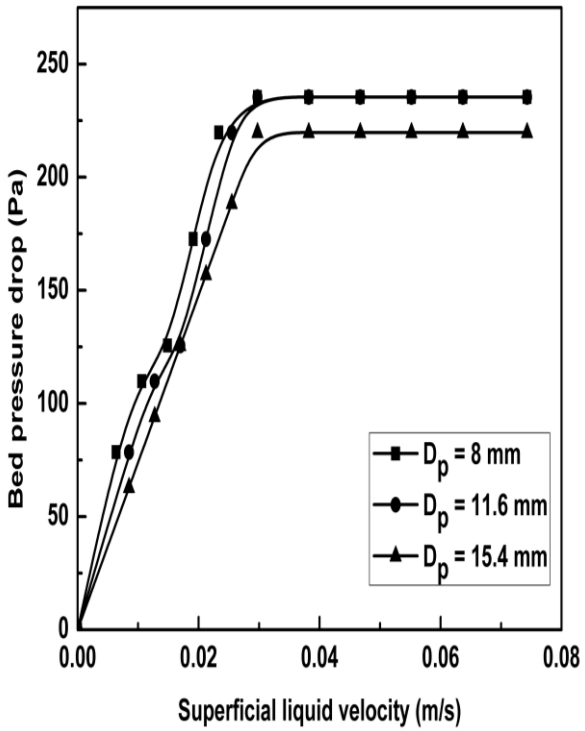

Fig. 4.2. Variation of bed pressure drop with liquid velocity for plastic beads of different size of initial static bed height of 24.7 cm.

Figs. 4.1 and 4.2 show the variation of pressure drop with superficial liquid velocity in liquid-solid system for different static bed heights and particle sizes. An increase in bed pressure drop has been observed with increased initial static bed height as seen in Fig. 4.1. It is obvious that higher static bed height (higher bed mass) requires a higher amount of drag to make the bed fluidize, thus a higher value of pressure drop as observed. There is a little difference in fluidized bed pressure drop in case of different particle size; smaller size particle because of higher bed mass due to less void fraction and little higher density has little higher pressure drop (Fig. 4.2). The pressure drop for 8mm and 11.6 mm particles observed to be the same as it has not been possible to measure a small difference in pressure drop in monometer with carbon tetrachloride as the manometric fluid. The pressure drop after incipient of fluidization has been assumed to be constant. The experimental pressure drop has been found to be close to that can be obtained from basic force balance, indicating the absence of wall effect.

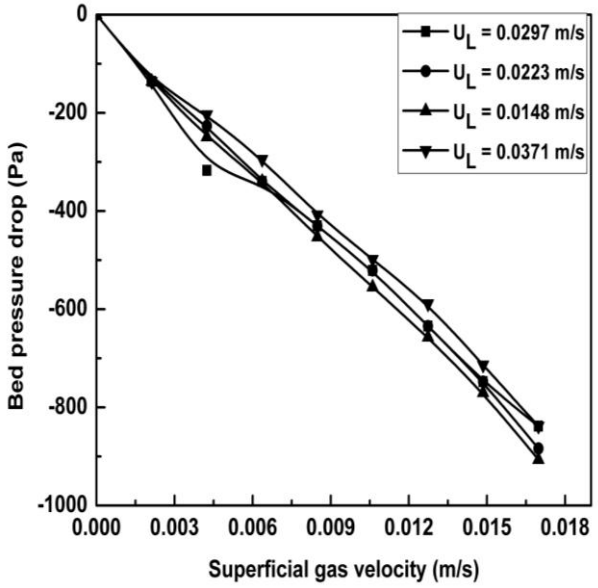

Fig. 4.3. Variation of bed pressure drop with gas velocity for different values of liquid velocities at H_S = 0.122 m and D_p of 0.0154 m.

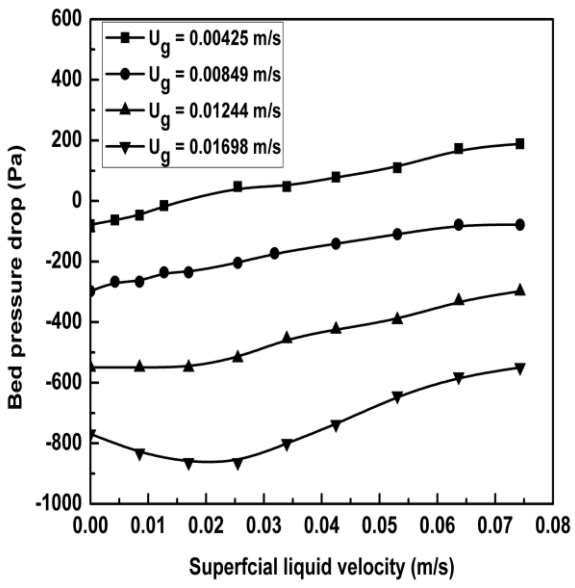

Fig. 4.4. Variation of bed pressure drop with liquid velocity for different values of gas velocities at H_S = 0.122 m and D_p of 0.0154 m.

Fig. 4.3 shows the variation of bed pressure drop with gas velocity at different constant liquid velocities. It is clear that with increase in gas velocity there is decrease in bed pressure drop. This is negative as the initial pressure drop is made zero with no gas only constant liquid velocity. With increase in gas velocity the bed pressure drop decreases because of higher gas holdup in the bed which cause decrease in hydrostatic pressure at the bottom of the bed. When the bed pressure drop is measured for the variation of liquid velocities at constant gas velocities exactly same values of pressure drop for particular gas and liquid velocities has not been obtained as in Figs. 4.3 and 4.4, because of different initialization of pressure drop values to zero at the starting of varying the gas or the liquid velocity. Fig. 4.4 shows an increase in bed pressure drop with liquid velocity; this is due to increased liquid holdup in the bed with increase in liquid velocity.

In case of gas-liquid-solid fluidization with liquid as the continuous phase, the minimum fluidization velocity is called as the minimum liquid fluidization velocity (U_{Lmf}). U_{Lmf} is the superficial liquid velocity at which the bed becomes fluidized for a given superficial gas velocity. The minimum liquid flow rate required to achieve fluidization is determined from the bed pressure drop vs. superficial liquid velocity plot at a constant gas velocity. The point

of intersection of the line of different slope is taken as U_{Lmf}. Visual observation determines U_{Lmf} as either the velocity at which the bed first begins to expand or as the velocity at which any particle within the bed continuously shifts position with neighboring particles (Jena, 2010). U_{Lmf} in this study has been obtained from the plot of pressure drop and superficial liquid velocity (Figs.4.1 and 4.2) for liquid-solid system i.e. at gas velocity zero. With increase in gas velocity it has been observed that the U_{Lmf} decreases, but this has not been quantified because of difficulty in measuring the same for low density particles. For moderate and high density particles this can be done. Fig. 4.1 shows no variation in U_{Lmf} with bed height, but Fig. 4.2 shows a variation in U_{Lmf} with particle size, higher the particles size higher the $U_{Lmf.}$

4.1.2. Bed expansion:

The knowledge of expanded bed height is essential for sizing of the system. For a fluid velocity more than the minimum fluidization the static solid bed get expanded with to and fro motion of the solid particles. As the fluid velocity excess than the minimum fluidization is increased the bed gradually expanded to higher heights. The expanded bed height in the present study has been measured by visual observation. The bed expansion study as carried out by varying liquid velocity (at constant gas velocity), different statics bed heights and varying gas velocity (at constant liquid velocity) have been presented in Figs. 4.5 through 4.8. Bed expansion is also represented by bed voidage. Bed voidage represents the fraction of the expanded bed contains gas and liquid in case of three-phase fluidization. Fig. 4.5 shows an increase in bed expansion ratio with increase in liquid velocity for liquid-solid fluidized bed. It is observed that the bed expansion ratio is not a function of initial static bed height, thus for a higher initial static bed height the expanded bed height is more for a particular value of liquid velocity. Fig. 4.6 shows the variation of bed expansion ratio with liquid velocity at different particle size for the liquid-solid system. The plot shows an increase in bed expansion ratio with decrease in particle size i.e. smaller size particles lifted to higher height in the bed. Fig. 4.7 shows the variation of bed expansion ratio of gas-liquid-solid fluidized bed with liquid velocity at different constant gas velocities. With both increase in liquid and gas velocities the bed expansion ratio increases but monotonic with varying slope, the initial slope

is changed midway and again achieved. At zero liquid velocity when gas is introduced into the bed the bed expanded but entire particles are not in fluidization few particles riven by the gas and as the liquid velocity increased there off the bed expanded then the rate of expansion decreased and again increased.

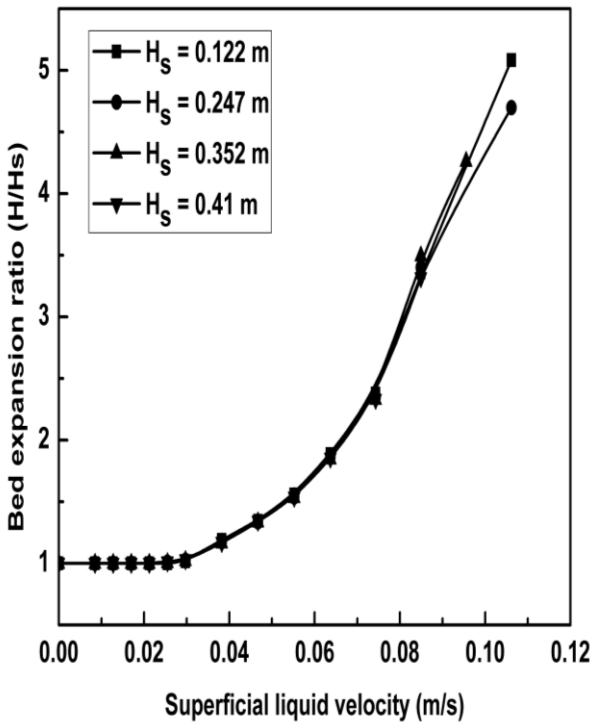

Fig. 4.5. Variation of bed expansion ratio with superficial liquid for 0.0154 m plastics beads at different static bed heights.

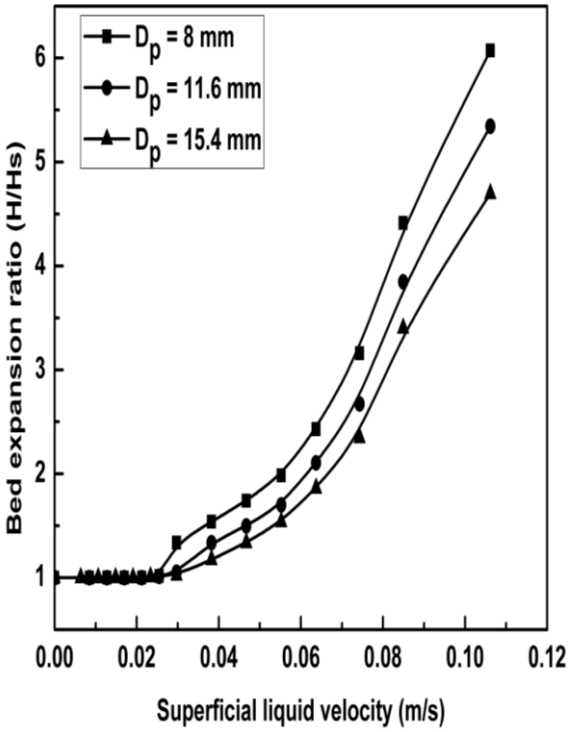

Fig. 4.6. Variation of bed expansion ratio with superficial liquid for plastics beads of different size in liquid-solid fluidization.

Fig. 4.8 shows the variation of bed expansion ratio of gas-liquid-solid fluidized bed with gas velocity at different constant liquid velocities which are either fraction of minimum fluidization velocity (U_{Lmf}) or multiple of it. For 0.0154m particles the U_{Lmf} has been observed to be 0.0297 m/s, thus liquid velocities of the multiples 0.5, 0.75, 1, 1.25 and 1.5 of this value has been used. It is observed from Fig. 4.8 that there is a continuous increase in bed expansion ratio with gas velocity to some value of gas velocity and after which it decreases. The behaviour observed with low density particle is peculiar. This has also been reported by Nore et al. (1992)

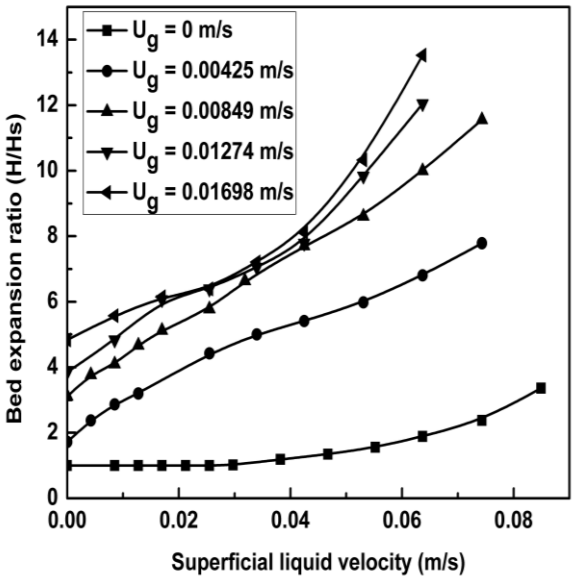

Fig. 4.7. Variation of bed expansion with liquid velocity at different values of gas velocities for 0.0154 m plastics beads at H_S = 0.122 m.

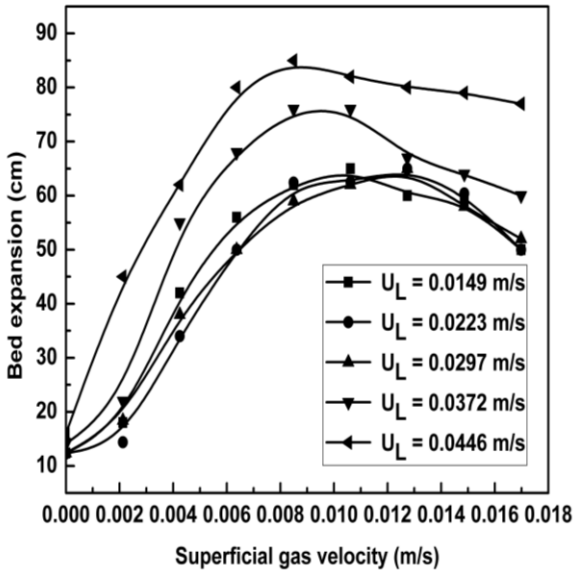

Fig. 4.8. Variation of bed expansion with gas velocity at different values of liquid velocities for 0.0154 m plastics beads at H_S = 0.122 m.

4.2. Computational results:

A series of numerical calculation are carried out by ANSYS FLUENT 13.0 and the results are presented graphically in order to show the effect of variables such as: superficial liquid and gas velocities on the hydrodynamic properties of three-phase fluidized bed. As mentioned earlier three different geometrical models are considered for simulation in the present work, those are: 2D geometry without distributor, 3D geometry without distributor and 2D geometry with distributor of orifice size 0.002 m. This has been done to compare the results of simulation with previous results found in literature on the 2D and 3D models without distributor carried out under similar conditions and to compare the result obtained from the simulation of 2D model with distributor with one without distributor. 3D model with distributor has not been carried out because of requirement of high computational power which is out of scope of the present work. In all the simulations a time step size of 0.001s has been used. The convergence criteria for all the numerical simulations are based on monitoring the mass flow residual and the value of 1.0 e^{-04} was set as converged value. The residual plot of the progress of the simulation is shown in Fig. 4.9. The following under relaxation factors have been used for different flow quantities: pressure = 0.3, density = 1, body forces = 1,

momentum = 0.2, volume fraction = 0.5, granular temperature = 0.2, turbulent kinetic energy = 0.8, turbulent dissipation rate = 0.8 and turbulent viscosity =1. All the simulations have been carried out still the system reach the quasi steady-state, the average flow behaviuors are time independent. This is achieved by monitoring the expanded bed height and the phase volume fractions. Solid, liquid and gas phase dynamics have been represented in the form of contour, vectors and XY plots and are analysed. Fig. 4.10 shows the variation in the bed profile with the physical time of simulation. It is observed from the figure that the bed profile is almost the same after 25 sec of simulations time. Simulation continued for 60 sec and the average over last 20 s are used in the analysis. Once the fully developed quasi steady state is reached, the average quantities in term of time, axial, and radial direction are calculated.

Figs. 4.11 and 4.12 show the comparison of bed expansion and gas holdup of 2D and 3D fluidized bed without distributor. Hydrodynamics of 2D and 3D fluidized bed without distributor found to be in close agreement. So in all the subsequent work simulation for 3D model without distributor and 2D fluidized bed with distributor has been carried out.

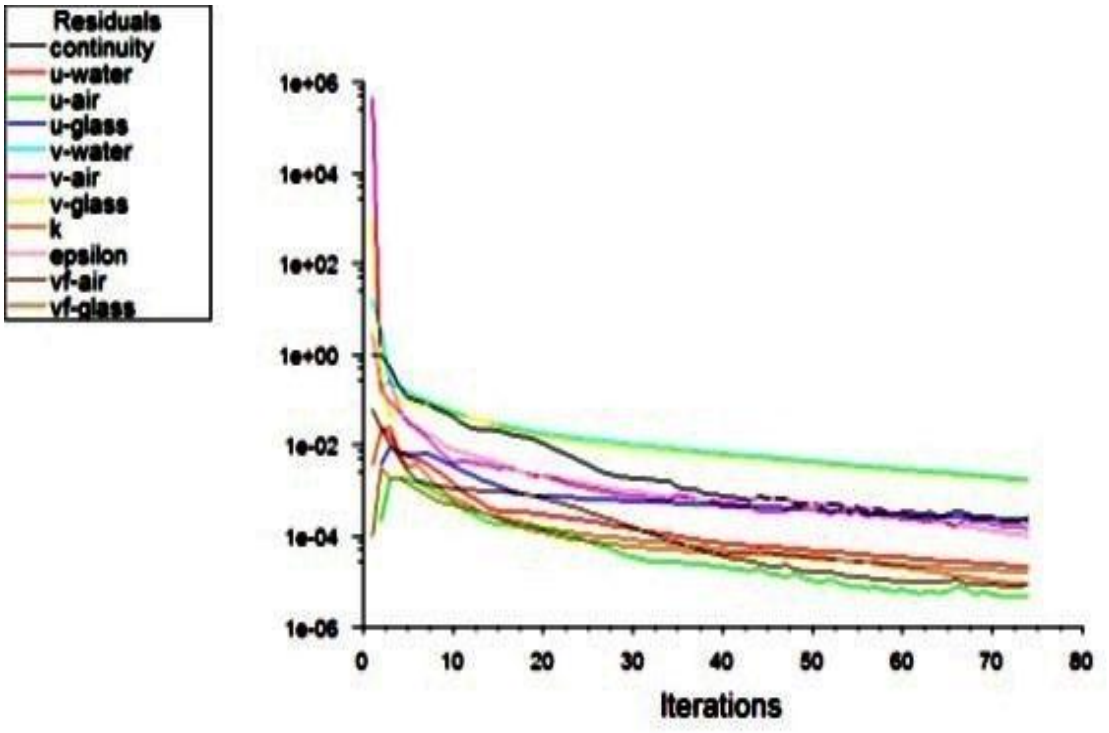

Fig. 4.9. Plot of residuals showing the progress of simulation

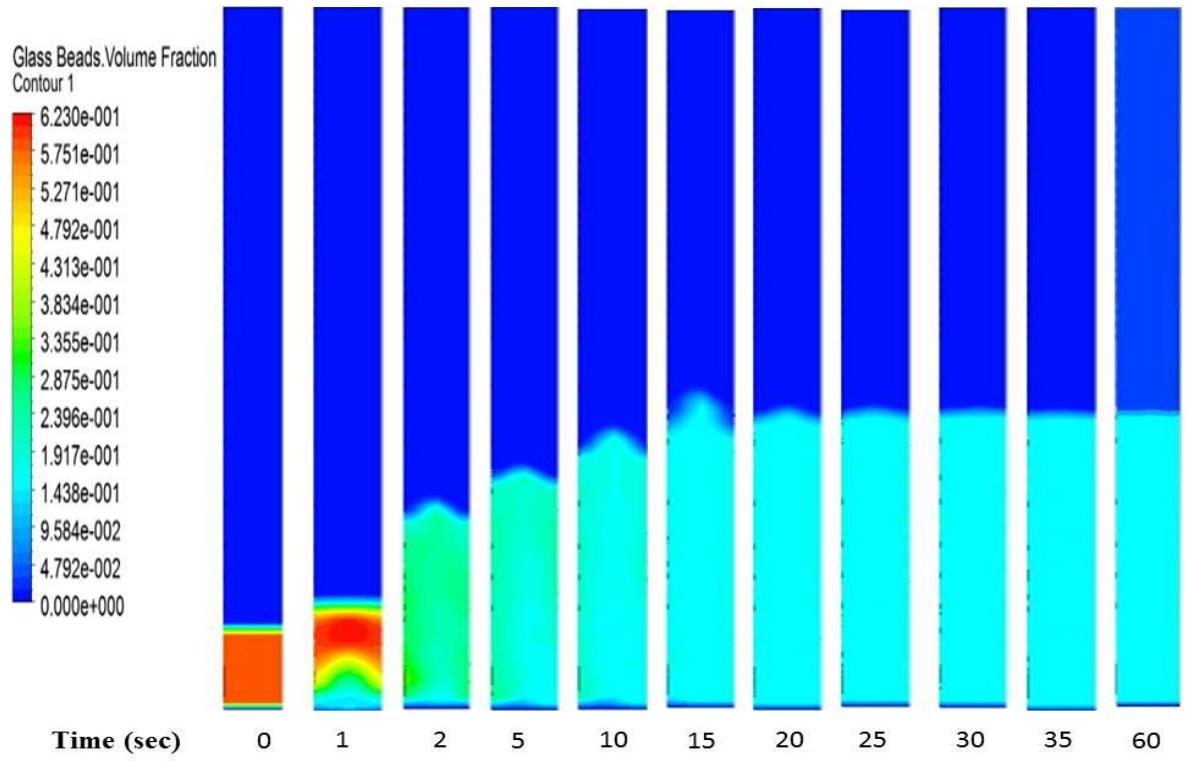

Fig. 4.10. Contour of volume fraction of 2.18 mm glass beads of initial statics bed height of 0.213 m inside 3D fluidized bed at liquid velocity of 0.138 m/s and gas velocity of 0.0375 m/s at different physical time of simulation

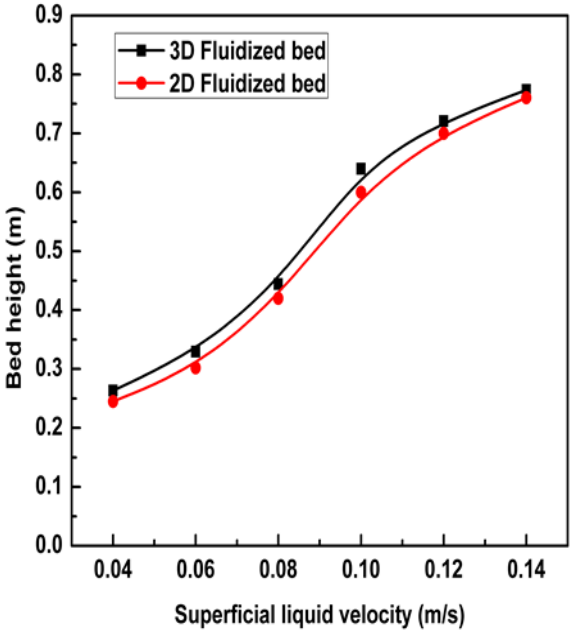

Fig. 4.11. Comparison of bed height of 2D and 3D fluidized bed without distributor.

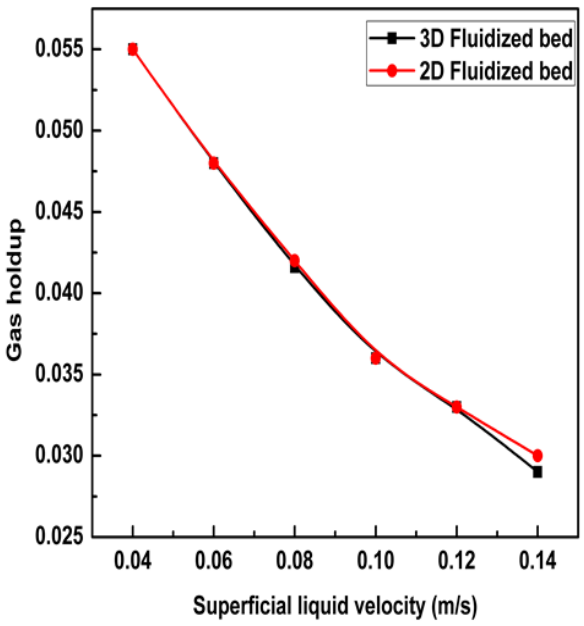

Fig. 4.12. Comparison of gas holdup of 2D and 3D fluidized bed without distributor.

4.2.1. Phase volume fractions:

Solid, liquid and gas phase volume fraction in the bed are represented in the form of contour. Fig. 4.13 shows the contour of volume fraction of solid, liquid and gas in the column obtained at liquid velocity of 0.14 m/s and gas velocity 0.0375 m/s for initial statics bed height 0.213 m glass beads diameter 2.18 mm in 3D fluidized bed after the quasi steady state is achieved. Fig. 4.14 shows the contour of volume fraction of solid, liquid and gas at liquid velocity 0.12 m/s and gas velocity 0.0125 m/s for initial statics bed height 0.171 m and glass beads diameter of 2.18 in 2D fluidized bed having distributor of pore size 2 mm after quasi steady is achieved. From Figs. 4.13 and 4.14, it is observed that the distribution of volume fraction of all the phases inside fluidized section of the 2D fluidized bed model with distributor is not uniform compared to that of the 3D fluidized bed model. The contour of volume fraction of water indicates that water is less in fluidized section than the two-phase section above it.

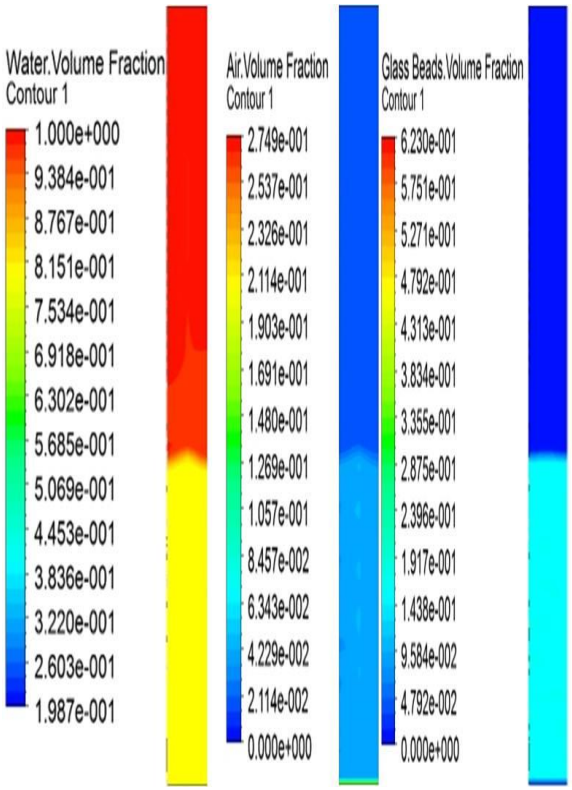

Fig. 4.13. Contour of volume fraction of solid, liquid and gas at liquid velocity 0.14 m/s and gas velocity 0.0375 m/s for static bed height of 0.213 m in 3D fluidized bed.

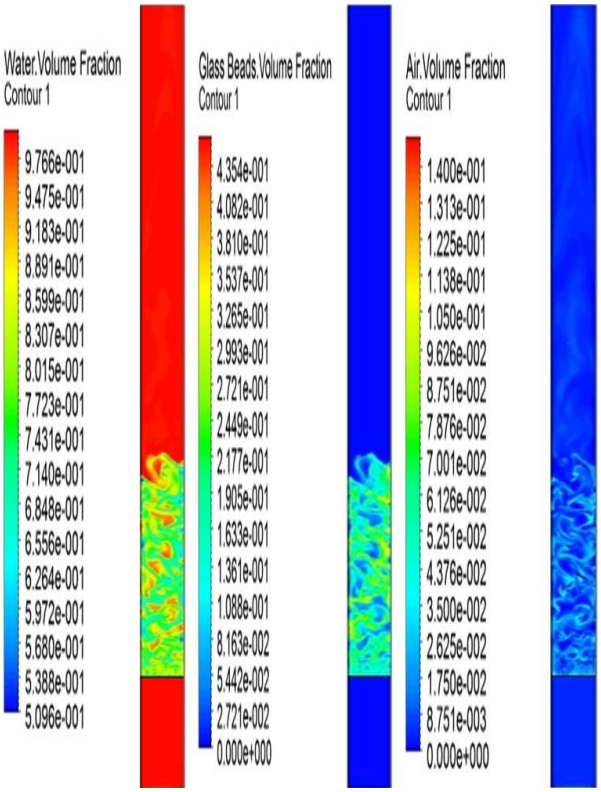

Fig. 4.14. Contour of volume fraction of solid, liquid and gas at liquid velocity 0.12 m/s and gas velocity 0.0125 m/s for static bed height of 0.171 m in 2D fluidized bed having distributor with pore size 0.002 m.

Similarly the contour of air indicate that gas holdup is significantly more in fluidized section of the bed compared to the two-phase region above. This is because of higher residence time of the smaller bubbles in the fluidized bed, but as the bubbles leave the three-phase region coalescence occurs and bubble size grows and the residence time decreases. Similar results are obtained by Jena (2010) and Nguyen et al. (2011).

4.2.2. Phase velocity:

Fig. 4.15 shows the velocity vector and contour of gas at superficial liquid velocity of 0.14 m/s and gas velocity of 0.0125 m/s. From the figures it is observed that the water velocity is more fluctuating in case of fluidized bed with distributor than in case of the bed without distributor. This indicates the effect of the distributer on the velocity vector. From the vectors it is seen that the velocity of gas phase is less in the fluidized section compared to that of two phase section which resulted in increasing the residence time of the gas phase as a result the volume fraction of the gas phase is more in fluidized section. But in the two-phase section there is an increased in the velocity of the gas phase as compared to that of liquid phase. The velocity vector when compared to that of 2D fluidized bed model it is seen that the velocity of all three-phases are less vigorous and back mixing, which is generally seen in the experiment. The presence of distributor produces more turbulence and better back mixing of the fluid in the bed which is necessary for intimate contact between the phases. In the bed without distributor variation in velocity is observed and the flow is not uniform which is due to the interaction of water of glass beads, air. The test section of the fluidized bed (above the distributor) has been divided into four equal sections to have a better and clear view of the vector plots. It is also observed from Fig. 4.16 that water attain nearly uniform velocity in the two phase region in the fluidized bed where glass beads are absent but complete uniform in velocity is not attained. This may be because of the migration of the turbulence affected from the distributor carried to the outlet although it diminishes gradually. Figs. 4.17 and 4.18 show the velocity vector and contour of the water inside the fluidized bed. These figures indicate similar behaviour of the beds with and without distributor as discussed for Figs. 4.15 and 4.16.

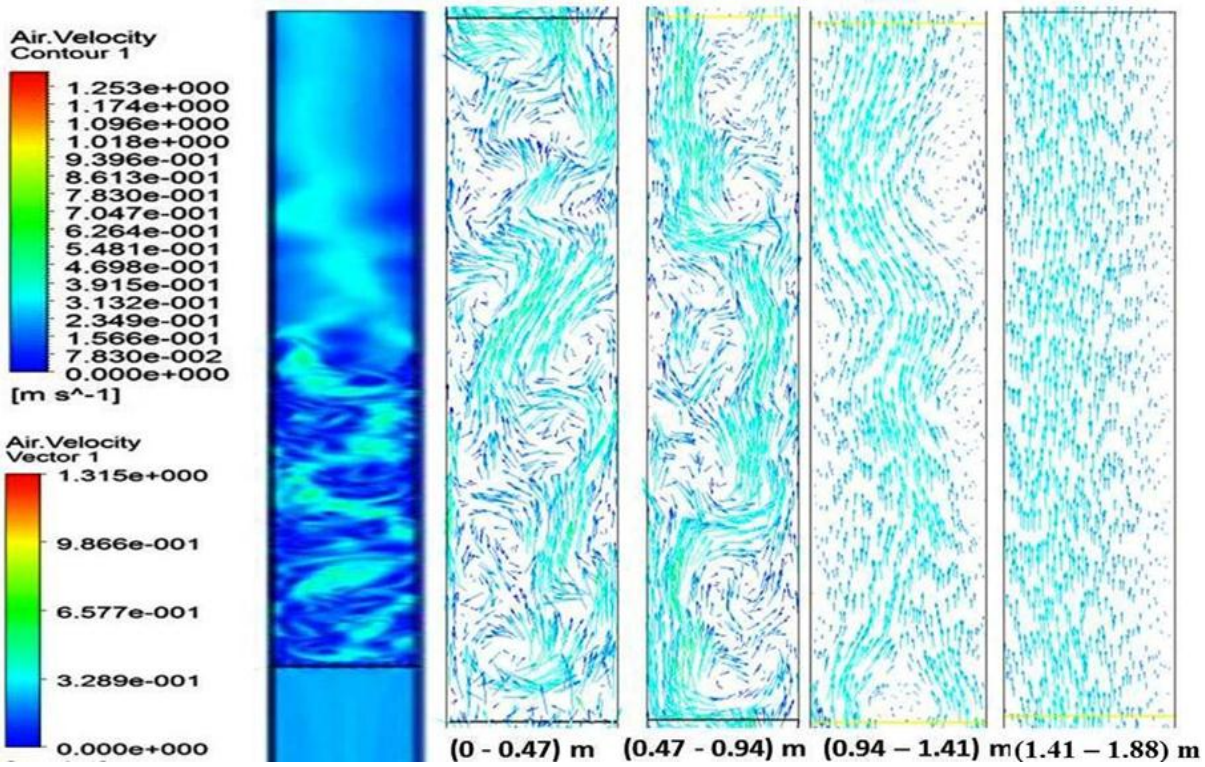

Fig. 4.15. Velocity vector and contour of gas inside the fluidized bed system with distributor.

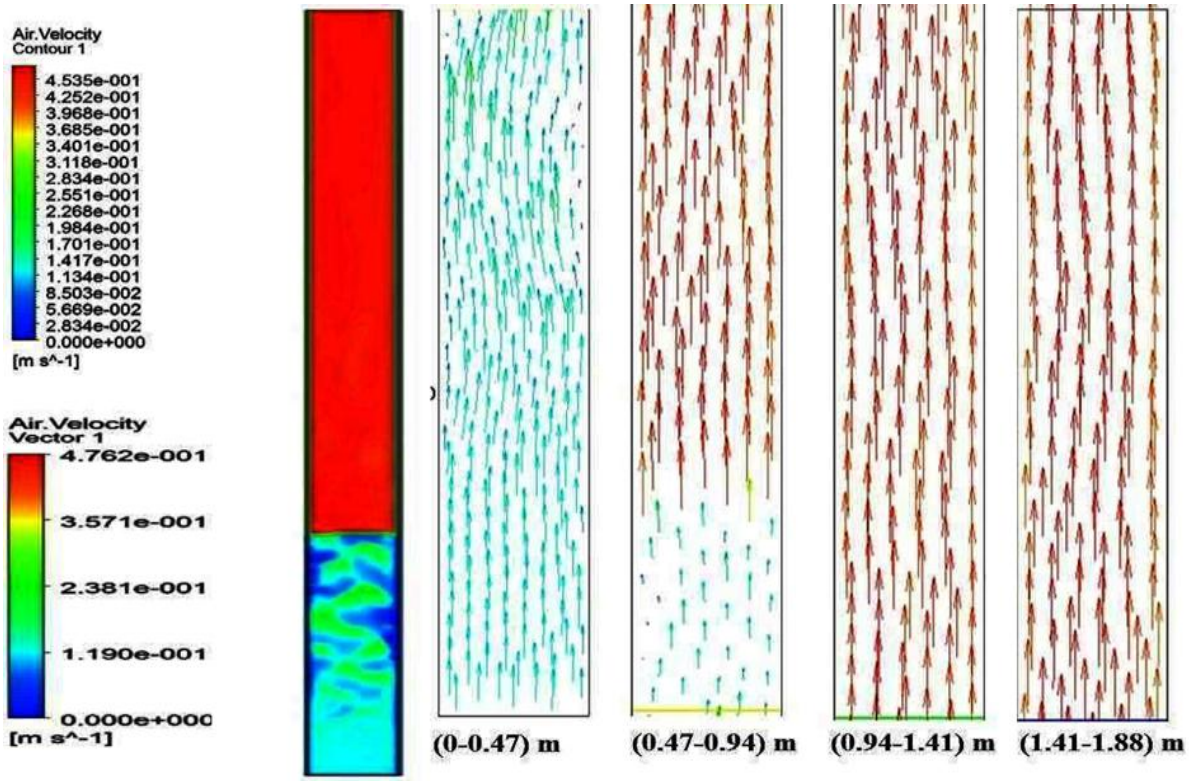

Fig. 4.16. Velocity vector and contour of gas inside fluidized bed without distributor.

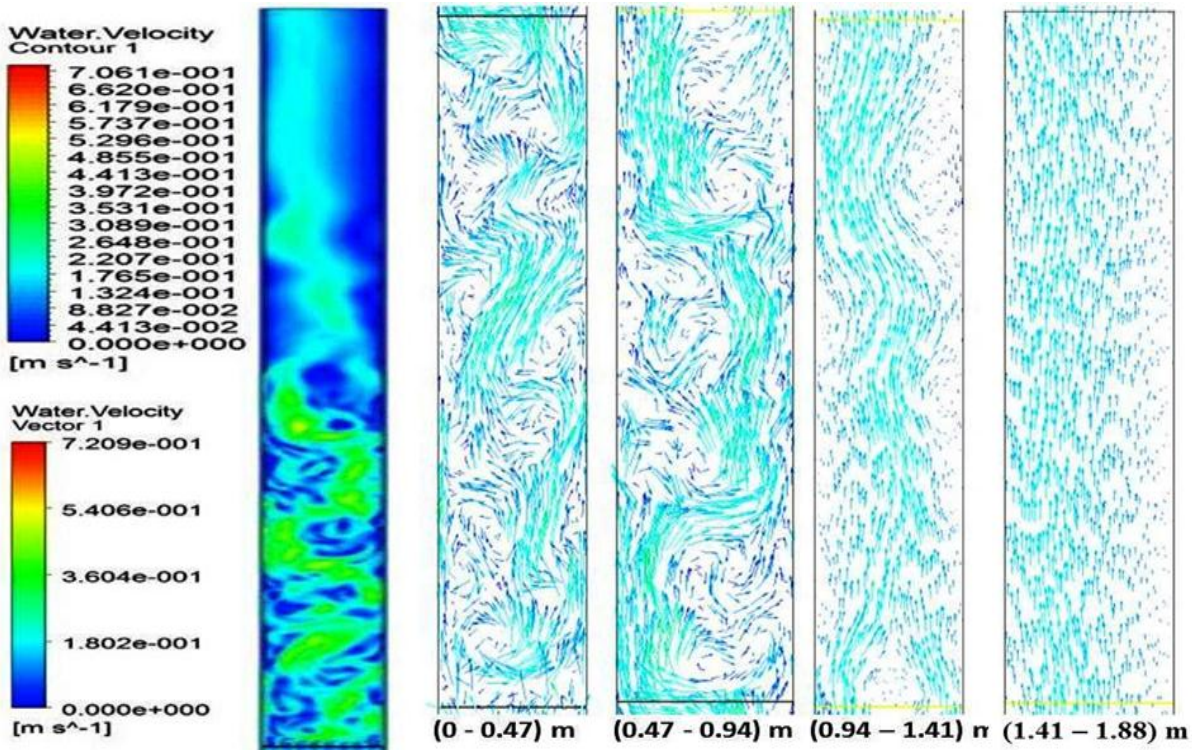

Fig. 4.17. Velocity vector and contour of liquid inside the fluidized bed system with distributor.

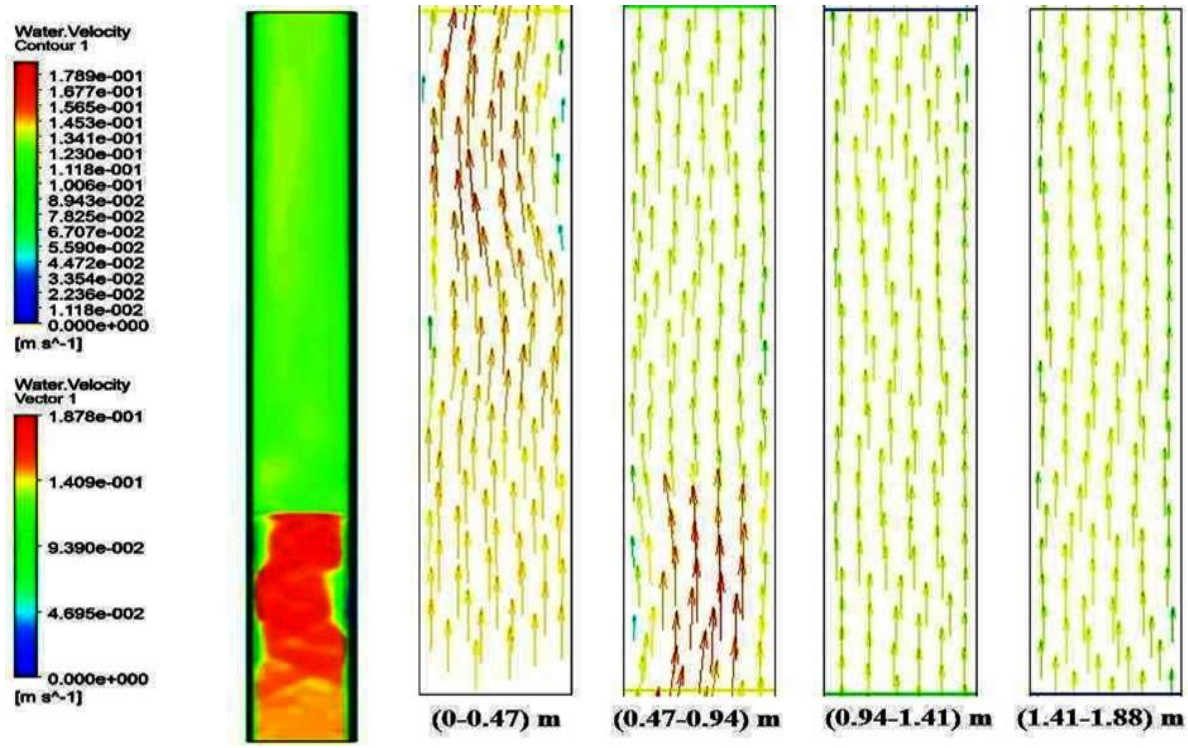

Fig. 4.18. Velocity vector and contour of liquid inside the fluidized bed system without distributor.

Fig. 4.19 shows the contour and velocity vector of the solid phase i.e. glass beads. This figure also indicates the fluctuation in velocity.

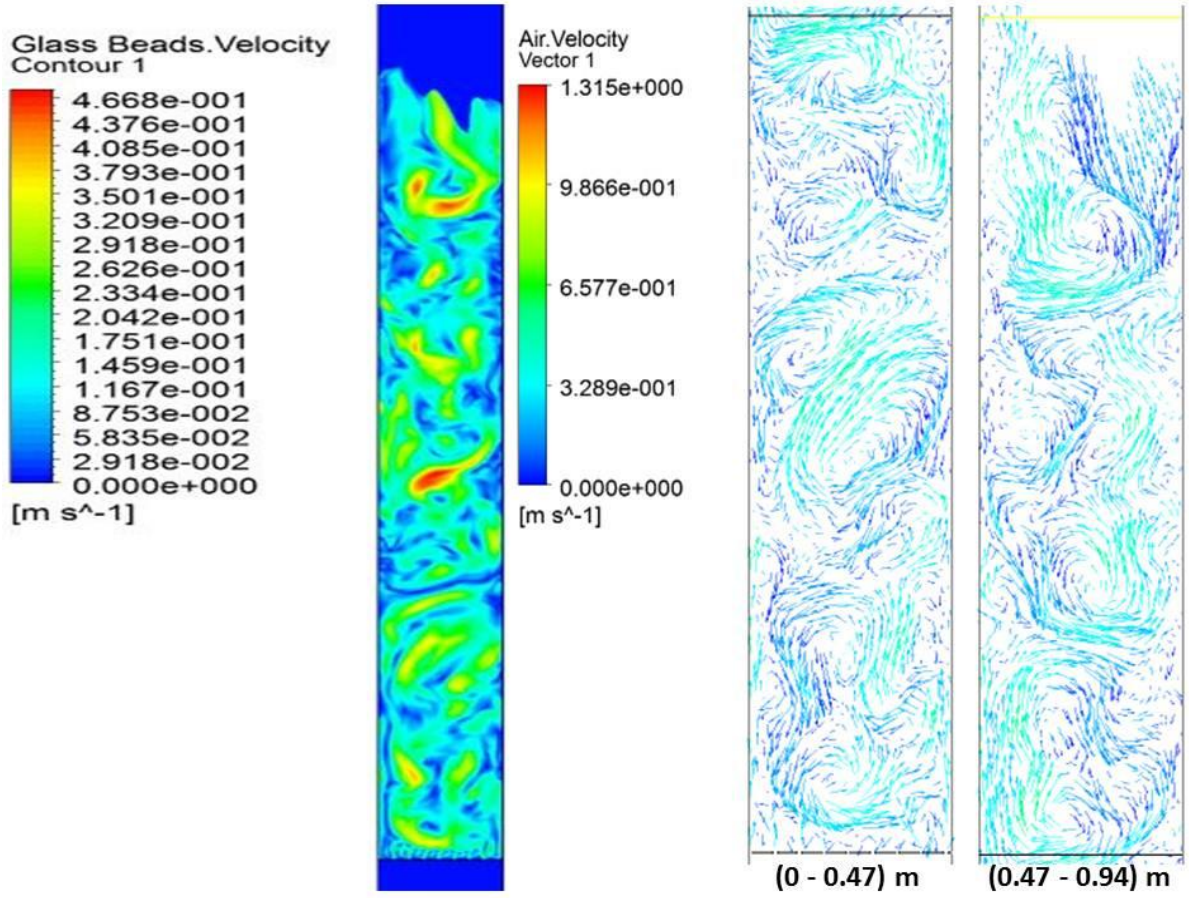

Fig. 4.19. Velocity vector and contour of solid inside the fluidized bed system with distributor.

Fig. 4.20 shows the velocity contour of air, water and glass beads at inlet liquid velocity 0.08 m/s and gas velocity 0.0125 m/s at 0.2m above the inlet i.e. of 3D fluidized bed. From the contour it can be seen that the velocity vector of water is more in the fluidized section compared to that of gas-phase and solid-phase. Fig. 4.21 shows the comparison of water phase velocity varying radially at three different bed heights (0.1 m, 0.2 m and 0.3 m) for 3D fluidized bed without distributor and 2D bed with distributor. From the figure it is observed that fluidized bed with distributor has more fluctuation in velocity compared to that of fluidized bed without distributor. Similar radial variation of the air velocity has also been observed for the gas phase also (Fig. 4.22).

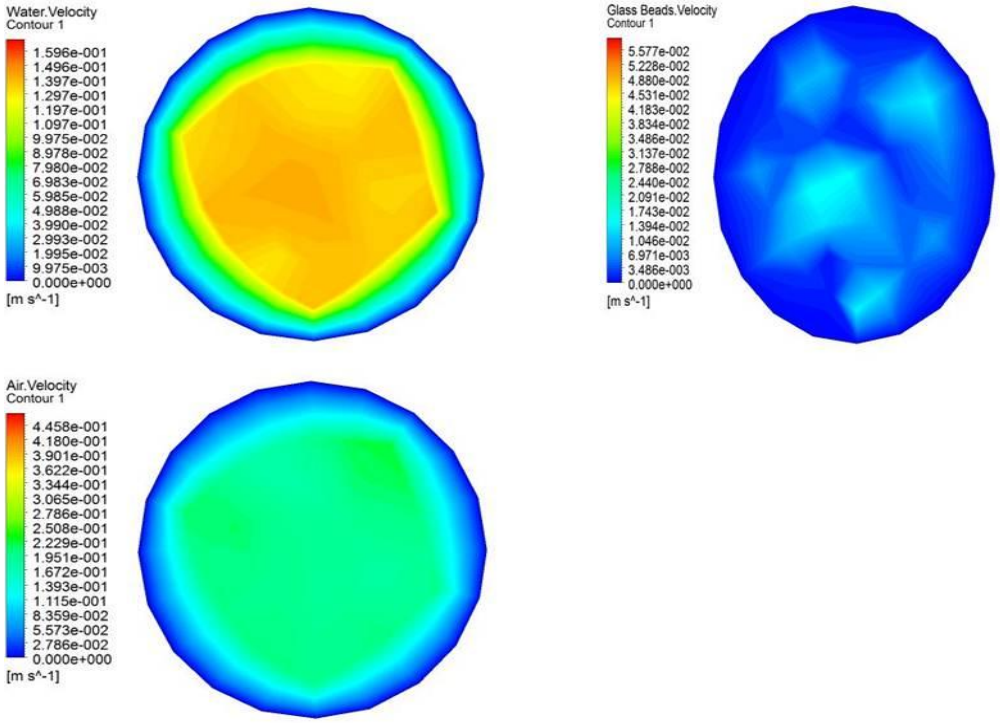

Fig. 4.20. Velocity contour of solid, gas and liquid at liquid velocity 0.08 m/s and gas velocity 0.0125 m/s for static bed height of 0.213 m in 3D fluidized bed at height 0.2 m from inlet.

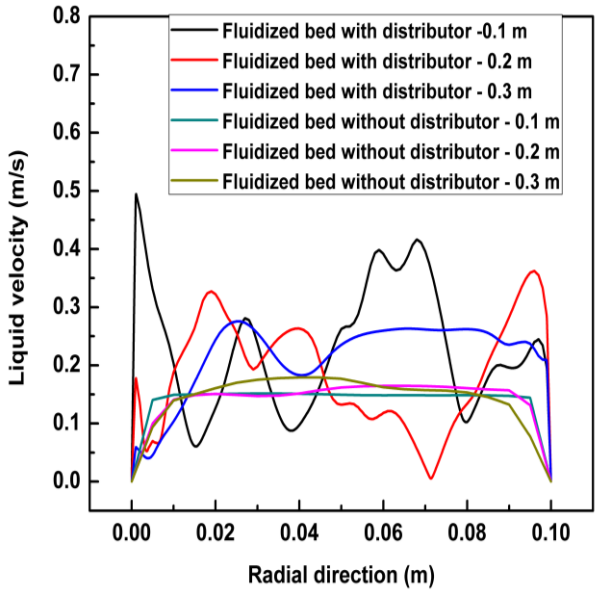

Fig. 4.21. Comparison of liquid velocity inside fluidized bed having distributor and without distributor.

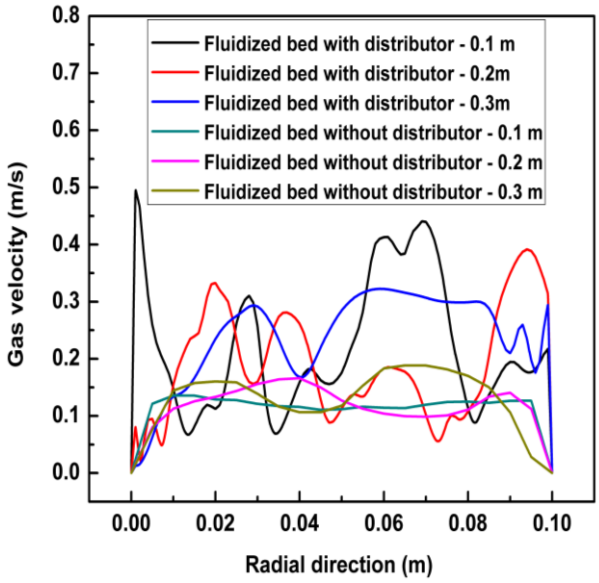

Fig. 4.22. Comparison of gas velocity inside fluidized bed having distributor and without distributor

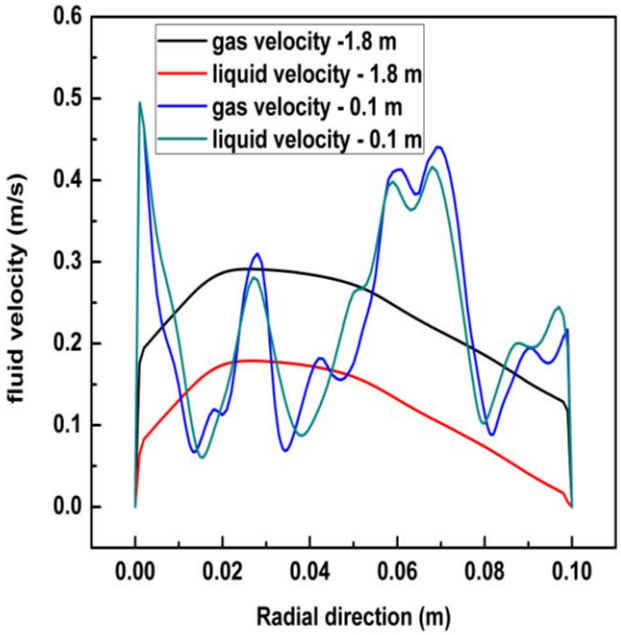

Fig.4.23. Comparison of gas and liquid velocity at same column height of a fluidized bed with distributor.

Fig. 4.23 shows comparison of the velocity of gas and liquid phase in the fluidized section and the two phase section above the fluidized section. It is observed from the figure that the velocity of gas and liquid phases are nearly same in the fluidized section at a height of 0.1 m from the bottom, but in the two phase section the velocity of gas is higher compared to that of the liquid phase. This shows that gas moves faster in the two phase region leading to decrease residence time of gas bubbles and in gas holdup in the two-phase region of the fluidized bed.

Fig. 4.24 shows the velocity vector of solid particles of diameter 2.18 mm at inlet liquid velocity 0.008 m/s and gas velocity 0.0125 m/s in 3D fluidized bed model. It is seen from the figure that the solid particle flows downward in the central region of the fluidized section at the top of the fluidized section with more vigorous solid particle circulation. In the lower section less movement of solid particles observed. Solid particles axial velocity is more in the central region of the fluidized bed and zero near to the wall as shown in Fig. 4.25. Similar result has been obtained by Panneerselvam et al. (2009), Nguyen et al. (2011), and Hamidpur et al. (2012).

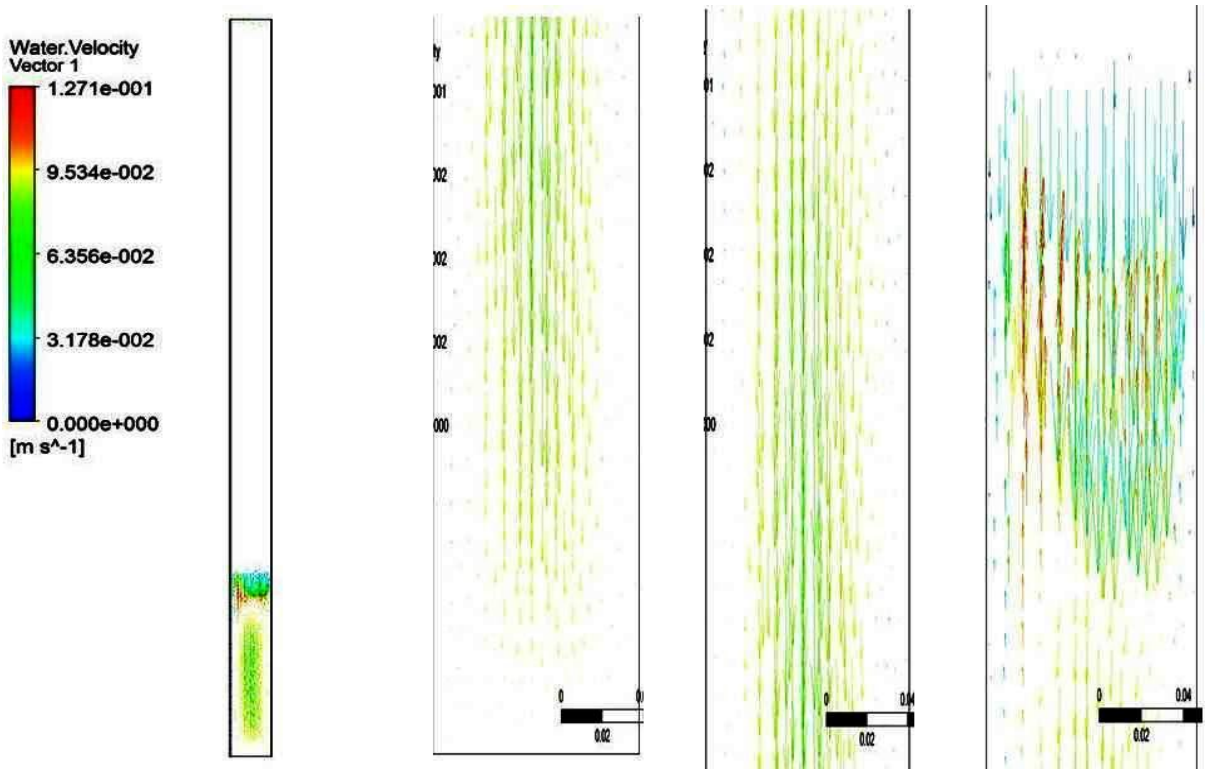

Fig. 4.24. Velocity vector of glass beads of diameter 2.18 mm at inlet liquid velocity 0.08 m/s and gas velocity 0.0125 m/s for statics bed height 0.213 m in 3D fluidized bed model.

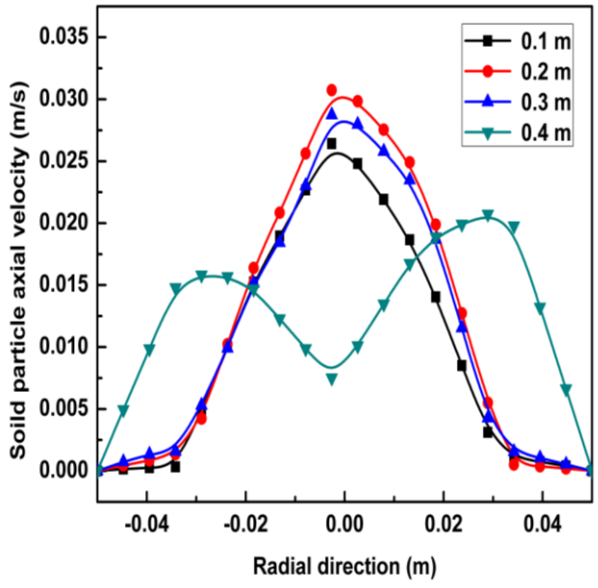

Fig.4.25. Solid particles axial velocity vs. radial direction at different height of glass beads [U_L = 0.08 m/s, U_g = 0.0125 m/s, and H_S = 0.213 m].

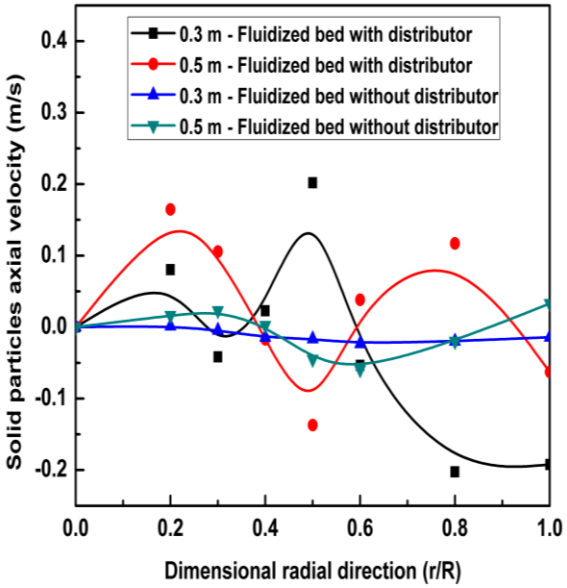

Fig.4.26. Comparison for solid particles axial velocity vs. dimensionless radial direction at different height [U_L = 0.14 m/s,Ug = 0.0125 m/s and Hs = 0.213 m].

Fig. 4.26 shows the comparisons for solid particle axial velocity of 2D fluidized bed having distributor of pore size 2 mm and 3D fluidized bed at inlet liquid velocity 0.12 m/s and inlet gas velocity 0.0125 m/s. It is evident from the plot that the axial velocity in 2D bed with distributor is more in magnitude and fluctuating type as compared to that in the 3D fluidized bed. This is due to the presence of distributor. It is seen from the plot that the solid particles are in to and fro motion some times in the direction of gas and liquid flow and sometimes in opposite direction to the flow of liquid and gas phases. From the plot (Fig. 4.25), it is observed that axial solid velocity is less in the lower section of the fluidized section and increases as we move toward the top of the bed where it attains maximum velocity. This occurs because of increased velocities of gas and liquid phases with the bed height and decrease in interaction with number of solid particles. At the bottom solid seems don't possess any velocity.

4.2.3. Bed expansion:

For fluid velocity higher than the minimum fluidization velocity, the solid bed expands. The expanded bed height gradually increases as the fluid velocity is increased.

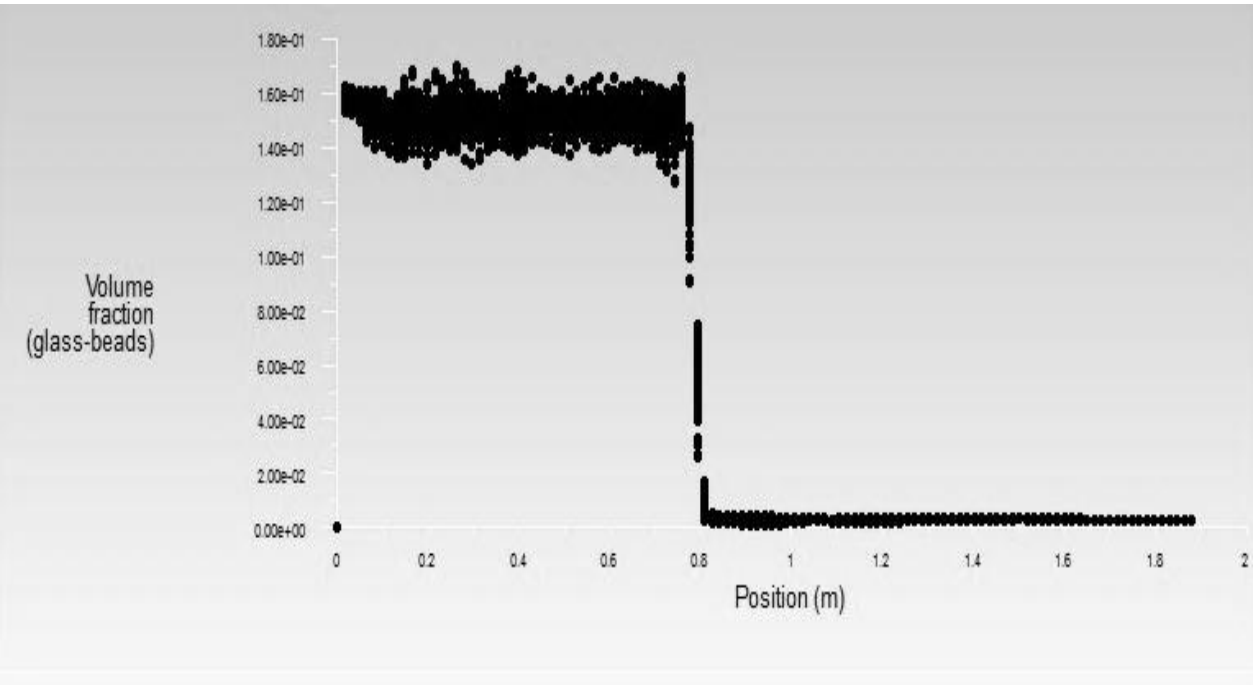

Fig. 4.27. XY plot of solid volume fraction.

In case of gas-liquid-solid fluidization, the bed expansion is seen with increase in liquid velocity (the primary phase) to a large and the gas velocity which depends upon the relative velocity between the two phases. The expanded bed height in this work is determined from the XY plot of solid volume fraction w.r.t. axial direction from the base of the column (as shown in Fig. 4.27). The point where the solid volume fraction sharply decreases to zero is taken as the height of the bed. It can be seen from the contour of the solid volume fraction in the bed (Fig. 4.28) that there is a steady increase in the bed height with increase in the liquid velocity above minimum fluidization velocity.

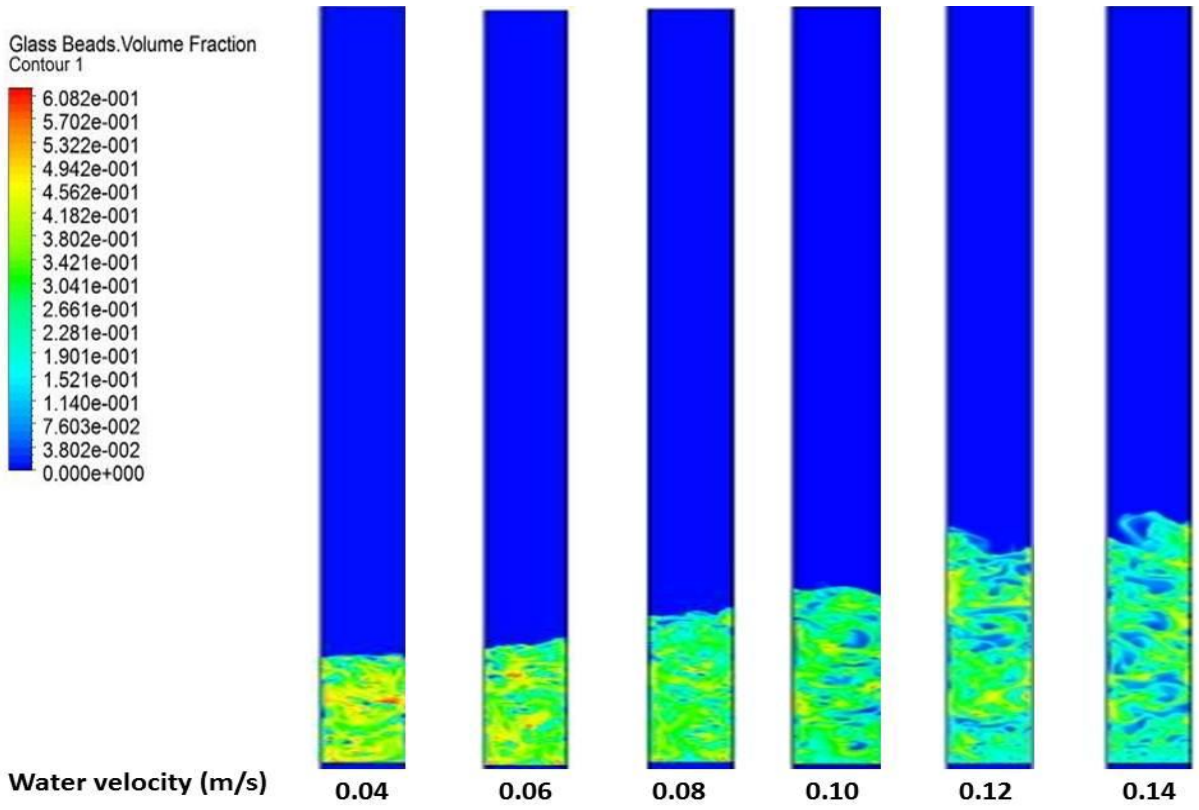

Fig. 4.28. Contour plot of variation in solid volume fraction with variation in liquid velocity.

Fig. 4.29 shows the variation of bed expansion of solid with liquid velocity at different constant gas velocities. It is evident from the plot that the bed expansion increases with increase in liquid velocity for constant gas velocity. The bed expansion is more for more gas velocity up to moderate value of liquid velocity and at higher liquid velocity the bed expansion is less with more gas velocity Fig. 4.30 show the CFD simulation result of bed

expansion (%) of the maximum bed height vs. superficial liquid velocity for fluidized bed having different static bed height of solid particles (i.e. 0.0213 m & 0.171 m). It is evident that the bed height increases for solid particle with higher initial static bed height. Similar results are obtained by Nguyen et al (2011).

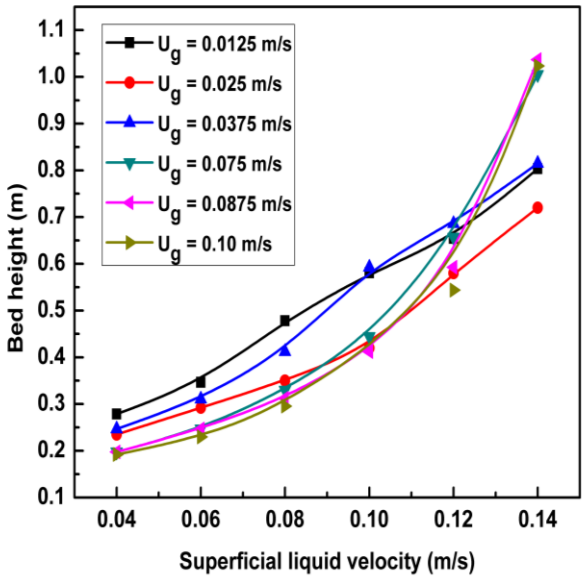

Fig. 4.29. CFD simulation result of bed expansion behavior of 2.18 mm glass beads at statics bed height 0.213 m in 3D fluidized bed at constant gas velocity.

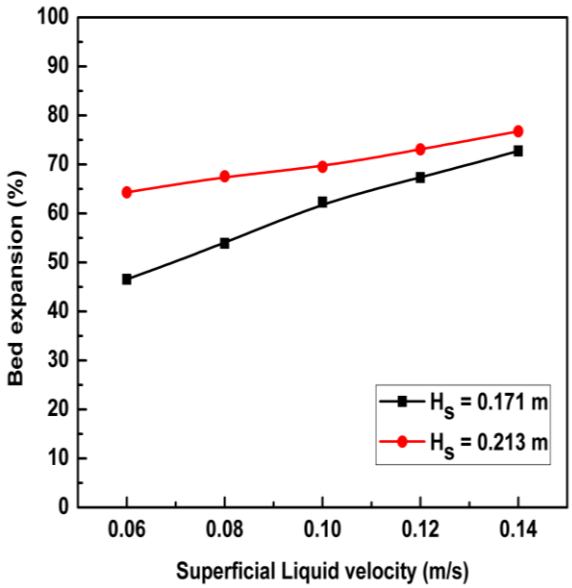

Fig. 4.30. Comparison of bed height obtained from CFD simulation of 2D fluidized bed with distributor at different statics bed height.

Fig. 4.31 shows the variation of bed expansion of solid particles with liquid velocity at different constant gas velocities in the 2D fluidized bed with distributor. It is observed from the plot that the bed expansion increases with increase in gas and liquid velocities. The bed expansion is more in case of bed with distributor as compared to that of the fluidized bed without distributor as observed from the values of bed expansion in Figs. 4.29 and 4.31. As it observed in the fluidized bed without distributor that the bed expansion decreases with increase in gas velocity is not accords in the fluidized bed with distributor. Fig. 4.32 shows the CFD simulation result of bed height varying with gas velocity at different liquid velocities of 3D fluidized bed model. It is evident from the plot that the bed height decreases with increasing gas velocity which corroborated the experimental finding that bed height increases with increasing gas velocity. The computational model used is based on the prescription by some investigators. They might have found a decrease in bed height with the increase in gas

velocity. The bed contraction truly occurs for particles of sizes close to 1 mm or less than that.

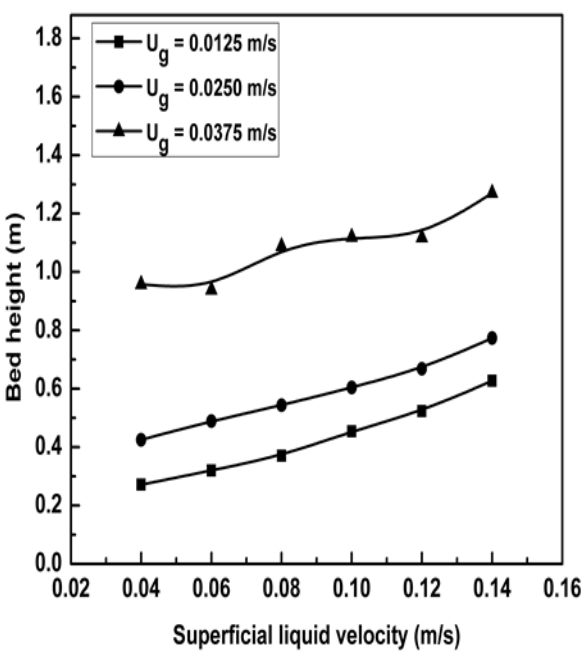

Fig. 4.31. CFD simulation result for variation of bed expansion with liquid velocity for different value of gas velocities at [H_S =0.171 m, and D_P = 2.18 mm].

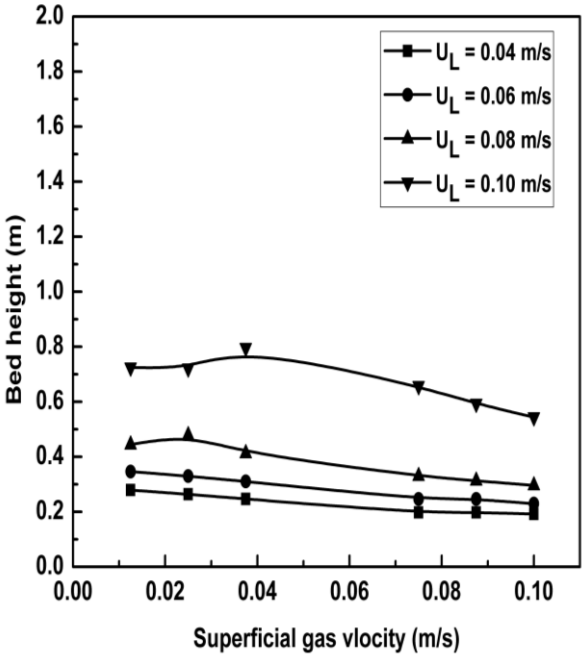

Fig. 4.32. CFD simulation result for variation of bed expansion with gas velocity for different value of liquid velocities at [H_S =0.171 m, and Dp = 2.18 mm].

Figs. 4.33 and 4.34 show the variation in expanded bed height with liquid velocity for different sizes of plastic beads for the liquid-solid and gas-liquid-solid system respectively. It is clear from both the plots that the bed expansion is more for smaller particles for a particular value the fluid velocity in comparison to bigger size particle. This phenomenon has been observed from experiments also. Fig. 4.35 shows the comparison CFD simulation result of bed expansion of low density solid particles to that of the experimental ones for the liquid-solid system. A very close agreement is seen between the results.

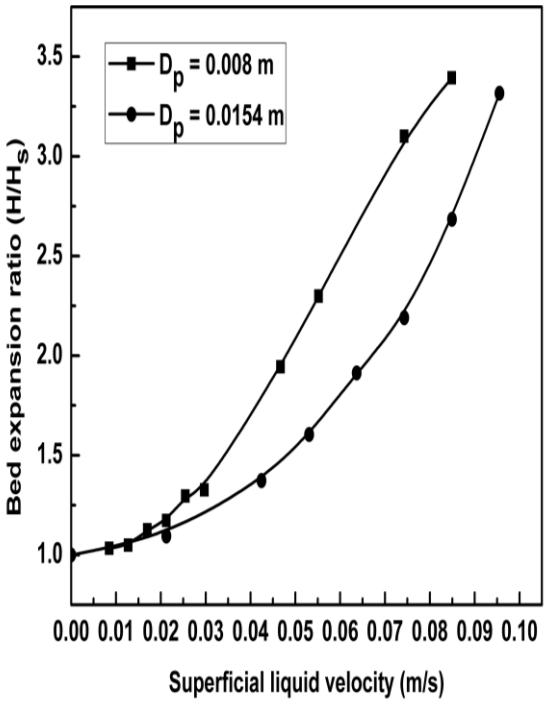

Fig. 4.33. CFD simulation result for variation of bed expansion ratio with liquid velocity for different low density particle size.

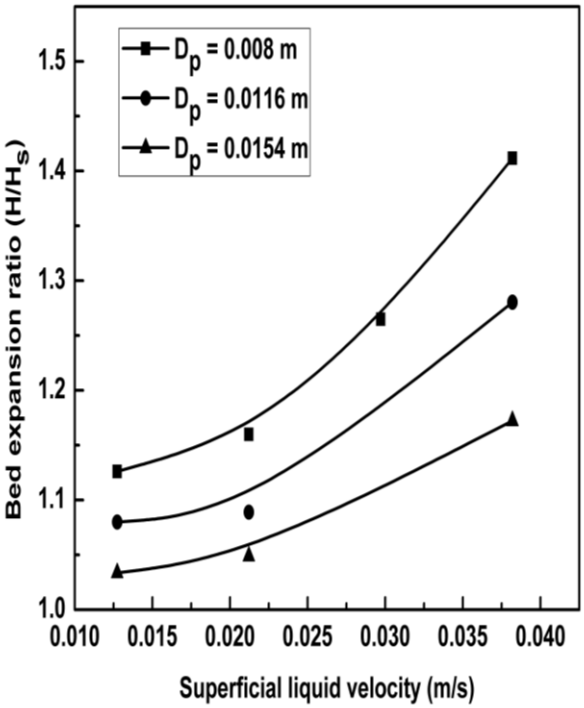

Fig. 4.34. Comparison of bed expansion ratio vs. superficial liquid velocity for low density solid particle of different size at constant gas velocity 0.0084 m/s.

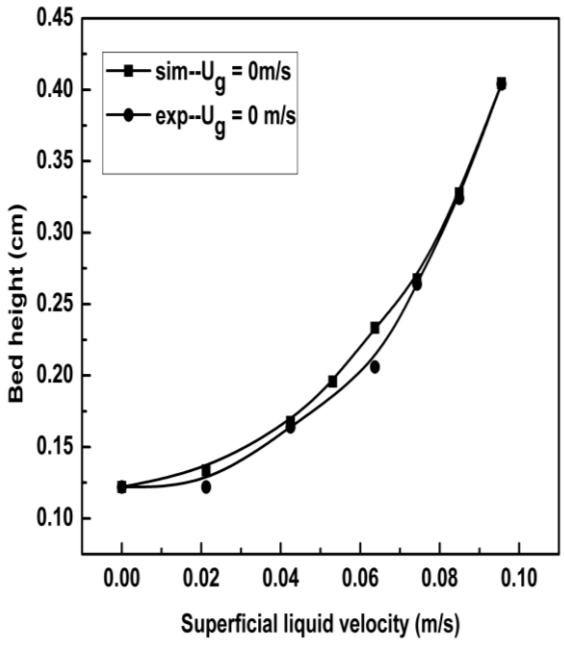

Fig.4.35. Comparison for simulation and experimental result of plastic beads.

4.2.4. Bed pressure drop:

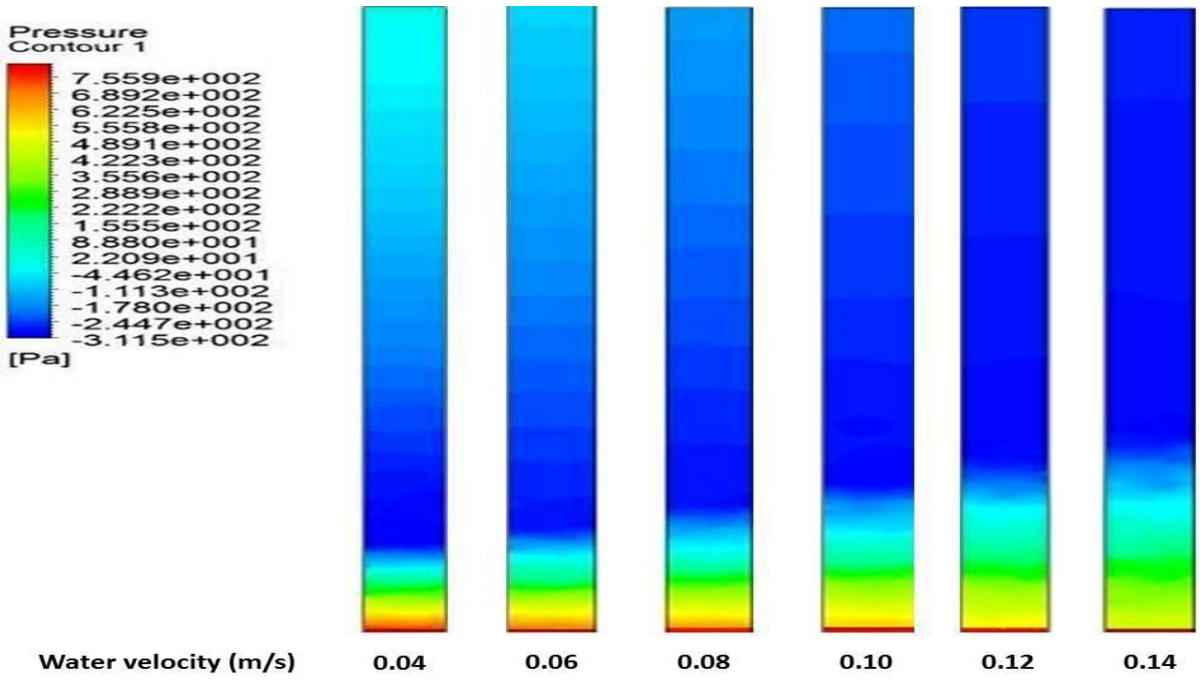

Fig. 4.36. Contour of bed pressure drop with variation with liquid velocity in the fluidized bed (2D) having distributor at a gas velocity of 0.0125 m/s.

The axial bed pressure drop in a fluidized bed varies from higher value at the bottom of the bed to zero value at the top of the column. The bed pressure drop can be determined from the difference of pressure at the inlet and outlet. Fig. 4.36 shows the contour of statics gauge pressure. It is evident from the figure that the pressure is higher at the inlet and gradually decreases and became zero at the outlet.

Fig. 4.37 shows the plot of bed pressure drop vs. superficial liquid velocity obtained at different inlet values of gas velocities after the minimum fluidization is achieved. It is evident from the plot that pressure drop increases when superficial liquid velocity is increased. Also when the gas velocity is small (U_g = 0.0125 m/s) there is no substantial increase in pressure drop with liquid velocity; more is the gas velocity more is the variation in bed pressure drop. This can be attributed to the fact that at lower gas velocity, the volume fraction of the gas is low and does not change a lot with the variation with liquid velocity. But at higher gas

velocity and increase in liquid velocity cause a decrease in gas holdup (increase in liquid holdup), thus leading to increase in pressure drop.

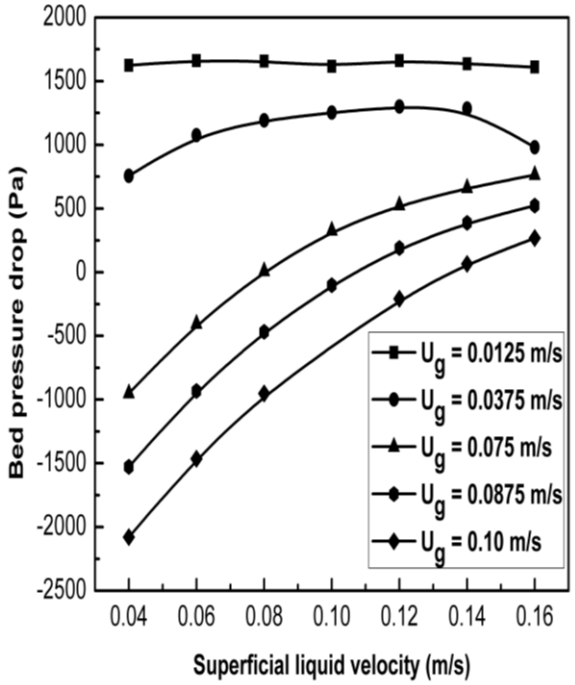

Fig. 4.37. Variation of bed pressure drop vs. superficial liquid velocity for 3D fluidized bed at constant gas velocity [H_S = 0.213 m and Dp = 2.18 mm].

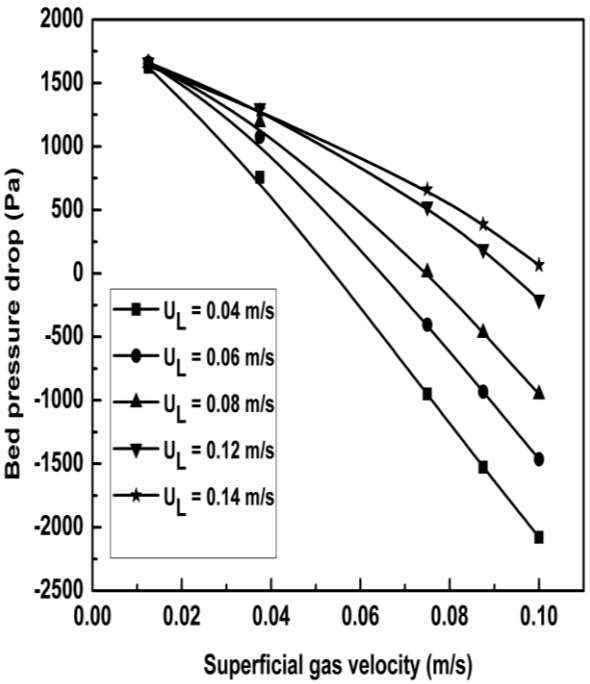

Fig. 4.38. Variation of bed pressure drop vs. superficial gas velocity for 3D fluidized bed at constant liquid velocity [H_S = 0.213 m and D_P 2.18 mm].

Fig. 4.38 shows the variation of bed pressure drop with superficial gas velocity. In the plot the effect of superficial liquid velocity on pressure drop is also seen. Fig. 4.39 shows the variation of bed pressure drop vs. superficial liquid velocity for 2D fluidized bed having distributor of pore size 2 mm. It is seen from the plot that the bed pressure increases with increase in superficial liquid velocity at constant gas velocity. For gas velocity of 0.0125 m/s for bed without distributor (Fig. 4.37) shows no variation in pressure drop with liquid velocity whereas an increase in bed pressure drop is observed in case of bed with distributor. Fig. 4.40 shows the comparison of bed pressure drop vs. superficial liquid velocity of 3D fluidized bed without distributor and 2D fluidized bed with distributor of pore diameter 2 mm for constant gas velocity 0.025 m/s for static bed height 0.213 m. It is evident from the figure that the pressure drop of 2D fluidized bed with distributor finds close agreement with the 2D

fluidized bed without distributor, but a variation in bed pressure drop of bed with distributor is seen which is not in case of bed without distributor.

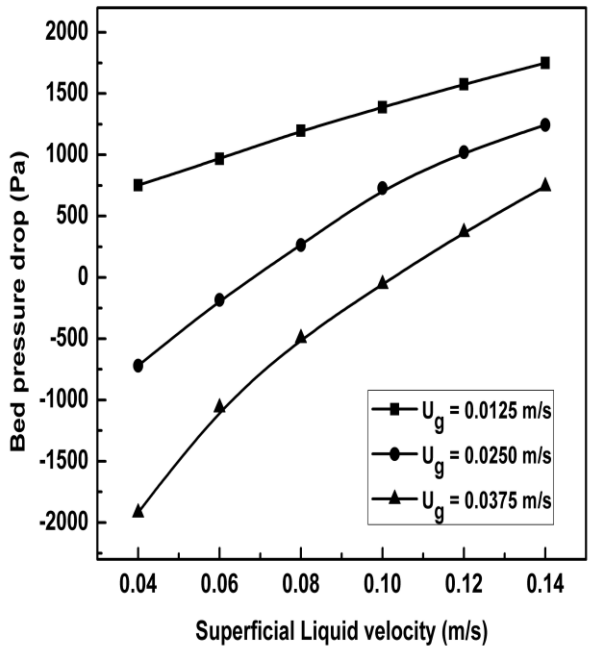

Fig. 4.39. Variation of bed pressure drop vs. superficial liquid velocity for 2D fluidized bed with distributor at constant gas velocity [H_S = 0.171 m and D_P = 2.18 mm].

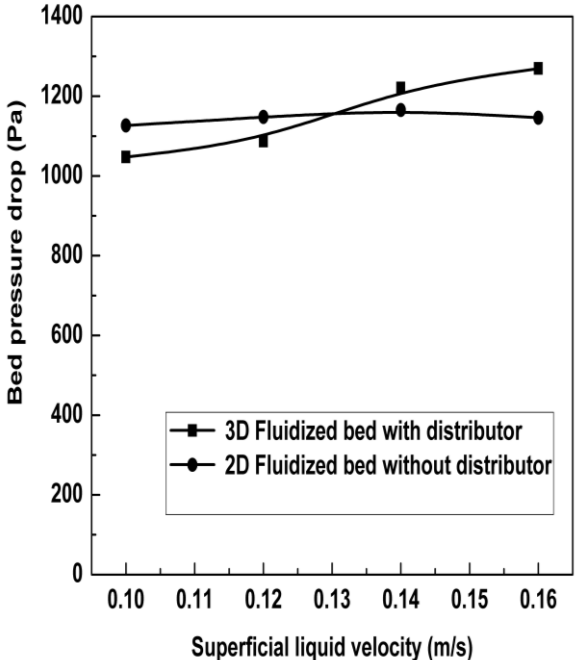

Fig. 4.40. Comparison of bed pressure drop vs. superficial liquid velocity of 3D fluidized bed and 2D fluidized bed with distributor having pore size 2 mm

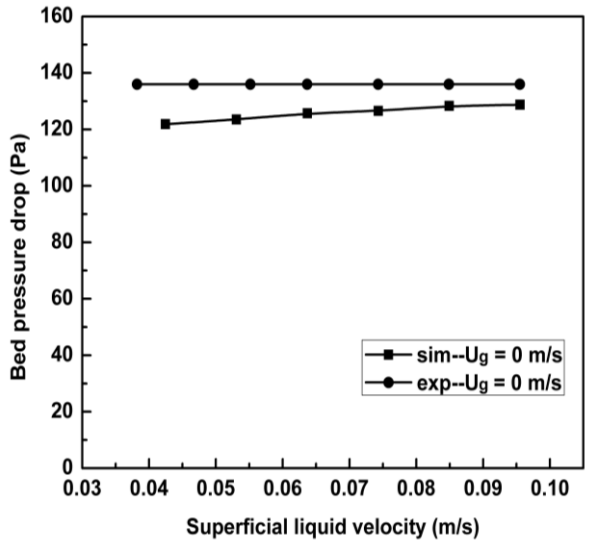

Fig. 4.41. Comparison of bed pressure drop vs. superficial liquid velocity of 2D fluidized bed and 2D fluidized bed with distributor having pore size 2 mm.

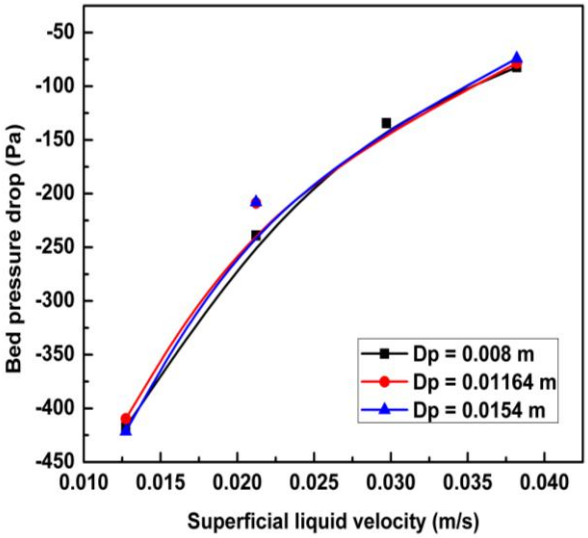

Fig. 4.42. Comparison of bed pressure drop vs. superficial liquid velocity for low density solid particle of different size [Ug = 0.0084 m/s, ρ = 1155 kg / m^3 and H_S = 0.122 m].

Fig. 4.41 shows a comparison of experimental and simulated values of bed pressure drop for liquid-solid system. A close agreement between the results is seen. Fig. 4.42 shows the bed pressure drop for low density solid particles of different particle size, no significant variation in bed pressure drop with particle size is observed because of same bed mass and bed voidage of all particle sizes are assumed in simulation.

4.2.5. Solid granular temperature:

Since Kinetics Theory of Granular Flow (KTGF) is used to define the solid phase. Granular temperature indicates the random part of the velocities of solid particles (Goldhirsch, 2008). In fluidized bed granular temperature increases with the increase in the particle oscillation. Fig. 4.43 shows the plot of axial direction of the fluidized bed (i.e. height) vs. glass beads granular temperature for inlet liquid velocity 0.14 m/s and inlet gas velocity 0.0375 m/s after quasi- steady is attained.

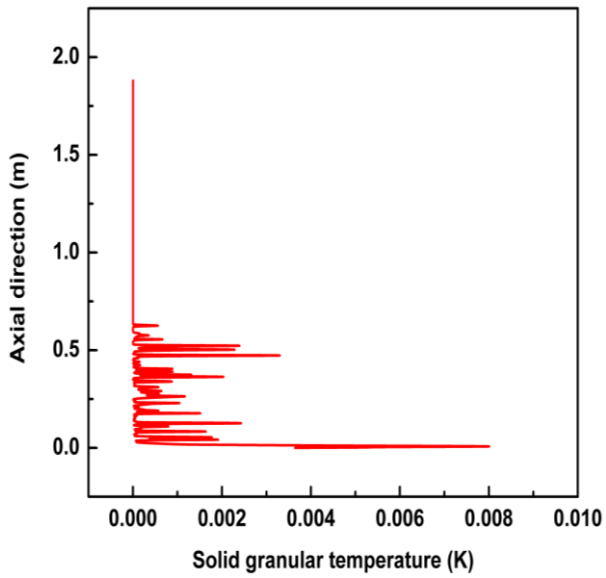

Fig. 4.43. Plot of fluidized bed axial direction vs. solid granular temperature of 3D fluidized bed for liquid velocity 0.14 m/s and gas velocity 0.0375 m/s of static bed height 0.213 m.

Fig. 4.44 show glass beads granular temperature vs. radial direction at different height (0.1 m, 0.3 m, and 0.5 m) of the fluidized bed for superficial liquid velocity 0.12 m/s and gas velocity 0.0125 m/s at different physical simulation time after quasi steady state is obtained. It is evident that granular temperature is higher at the higher section of the fluidized bed because

the volume fraction of the solid particles is less which oscillates the solid particle which led to increase in the temperature of the glass beads. But in the lower section the volume fraction of the solid particle are higher which reduces the particle oscillation which led to decrease in the granular temperature.

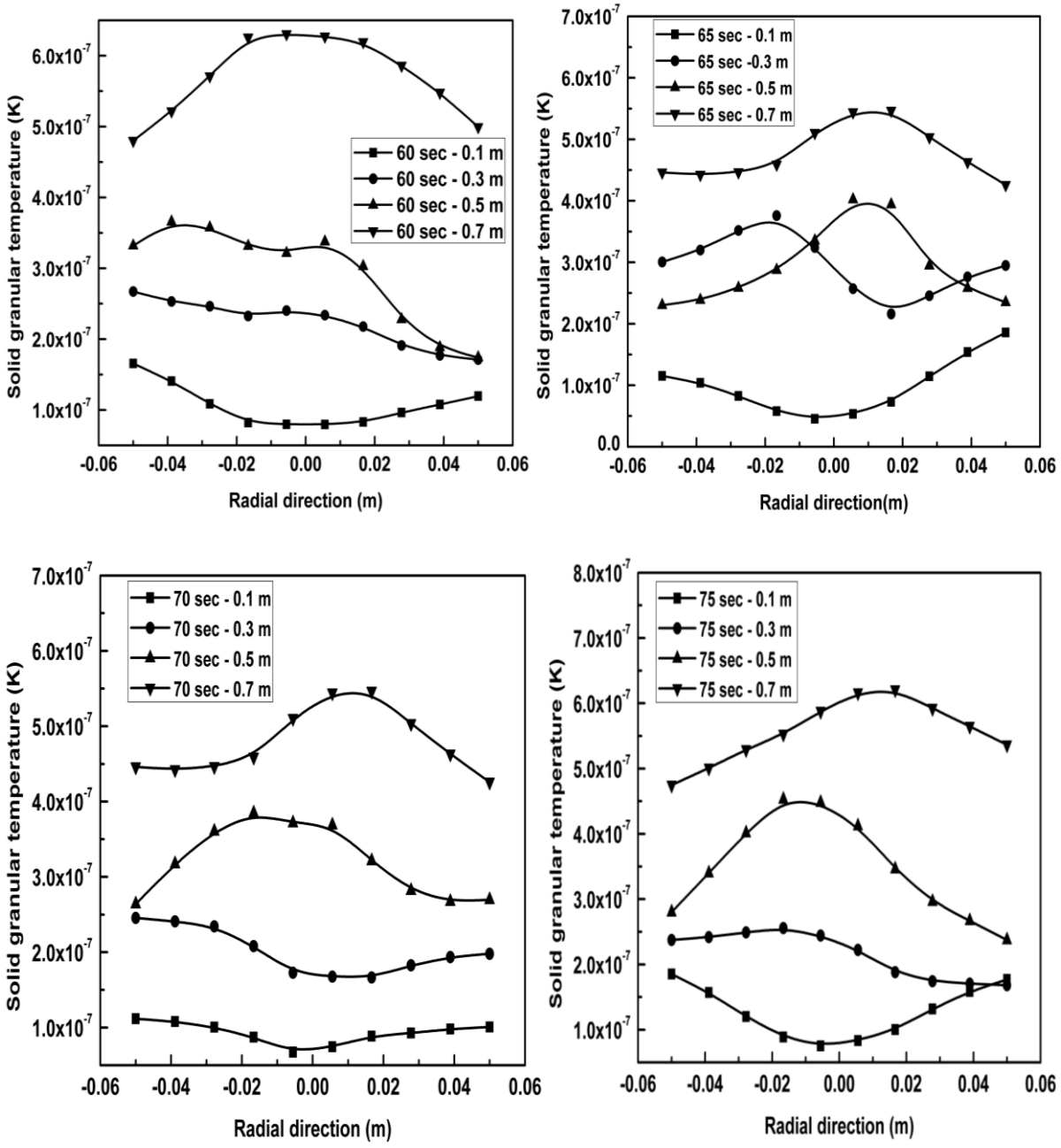

Fig. 4.44. Variation of solid granular temperature vs. radial direction of 3D fluidized bed at different height of the fluidized section at different time interval (60, 65, 70 and 75 sec).

4.2.6. Gas holdup:

Gas holdup is obtained as mean-area weighted average volume of the gas phase at sufficient number of axial position in the fluidized portion of the bed. As it is seen from the XY plot (Fig. 4.45) of gas (air) volume fraction along the axis of the column, the volume fraction of gas is not same in all the portion in the fluidized portion of the column. Hence area weighted average of volume fraction of air is determined at height 0.05 m apart along the length of the column. These value are averaged to give the average gas holdup in the bed. The contour plots of gas volume fraction at different inlet superficial liquid velocity of 2D fluidized bed model with distributor are shown in Fig. 4.46. It is seen from the contour that the volume fraction of gas is higher in the fluidized section compared to that of the two-phase section above the fluidized section. Also it is observed from the figure that the volume fraction of the gas varies randomly inside the fluidized section of the bed. Fig. 4.47 shows the variation of gas holdup radially for 3D fluidized bed it is observed that the gas holdup does not varies in the radial direction. But Literature reveals that the gas holdup remain higher in the center of the fluidized bed and decreases near to the wall (Hamidpur et al, 2012, Panneerselvam et al, 2009, Muthiah et al, 2009).

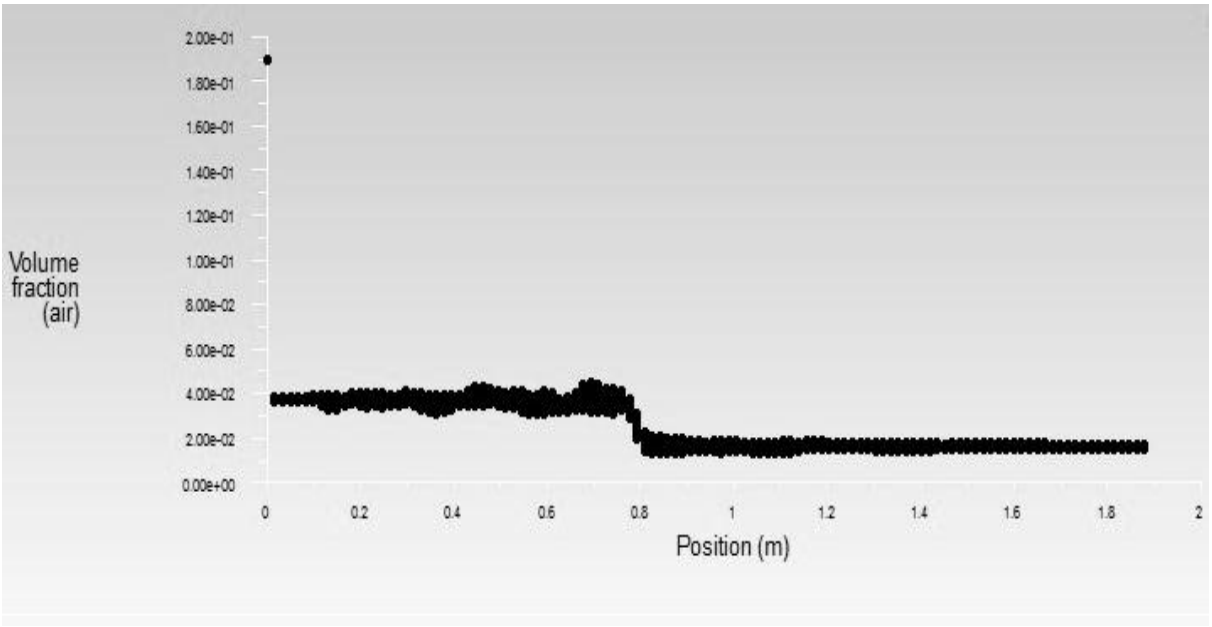

Fig. 4.45. XY plot of gas volume fraction.

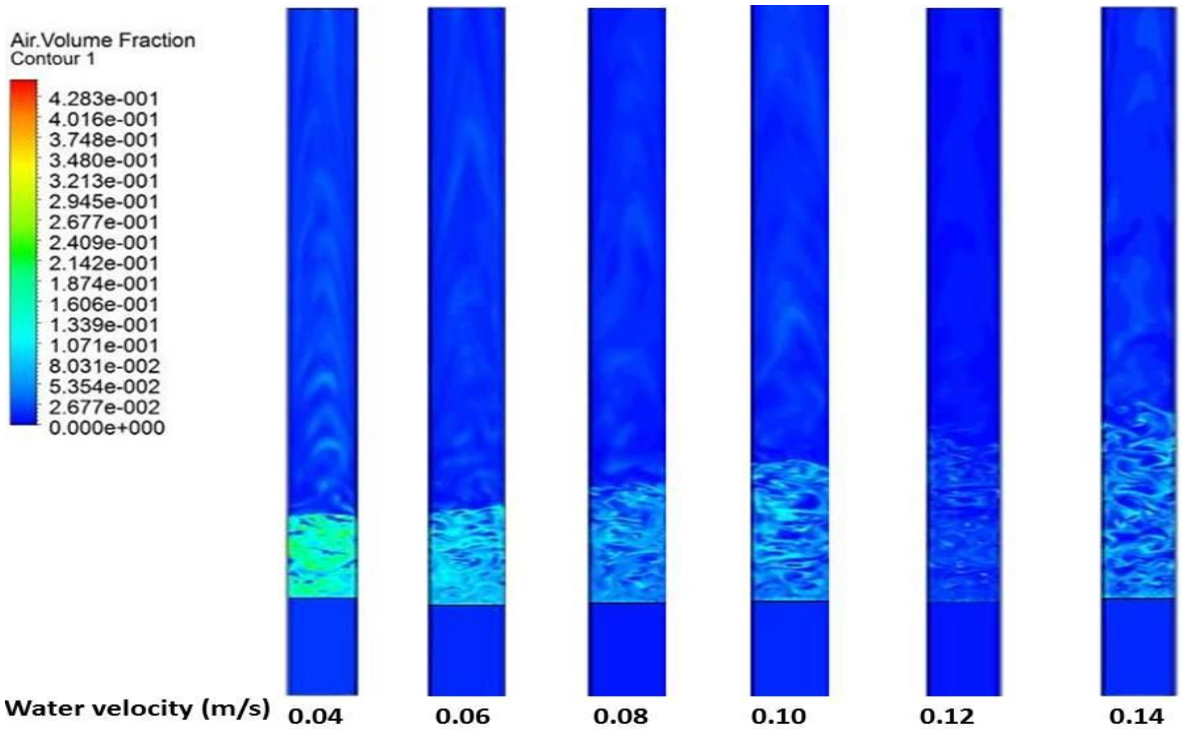

Fig. 4.46. Contour of volume fraction of gas at different inlet liquid velocity.

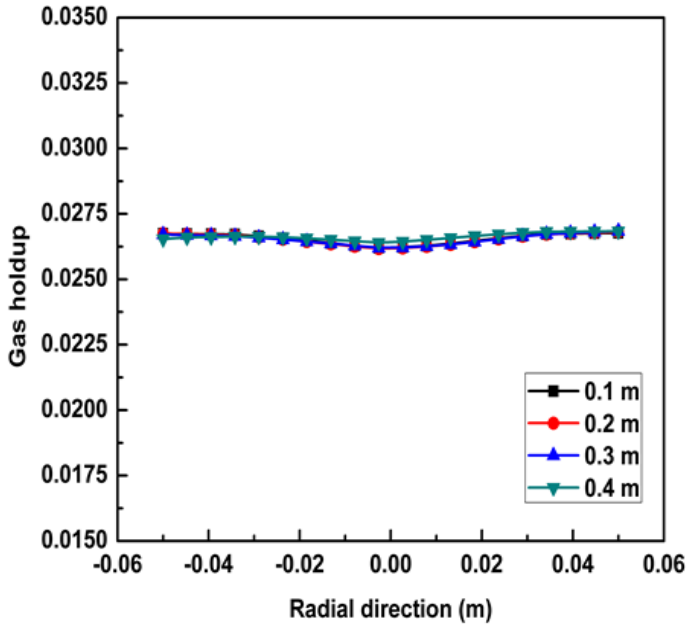

Fig. 4.47. Variation of gas holdup radially at different height of the fluidized bed for glass beads [H_S = 0.213 m, D_P = 2.18 mm, U_L = 0.08 m/s and U_g = 0.0125 m/s].

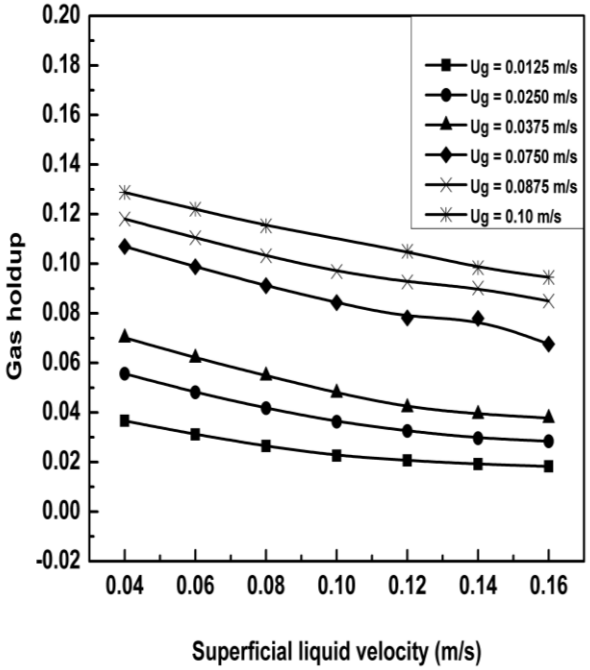

Fig. 4.48. Variation of gas holdup with superficial liquid velocity at different value of gas velocity for 2.18 mm glass beads for 3D fluidized bed model at static bed height 0.213 m.

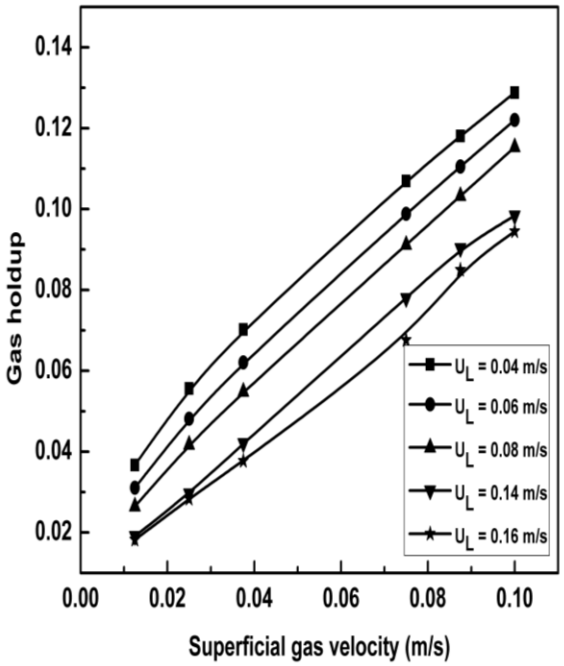

Fig. 4.49. Variation of gas holdup with superficial gas velocity at different value of liquid velocity for 2.18 mm glass beads for 3D fluidized model at static bed height 0.213 m.

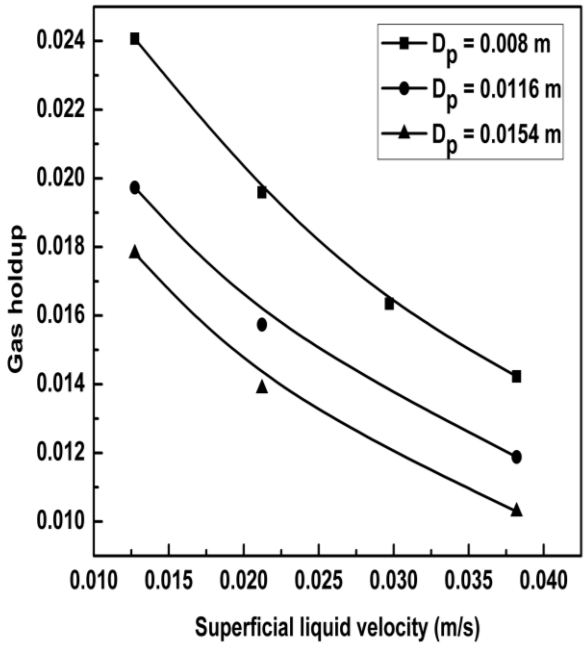

Fig. 4.50. Comparison of gas holdup vs. superficial liquid velocity for low density solid particle of different size at constant gas velocity 0.0084 m/s.

Fig. 4.48 shows the variation of gas holdup (air) with superficial liquid velocity at different values of gas velocities for 3D fluidized bed. It is evident from the plot that the gas holdup decreases with increasing liquid velocity. Similarly from Fig. 4.49 it is observed that the gas holdup monotonically increases with increase in gas velocity. Same behaviour has been observed in literature (Jena, 2010; Nguyen et al. 2011). Fig. 4.50 shows variation of gas holdup for different particle diameter of low density material, it is observed that the gas holdup for smaller particle size is higher compared to that of larger particle size.

CHAPTER-5

Conclusion and future work

Hydrodynamic characteristics of three-phase fluidized bed with low density solid particles have been determined by experiment. From the experimental result it is observed that; bed pressure drop varies with inventory of solid (i.e. initial static bed height) but not a function of particle size. For the gas-liquid-solid system it is difficult to quantify the bed pressure drop as it varies with gas and liquid velocities because of variation in gas and liquid volume fractions. This phenomenon is severe when the experiment is carried out by varying a particular fluid velocity keeping the other constant. The minimum fluidization velocity (U_{Lmf}) is not a function of initial static bed height but a function of particle size. The (U_{Lmf}) for 0.0154 m, 0.0116 m and 0.008 m particles are found to be 0.029 m/s, 0.027 m/s and 0.024 m/s respectively for fluidization in the absence of gas phase. The bed expansion ratio is not a function of the static bed height but a strong function of particle size, liquid and gas velocities.

CFD simulation on hydrodynamics of three-phase fluidized bed has been carried out by employing the Eulerian multiphase model. The distribution of volume fraction of all the three phases inside fluidized section of the fluidized bed model with distributor is not uniform compared to that of the fluidized bed model without distributor. The simulation results also indicate that there is more fluctuation in velocity of all three phases i.e. air, water and glass beads in case of bed with distributor than the bed without distributor. The presence of distributor provides better back mixing and vigorous intimate contact between various phases in the bed which is a desirable phenomenon. Thus every physical fluidized bed contains a distributor plate.

The CFD simulation result of bed expansion of low density solid particles find close agreement to that of experimentally obtained result. The bed pressure drop obtained from CFD simulation agree well with the experimental values. Both the bed expansion and pressure

drop values indicate that the drag model used in CFD simulation has satisfactorily describe the three-phase (gas-liquid-solid) phenomena. The bed expansion behaviour with variation in gas velocity obtained from CFD simulation to some extent has corroborated the experimental findings. Experimental result has shown an increase in bed expansion with gas velocity, on the other hand CFD simulation has shown slight decrease in bed expansion. The CFD simulation exhibited a solid circulation pattern for all the operating conditions, which is consistent with the observations reported by various earlier investigators. The good agreement between the values obtained from CFD simulation and experimental ones for the range of the present operating variables justify that the Eulerian multiphase granular flow approach is capable to predict the overall performance of gas-liquid-solid fluidized bed.

5.1. Future work

- CFD simulation of 3D fluidized bed with distributor will be studied and compare the result obtained with the 2D fluidized bed with distributor.
- Effect of distributor on hydrodynamics properties of three-phase fluidized bed with low density solid particles need to be carried out.
- CFD study on the effect of different bubble size on hydrodynamics of fluidized bed for low density material need to study.
- Beside Eulerian multiphase phase model, discrete phase model need to be apply to solid and gas phase.
- CFD study of the bubble break-up and bubble formation inside the three-phase fluidized need to be carry out.

References:

Allia, K., Tahar, N., Toumi, L., Salem, Z., 2006. Biological treatment of water contamination by hydrocarbon in three-phase gas-liquid-solid fluidized bed. Global NEST Journal, Vol-8 (1), 9 – 15.

Annaland, M., S., Deen, N., G., Kuipers, J., A., M., 2005. Numerical simulation of gas–liquid–solid flows using a combined front tracking and discrete particle method. Chemical Engineering Science 60, 6188 – 6198.

Beaton, W.L, McDaniel, N.K., McWhirter, W.E., Petersen, R.D., van Dnesen, R.P., 1986. Resid hydrocracker expands cnide processing flexibility. Oil Gas Journal 84 (27), 47 - 53.Briens and Ellis (2005)

Bunner, B., Tryggvason, G., 1999. Direct numerical simulations of dispersed flows. In: Proceedings of the Ninth Workshop on Two-Phase Flow Predictions, Germany, 13 – 19.

Glover G.M.C, Generalis S., C., 2004. Gas-liquid-solid flow modelling in a bubble column. Chemical Engineering and Processing 43,117 – 126.

Cao, C., Liu, M., Wen, J., Guo, Q., 2009. Experimental measurement and numerical simulation for liquid flow velocity and local phase hold-ups in the riser of a GLSCFB. Chemical Engineering and Processing: Process Intensification 48, 288 – 295.

Chen, C., Fan, L.S., 2004. Discrete Simulation of Gas-Liquid Bubble Columns and Gas-Liquid-Solid Fluidized Beds. AIChE Journal 50, 288 – 301.

Cheung, S.C.P., Yeoh, G.H., Tu, J.Y., 2007.On the numerical study of isothermal vertical bubbly flow using two population balance approaches.Chem.Eng.Sci.62, 4659 – 4674.

Feng, W., Wen, J., Fan, J., Yuan, Q., Jia, X., Sun, Y., 2005. Local hydrodynamics of gas-liquid-nanoparticles three-phase fluidization. Chemical Engineering Science 60, 6887 – 6898.

Fan, L.S., 1989. Gas-Liquid-Solid Fluidization Engineering. Butterworth Series in Chemical Engineering, Butterworth Publishers, Boston, MA.

Fluent 6.2.16. Fluent 6.2.16 User's Guide, Fluent Inc. 2004.

Fluent 6.2.16. Fluent 6.2.16 Theory's Guide, Fluent Inc. 2004.

Grevskott, S., Sannaes, B. H., 1996. Liquid circulation, bubble size distribution and solid circulation in two and three phase bubble column. Chemical Engineering Science 51, 1703 – 1713.

Goldhirsch, I., 2008.Introduction to granular temperature. Powder Technology 182, 130 – 136.

Hamidpour, M., Chen, J., Larachi, F., 2012. CFD study on hydrodynamics in three-phase fluidized beds-Application of turbulence models and experimental validation. Chemical Engineering Science 78, 167 – 180.

Jena, H.M., Roy, G.K., Meikap, B.C., 2005. Development and Comparative Study of a Semi-Fluidized Bed Bioreactor for Treatment of Wastewater from ProcessIndustries. Process & Plant Engineering – Environment Management 23, 70 – 75.

Jena, H.M., Roy, G.K., and Meikap, B.C., 2008. Prediction of gas holdup in three-phase fluidized bed from bed pressure drop measurement. Chemical Engineering Research and Design 86, 1301-1308.

Jena, H.M, 2010. Hydrodynamics of Gas-Liquid-Solid Fluidized and Semi-Fluidized Beds. Ph.D. Thesis, National Institute of Technology, Rourkela.

Jianping, W., Shonglin, X., 1998. Local hydrodynamics in a gas-liquid-solid three- phase bubble column reactor. Chemical Engineering Journal 70, 81 – 84.

Jiradilok, V., Gidaspow, D., Breault, R.W., 2007. Computation of gas and solid dispersion coefficients in turbulent risers and bubbling beds. Chem.Eng.Sci.62, 3397 – 3409.

Laborde-Boutet, C., Larachi, F., Dromard, N., Delsart, O., Schweich, D., 2009. CFD simulation of bubble column flows: Investigations on turbulence models in RANS approach. Chem.Eng.Sci.64, 4399 – 4413.

Le Page, J.-F., Chatila, S.G., and Davidson, M., 1992. Resid and Heavy Oil Processing. IFP, Editions Technip, Paris.

Li, Y., Zhang, J., Fan, L., S., 1999. Numerical simulation of gas-liquid-solid fluidization systems using a combined CFD-VOF-DPM method: bubble wake behavior. Chemical Engineering Science 54, 5101 – 5107.

Li, Y., Yang, G., Q., Zhang, J., P., Fan L., S., 2001. Numerical studies of bubble formation dynamics in gas-liquid-solid fluidization at high pressures. Powder Technology 116, 246 – 260.

Matonis, D., Gidaspow, D., Bahary, M., 2002. CFD Simulation of Flow and Turbulence in a Slurry Bubble Column. AIChE Journal 48 (7), 1413 – 1429.

Mitra-Majumdar, D., Farouk, B., Shah, Y.T., 1997. Hydrodynamic modeling of three- phase flows through a vertical column. Chemical Engineering Science 52, 4485 – 4497.

Muthiah, P., Ponnusamy, K., Radhakrishnan T.K., 2009. CFD Modeling of Flow Pattern and Phase Holdup of Three Phase Fluidized Bed Contactor. Chemical Product and Process Modeling, Volume-4, Issue-1, Article – 36.

Nguyen, K., T., Huang S., C., 2011. Simulation of Hydrodynamic Characteristics of Glass Beads in Gas-Liquid-Solid Three Phase Fluidized Beds by Computational Fluid Dynamics. Journal of Engineering Technology and Education, Vol. - 8, No - 2, 248 – 261.

Nore, O., Briens, C., Margatis, A., Wield, G., 1992. Hydrodynamics, gas-liquid mass transfer and particle-liquid heat and mass transfer in a three-phase fluidized bed for biochemical process application. Chemical Engineering Science 47, 3573 – 3580.

O'Rourke, P.J., Zhao, P. (P.), Snider, D., 2009. A model for collisional exchange in gas/liquid/solid fluidized beds. Chemical Engineering Science 64, 1784 – 1797.

Padial, N., T., Heyden, V., W., B., Rauenzahn, R., M., Yarbro, S., L., 2000. Three-dimensional simulation of a three-phase draft-tube bubble column. Chemical Engineering Science 55, 3261 – 3273.

Pan, Y., Dudukovic, M.P., Chang, M., 1999. Dynamic simulation of bubbly flow in bubble columns. Chemical Engineering Science 54, 2481 – 2489.

Pan, Y., Dudukovic, M.P., Chang, M., 2000. Numerical investigation of gas-driven flow in 2-D bubble columns. A.I.Ch.E. Journal 46, 434 – 449.

Panneerselvam, R., Savithri, S., Surender, G.D., 2007.CFD based investigations on hydrodynamics and energy dissipation due to solid motion in liquid fluidised bed. Chem.Eng.J.132, 159 – 171.

Panneerselvam, R., Savithri, S., Surender, G.D., 2009. CFD simulation of hydrodynamics of gas–liquid–solid fluidised bed reactor. Chemical Engineering Science 64, 1119 – 1135.

Rafique, M., Chen, P., Dudukovic, M., 2004. Computational modeling of gas-liquid flow in bubble columns. Reviews in Chemical Engineering 20, 225–375.

Rajasimman, M., Karthikeyan, C., 2006. Aerobic digestion of starch wastewater in a fluidized bed bioreactor with low density biomass support. Journal of Hazardous Materials 143, 82 – 86.

Schallenberg, J., Enß, J., H., Hempel, D., C., 2005. The important role of local dispersed phase hold-ups for the calculation of three-phase bubble columns. Chemical Engineering Science 60, 6027 – 6033.

Shah, Y.T., 1979. Gas-liquid-solid reactor design. McGraw-Hill, New York.

Sivaguru, K., Begum K., M., Anantharaman, N., 2009. Hydrodynamic studies on three-phase fluidized bed using CFD analysis. Chemical Engineering Journal 155, 207 – 214.

Sokół, W., Halfani, M.R., 1999.Hydrodynamics of a gas-liquid-solid fluidized bed bioreactor with a low density biomass support. Biochemical Engineering Journal 3, 185 – 192.

Sokół, W., 2001. Operating parameter for a gas-liquid-solid fluidized bed bioreactor with a low density biomass support. Biochemical Engineering Journal 8, 203 – 212.

Sokół, W., Korpal, W., 2004.Determination of the optimal operational parameters for a three-phase fluidized bed bioreactor with a light biomass support when used in treatment of phenolic waste waters. Biochemical Engineering Journal 20, 49 – 56.

Sokolichin, A., Eigenberger, G., Lapin, A., 2004. Simulation of buoyancy driven bubbly flow: established simplifications and open questions. AIChE Journal 50, 24 – 45.

Wild, G., Poncin, S., 1996. Chapter 1: Hydrodynamics. In: Three-Phase Sparged Reactors, Nigam, K.D.P., and Schumpe, A., ed., Gordon and Breach Publishers, Amsterdam, The Netherlands.

Wiemann, D., Mewes, D., 2005. Calculation of flow fields in two and three-phase bubble columns considering mass transfer. Chemical Engineering Science 60, 6085 – 6093.

Zhang, J., 1996. Bubble Columns and Three-Phase Fluidized Beds: Flow Regimes and Bubble Characteristics, PhD thesis, UBC, Vancouver.

Zhang, J., Grace, J.R., Epstein, N., 1997. Flow Regime Identification in Gas-Liquid Flow and Three-Phase Fluidized Beds. Chemical Engineering Science 52, 3979 – 3992.

Zhang, J., Li, Y., Fan, L., S., 2000a. Numerical studies of bubble and particle dynamics in a three-phase fluidized bed at elevated pressures. Powder Technology 112, 46 – 56.

Zhang, J., Li, Y., Fan, L., S., 2000b. Discrete phase simulation of gas-liquid-solid fluidization systems: single bubble rising behavior. Powder Technology 113, 310 – 326.

Zhang, X., Ahmadi, G., 2005. Eulerian-Lagrangian simulation of liquid-gas-solid flow in three- phase slurry reactor. Chemical Engineering Science 60, 5089 – 5104.